

# Functional and Responsive Polymers via Controlled Radical Polymerization

Présentée le 20 novembre 2020

à la Faculté des sciences et techniques de l'ingénieur  
Laboratoire des polymères  
Programme doctoral en science et génie des matériaux

pour l'obtention du grade de Docteur ès Sciences

par

**Jian WANG**

Acceptée sur proposition du jury

Prof. F. Stellacci, président du jury  
Prof. H.-A. Klok, directeur de thèse  
Prof. J. Vancso, rapporteur  
Dr J. Yu, rapporteur  
Dr E. Benetti, rapporteur

## *Acknowledgements*

The work described in this Thesis was performed at the École Polytechnique Fédérale de Lausanne (EPFL) from November 2015 until August 2020 under the supervision of Prof. Harm-Anton Klok.

*This work was financially supported by SNSF (Swiss National Science Foundation)*

*and CSC (China Scholarship Council)*

## **Acknowledgements**

When I first came to Switzerland in 2015, I didn't aware that what a wonderful and amazing journey I would experience in the following 5 years. I still remember that during the first meeting with Prof. Harm-Anton Klok, he noticed that I was nervous and he was trying his best to make me relax by showing me his close relationship with Chinese universities and his name stamp in Chinese (钟翰堂), an old school Chinese name, but more like an artist instead of a scientist. This was really a great start of my PhD study because during all the meetings in these 5 years, the atmosphere was always very nice and no matter what kind of questions I was faced with, HAK can always cheer me up and motivate me to find better solutions on the questions. I really enjoyed all the meetings during these 5 years and I have learnt a lot not only about the way of thinking scientific questions, but also about the attitude towards science and life. Eva, the "boss" of our boss, gave me really warmly welcome when I first came to Switzerland and supported me a lot on every aspect of my life. HAK and Eva really behave like my host parents and I will always be grateful for the kindly help, guidance and support from HAK and Eva all my life. Thank you, HAK and Eva!

Besides my host parents, I would like to thank to my thesis committee: Prof. Francesco Stellaci, Prof. Julius Vancso, Prof. Edmondo Benetti and Prof. Jing Yu for taking the time to review my thesis for their patience and valuable discussion about my research. I would like to thank our collaborators Prof. Dragan Damjanovic for all his help, his advice and for the nice discussions. Besides, I would like to thank two members of his group, Dr. Kanghyun Chu and Lukas Riemer, who were kind enough to teach me almost

## *Acknowledgements*

everything I know in pyro/piezoelectric material and help me to setup pyroelectric and piezoelectric measurement. I really enjoyed my time working in Dragan's lab because I can always discover some fancy results. I also would like to greatly acknowledge Prof. Dominique Pioletti and two of his group members Peyman and Naser for the kindly help in the bioadhesion measurement. I also want to express my gratitude to Prof. Terry W. J. Steele from Nanyang Technological University, Singapore. I believe that your contribution to my PhD thesis enriched this interdisciplinary work. Thanks a lot! Additionally, special thanks should also be given to the Swiss National Science Foundation and China Scholarship Council (201506360078) for providing financial support.

Then, I would like to express my great thanks to all my nice colleagues, the past and current LP members. Philippe, Jacques and Yann, thank you so much for always being supportive, helping us solving technical problems and enabling us to work in a safe condition. Cindy and Susanne, thank for so much for helping me with all the paper work and organizing nice parties for the whole group. Thank you Nariye for showing me the experimental process of ATRP. Thank you Piotr for sharing me a lot of experience in experiments and funding application. I enjoyed all our talks on culture, history, food and Japanese animation. Thank you Yashushi, I enjoyed a lot our talks not only on science but also on ancient history of Japanese and Chinese. Arda, my first officemate, thank you for showing me again everybody's name (I have problems in memorizing names) and giving me a lot of useful suggestions on how to work in the lab and project. Maxime, Claudia, Justin, Ioana, thank you for challenging me so hard during my

## *Acknowledgements*

presentations and those advices you gave were really helpful. Jan, thank you for helping me to improve my English in my first year. Those advices you gave on the degrafting project works very well. Michael, thank you for showing me the basic principle and analyzing skills of NMR. Friederike, Ghezae, Alex, thank you for sharing the office and lab with me and tolerating my messy table both in the office and in the lab. I really enjoy those talks and gossips on science and life. Julian, my friend, I really really enjoyed the time we had dinner and drinks together. Our experience on hiking is also quite unique, the bitter wine we found in the forest was not so nice to drink, but is a very precious memory for me. We always have a lot of topics to share with each other and I enjoyed all the talks with you on science and life. It is a pity for me that I never dare to try via ferrata, otherwise we could have spent more time together. I am so grateful for our priceless friendship and for the nice moments we had together. Tanja, we shared almost the same PhD period and thank you for your kindly help especially at the beginning of my PhD. I remember the time we spent in Kandersteg when I was shy, you always had the patience talking with me explained me everything. Markus and Tianyu, thank you for those dinners you organized and I really enjoyed the hotpot time we spent together and those talks on Chinese foods and the Spring Festival. Cristiana, thank you for being so kind to me and it is really a pity that we could finish the nanogel project together. Lisa, thank you for helping me in a lot of translation work and for teaching me to make macaron, without you I would never manage to handle the apartment renting process and to cook macaron.

## *Acknowledgements*

Corey, I really appreciate the feedback you gave on all my English writing and we also shared the great moment when Toronto Raptors won the NBA championship. Zhao, after 3 years being the only Chinese in LP, you came to join the lab. I am really happy to have you here and I enjoyed the time with you gossiping news in China and you seems to know everything happens in the entertainment circle. Feng, thank you for the tough questions on my research and my private defense presentation. Your questions always drive me to think deeply into my research. Special thanks should be given to Xinyue, behave like my sister, is always trying to help me in all the aspects of my life. It is really amazing to have you as my colleague again in Switzerland! I really want to express my sincere thanks to all the other LP members: Kuljeet, Alice, Maria, Sabrina, Sophia, Anna Lena and I enjoyed the fondue party and barbecue a lot with you. It is a great honor for me to have you as my colleagues.

I would like to give my sincere thanks to all my basketball teammates in Switzerland, including Fei Mi, Yue Zhou, Xiujiang Shen, Jiangtao Zhou, Hao Xue, Jianqi Hu, Simon Zhang, Runze Mao, Hairun Guo, Antonius, without all your efforts, we couldn't have won the championship of the Switzerland basketball game among Chinese students. I also want to express my thanks to all my Chinese friends in Switzerland, especially including Xiaopeng Huang, Junrui Zhang, Lin Sun, Minghua Zhu, Shuang Wu, Zhaoyang Wang, Zhiwen Jiang, Xiaodong Yang, Shan Jiang, Meng Li, Dr. Zhi Luo, Xiaoxuan Ding, Huayan Yang, Suiyang Liao, Lixia Wei, Chaoqun Dong, Lulu Liu, Lingfeng Zhang, Dr. Xiaolong Wang, Sichen Mi, Yang Liu, Dr. Zhangjun Huang, Prof. Jingshan Luo, Dr. Zaiwei Wang, Dr. Shoufan Cao, Dr. Huachuan Du, Dr. Shaowen

## *Acknowledgements*

Dong, Dr. Li Dong, Dr. Rensheng Pan, Hui Chen, Jing Hou, Xiaotian Zhang, Jason, Runzhe Liu, Lichen Bai, Prof. Longfang Ye, Dr. Wanzhe Chen, Prof. Qifeng Zhang, Prof. Fang Song, Prof. Tao Xu, Prof. Xiang Xu, Prof. Wei Zhong, Prof. Yifan Li, Dr. Xinyu Wang, Dr. Dong Liu, Dr. Xiao Di, Dr. Zhenzhu Meng, Jun Huang and Dr. Jiuqiu Liu. Thanks for enjoying each ping-pong and basketball match, hot-pot dinner, dumpling dinner, barbecue and card games. Special thanks should be given to Xiaopeng Huang and Lin Sun, being like my old and little brothers, are always ready to help me in every aspect of my study and life. Especially Xiaopeng, it is an amazing experience to stay with you for 4 more years in Switzerland. You are my first academic brother and your tough questions on my research always help a lot. Your encouragement and your support can always cheer me up. I always enjoyed the time we played pingpong together and I am indebt a big thank to you for all your help.

I would express my sincerely thanks to my beloved parents, Libin Wang and Yuhong Ren, for raising me up and giving me unconditional love and life-long support and encouragement. Although PhD work is tough and I didn't spend that much time with you, my heart and my soul will always stay with you, my dear parents! I also must mention my brother, Bailin Wang, for taking care of my parents when I was not at home. I would also express my special thanks to my parents in law, Honggao Sheng and Dehui Wang, and my aunt in law, Hongqun Sheng for taking care of my wife and my children and for giving me the precious advices on my future career. Raising a child is not an easy task, your help have made me and my wife overcome these challenges easier.

## *Acknowledgements*

Last but not least, I am forever grateful to my wife, Jie Sheng. You gave me two most valuable gifts during my PhD study, Ray and Annie. It is a tough work to raise two children especially without my help. I own big thanks to you for supporting the whole family almost all by yourself. Without your help, support and belief, I will not achieve anything. You helped me in more ways than you can imagine and I would like to express my deepest love and thank to you from the bottom of my heart!

Jian Wang

13-9-20 Lausanne

## Table of Contents

<b>Summary.....</b>	<b>11</b>
<b>Zusammenfassung .....</b>	<b>14</b>
<b>List of Abbreviations and Symbols .....</b>	<b>17</b>
<b>1. Introduction.....</b>	<b>21</b>
1.1. Controlled Radical Polymerization (CRP) .....	21
1.1.1. A Brief Historical Overview .....	21
1.1.2. Typical Features of CRP .....	27
1.1.3. Different Types of CRP .....	28
1.1.4. The Comparison of NMP, ATRP and RAFT Processes.....	41
<b>2. Swelling-Induced Chain Stretching Enhances Hydrolytic Degrafting of Hydrophobic Polymer Brushes in Organic Media.....</b>	<b>44</b>
2.1. Introduction .....	44
2.2. Experimental section.....	47
2.2.1. Materials.....	47
2.2.2. Methods .....	48
2.2.3. Procedures.....	50
2.3. Results and Discussion .....	52
2.4. Conclusions .....	62
2.5. Supporting Information.....	63
<b>3. Mechanical Acceleration of Hydrolysis in Polymers Incorporating Main Chain Ester Bonds .....</b>	<b>70</b>
3.1. Introduction .....	70
3.2. Experimental Section .....	72

3.2.1. Materials.....	72
3.2.2. Methods .....	73
3.2.3. Procedures.....	74
3.3. Results and Discussion .....	78
3.4. Conclusions .....	90
3.5. Supporting Information.....	91
<b>4. Light-Activated, Bioadhesive Poly(2-Hydroxyethyl Methacrylate) Brush Coatings.....</b>	<b>103</b>
4.1. Introduction .....	103
4.2. Experimental Section .....	106
4.2.1. Materials.....	106
4.2.2. Methods .....	107
4.2.3. Procedures.....	108
4.3. Results and Discussion .....	111
4.4. Conclusions .....	124
4.5. Supporting Information.....	126
<b>5. Pyroelectric Properties of Polyelectrolyte Brushes .....</b>	<b>129</b>
5.1. Introduction .....	129
5.2. Experimental Section .....	130
5.2.1. Materials.....	130
5.2.2. Methods .....	131
5.2.3. Procedures.....	131
5.3. Results and Discussion .....	133
5.4. Conclusions .....	143
5.5. Supporting Information.....	145
<b>6. Conclusions and Perspectives .....</b>	<b>155</b>
<b>7. References.....</b>	<b>160</b>

## Summary

This Thesis is built around 4 topics, which share in common that they all take advantage of the assets of controlled radical polymerization to either (i) prepare well-defined model systems to address fundamental research questions with regard to the sensitivity of chemical bonds towards mechanical forces or (ii) to synthesize ultrathin, surface-grafted polymer brush films that can serve as light-activatable bioadhesives or which possess non-centrosymmetric materials properties.

**Chapter 2** demonstrates the use of SI-ATRP to prepare PtBMA brush films that are used as a model system to better understand the effect of weak mechanical forces on the hydrolysis of ester/amide and siloxane bond. The motivation originates from previous reports that describe the degrafting of hydrophilic polymer brushes in aqueous media. The fundamental question is that decoupling the effect of swelling and the water contribution to the rate of the hydrolysis is not possible. Using the hydrophobic brushes here, it has been possible for the first time to unambiguously decouple swelling and bond hydrolysis. Comparison of reaction rate constants measured in solvents of different quality suggested that degrafting correlates with brush swelling, demonstrating the mechanochemical nature of this process

In **Chapter 3**, the sensitivity of ester bond hydrolysis towards external mechanical forces is investigated. ATRP is used to construct a series of polystyrene polymers that contain two central ester bonds. Solution ultrasonication experiments, which were performed in THF and THF water mixture with different molecular weights and under different power densities provided evidences for an increase in the apparent rate

constants for ester hydrolysis with increasing mechanical force generated via mild ultrasonication.

**Chapter 4** and **Chapter 5** present the use of SI-ATRP to produce thin, functional polymer films. **Chapter 4** focuses on the development of thin polymer films that allow to control adhesion between synthetic materials and tissue. PHEMA brushes have been prepared that can be transformed, on-demand using UV light from a non-fouling surface coating into a bioadhesive interface. Two synthetic approaches towards such films are discussed. A first strategy involves direct irradiation of a PHEMA brush film with UV-light. The second strategy uses PHEMA brushes that have been post-modified to introduce photo-reactive diazirine moieties.

**Chapter 5** attempts to understand the pyroelectric behavior of thin PE brushes prepared via SI-ATRP. This chapter builds upon the serendipitous discovery that was made when a substrate modified with a PE brush was connected to an open circuit and subjected to an alternating sequence of temperature changes. Surprisingly, a clear current change was detected in the circuit upon the temperature change. We hypothesize that the pyroelectric current which is generated upon applying an alternating sequence of temperature changes because of a permanent dipole moment in the materials. This permanent dipole moment is believed to be the consequence of a non-neutral net charge within the polymer brush film.

**Keywords:** Controlled radical polymerization, Polymer brushes, Degrafting, Rate constant, Swelling ratio, Ester hydrolysis, Mechanochemistry, Solvent effects, Surface interaction, Bioadhesion, UV light activation, Pyroelectric current, Piezoelectric

materials, Polyelectrolyte brushes, Counterions, Dipole moment.

## **Zusammenfassung**

Diese Arbeit basiert auf vier Themen, die gemeinsam haben, dass sie alle die Vorteile der kontrollierten radikalischen Polymerisation nutzen. Entweder, (i) um genau definierte Modellsysteme zu entwickeln, mit deren Hilfe grundlegende Forschungsfragen in Bezug auf die Empfindlichkeit chemischer Bindungen gegenüber mechanischen Kräften beantwortet werden können oder (ii) für die Synthese ultradünner, oberflächengepfropfter Polymerbürsten, welche als lichtaktivierbare Bioadhäsive dienen oder nicht zentrosymmetrische Materialeigenschaften besitzen

**Kapitel 2** beschreibt die Anwendung von oberflächeninitiiert-er radikalischer Atomtransferpolymerisation (SI-ATRP) zur Herstellung von Poly (tert-butylmethacrylat) -Bürsten, die als Modellsystem dienen, um den Einfluss schwacher mechanischer Kräfte auf die Hydrolyse der Ester / Amid- und Siloxanbindung besser zu verstehen. Mit den hier vorgestellten hydrophoben Bürsten war es erstmals möglich, das Quellverhalten und Hydrolyse eindeutig zu entkoppeln. Ein Vergleich der Reaktionsgeschwindigkeitskonstanten, die in Lösungsmitteln unterschiedlicher Qualität gemessen wurden zeigt, dass das Ablösen mit dem Quellverhalten der Polymerbürsten korreliert, was die mechanochemische Natur dieses Prozesses nahelegt.

**In Kapitel 3** wird die Empfindlichkeit chemischer Bindungen, insbesondere Esterbindungen, gegenüber externen mechanischen Kräften untersucht. Mit Hilfe einer Reihe von Polystyrolpolymeren, welche zwei mittig platzierte Esterbindungen aufweisen, konnte in Ultraschallversuchen in trockenem, sowie feuchtem THF, Hinweise für eine Erhöhung der beobachteten Geschwindigkeitskonstanten für die

Esterhydrolyse mit zunehmender mechanischer Kraft gefunden werden. Dabei kamen Polymere unterschiedlichen Molekulargewichts, sowie Ultraschall verschiedener Leistungsdichten zur Anwendung.

**Kapitel 4** befasst sich mit der Entwicklung von Polymerfilmen, mit deren Hilfe die Haftung zwischen synthetischen Materialien und Gewebe kontrolliert werden kann. Die verwendeten Poly (2-hydroxyethylmethacrylat) (PHEMA) Bürsten können bei Bedarf von einer nicht verschmutzenden (non fouling) Oberflächenbeschichtung in eine bioadhäsive Grenzfläche transformiert werden. Eine derartige Transformation kann durch direkte Bestrahlung mit UV-Licht erzeugt werden. Durch Postmodifikation der Bürsten können photoreaktive Diazirineinheiten eingeführt werden, was die Anwendung milderer UV Strahlung erlaubt.

**Kapitel 5** beschreibt das pyroelektrische Verhalten dünner Polyelektrolytpolymerbürsten, basierend auf der Beobachtung, dass die Stromstärke innerhalb eines offenen Stromkreises, der ein mit einer Polyelektrolytpolymerbürste modifiziertes Substrat beinhaltet, durch Temperaturänderungen beeinflusst wird. Ein solcher Effekt ist für Nicht-Polyelektrolytpolymerbürsten nicht feststellbar. Dieser pyroelektrische Effekt kann vermutlich auf ein permanentes Dipolmoment im Material zurückzuführen werden. Es liegt nahe, dass dieses permanente Dipolmoment die Folge einer nicht neutralen Nettoladung innerhalb des Polymerbürstenfilms ist.

**Schlüsselwörter:** Kontrollierte radikalische Polymerisation, Polymerbürsten, Entfropfen, Geschwindigkeitskonstante, Quellverhältnis, Esterhydrolyse, Mechanochemie, Lösungsmittelleffekte, Oberflächenwechselwirkung, Bioadhäsion,

UV-Lichtaktivierung, Pyroelektrischer strom, Piezoelektrische materialien,  
Polyelektrolytbürsten, Gegenionen, Dipolmoment.

## **List of Abbreviations and Symbols**

A	Measured absorbance
Ac <sub>2</sub> O	Acetic anhydride
AcOH	Acetic acid
AFM	Atomic force microscopy
AIBN	2,2-azobisisobutyronitrile
ANOVA	Analysis of variance
ATRA	Atom transfer radical addition
BBPB	1,4-Bis(4-bromomethylphenyl)butane
BDMB	Butane-1,4-diyl bis(4-(bromomethyl)benzoate)
BPO	Benzoyl peroxide
Bpy	2,2'-Bipyridyl
BST	2-Phenyl-2-(2,2,6,6-tetramethylpiperidine-1-oxy)ethyl benzoate
CRP	Controlled radical polymerization
CTAB	Hexadecyltrimethylammonium bromide
DCC	Dicyclohexylcarbodiimide
DCM	Dichloromethane
$\bar{M}$	Polydispersity ( $M_w/M_n$ )
DMAP	4-(Dimethylamino)pyridine
DMF	Dimethylformamide
DMSO	Dimethyl sulfoxide
DNA	Deoxyribonucleic acid
Dnbpy	4,4'-Dinonyl-2,2'-bipyridyl
DP	Degree of polymerization

*List of Abbreviations and Symbols*

ESI	Electrospray ionization
$\epsilon$	Calculated molar extinction coefficient
FTIR	Fourier-transform infrared spectroscopy
GPC	Gel permeation chromatography
GTP	Group transfer polymerization
HBr	Hydrobromic acid
HCl	Hydrochloric acid
HIFU	High intensity focused ultrasound
HRMS	High resolution mass spectrometry
$K_{ATRP}$	Equilibrium constant of ATRP
$k_{ini}$	Apparent initial rate constant
$K_p$	Rate constant of propagation
Me <sub>4</sub> cyclam	1,4,8,11-Tetramethyl-1,4,8,11-tetraazacyclotetradecane
MEK	2-Butanone
MeOH	Methanol
$M_i$	Initial number average molecular weight of polymer
MMA	Methyl methacrylate
$M_n$	Number average molecular weight
$M_t$	Number average molecular weight of the sonicated sample at time t
MTS	1-Methoxy-1-(trimethylsiloxy)-2-methylprop-1-ene
$M_w$	Weight average molecular weight
NMP	Nitroxide-mediated radical polymerization
NMR	Nuclear magnetic resonance
PBS	Phosphate buffered saline
PE	Polyelectrolyte

*List of Abbreviations and Symbols*

PEG	Polyethylene glycol
PFM	Piezoelectric force microscopy
PHEMA	Poly(2-hydroxyethyl methacrylate)
PLGA	Poly(lactic-co-glycolic acid)
PMDETA	N,N,N',N'',N''-pentamethyldiethylenetriamine
PMETAC	Poly([2-(methacryloyloxy)ethyl]trimethylammonium chloride)
PMMA	Poly(methyl methacrylate)
PMPC	Poly(2-methacryloyloxyethyl phosphorylcholine)
PPEGMA	Poly(poly(ethylene glycol methacrylate))
PS	Polystyrene
PSPMA	3-Sulfopropyl methacrylate, potassium salt
PtBMA	Poly(tert-butyl methacrylate)
PVC	Polyvinyl chloride
PVDF	Polyvinylidene fluoride
RAFT	Reversible addition-fragmentation chain-transfer polymerization
$R_p$	Rate of polymerization
SD	Standard deviation
SI-ATRP	Surface-initiated atom transfer radical polymerization
SIP	Surface-initiated polymerization
SKPM	Scanning kelvin probe microscopy
SS	Styrene sulfonate
TEM	Transmission electron microscopy
TEMPO	2,2,6,6-Tetramethyl-1-piperidinyloxy
TFMDA	4-[3-(Trifluoromethyl)-3H-diazirin-3-yl]benzoic acid

*List of Abbreviations and Symbols*

THF	Tetrahydrofuran
TMOS	Tetramethoxysilane
UV light	Ultraviolet light
WCA	Static water contact angles
XPS	X-ray photoelectron spectroscopy

# 1. Introduction

## 1.1. Controlled Radical Polymerization (CRP)

### 1.1.1. A Brief Historical Overview

Since the concept of chain polymerization and the basic structure of a polymer molecule was first proposed by Staudinger one century ago,<sup>1</sup> polymer science and technology has evolved rapidly that has promoted the development of the society and changed the lifestyle of human beings. Thanks to the better understanding of the mechanism of polymerization, large amount of polymeric materials with various functions has been produced in nowadays.

Traditional polymerization reactions can be roughly divided into two types based on the reaction kinetics: step and chain polymerizations. Step polymerization is characterized as a stepwise-growth mechanism in which the polymer molecular weight increases in a slow, step-like manner as the reaction time increases. During step polymerization process, any two molecular units can react with each other and the monomer disappears in the early stage of the reaction. The polymer chain length increases steadily and the average molecular weight are increasing throughout the reaction. Moreover, the reaction system contains various stages and chain length and the product will present in a calculable distribution. Chain polymerization usually requires an initiation to start the chain growth. Growth occurs by addition of one unit at a time so the monomer concentration decreases steadily throughout the process. Since the polymer chains are formed from the beginning of the polymerization and the rate

of chain growth is extremely fast, the average chain length for reacted species remains approximately constant. In the reaction mixture, unreacted monomer and polymer coexist with very little amount of growing polymer chains.<sup>2</sup>

Conventional polymerization techniques have great importance in industry. For example, polyesters, polyamides, epoxy resin, alkyd resin and many engineering plastics are produced by step polymerization. As another key type of polymerization, chain polymerization has been used to produce polyolefins including some most widely used industrial materials polystyrene and PVC. However, there are still some limitations existing in conventional polymerization techniques including lack of precise control over molecular weight and dispersities and difficulty in synthesizing polymers with complex architectures or specific functions.

So-called “living”/controlled polymerization reactions allow to overcome these limitations and to access to polymers with well-defined architecture, precisely defined molecular weight and narrow dispersities as well as complex functional groups. The first living polymerization was realized by Michael Szwarc<sup>3</sup> who eliminated transfer and termination reactions from chain growth polymerization using living anionic polymerization and non-polar monomers in 1956. After that, a number of studies has been conducted and has provided a good understanding of living anionic polymerizations.<sup>4</sup> In general, styrene derivatives and (meth)acrylate monomers are two best established systems in living anionic polymerization.

The difficulty of living anionic polymerization of functionalized styrene derivatives is the compatibility of the functional groups with anionic initiators and the propagating

chain-end polystyrylanions. In general, two strategies have been utilized to overcome this problem. The first strategy involves protection of the functional group, which result in a protected monomer, followed by deprotection to regenerate the original functional group after the polymerization. The second strategy incorporated an electron-withdrawing functional group onto the benzene ring of styrene, which as a result decreased the reactivity of the chain-end carbanion.<sup>5</sup> The molecular weight of living anion polymerization of styrene derivatives can be controlled from  $10^2$  to  $10^6$  kDa with a narrow molecular weight distribution ranging from 1.01 to 1.10. A reactive and stable benzyl-type polystyrylanion is generated at the end of the polymer chain, which allows to create specially designed polymers with precise molecular architectures.<sup>5</sup> The development of living anionic polymerization of alkyl (meth)acrylates was originally hindered by the existence of ester enolates in an equilibrium with aggregated form, which leads to broadening the molecular weight distribution. To overcome this problem, researchers tried to influence the equilibrium dynamics of aggregated ion pairs by using sterically hindered alkyl metal initiators in conjunction with ligands that are capable of coordinating with enolate ion pairs.<sup>6-10</sup> As a result, the use of appropriate additive/ligand in conjunction with initiator brings perfect control of the polymerization in both polar and non-polar solvents.

The first living cationic polymerization was reported by Higashimura and Sawamoto for alkyl vinyl ethers initiated with a combination of hydrogen iodide and iodine in 1984 and shortly thereafter by Faust and Kennedy for isobutylene.<sup>11-13</sup> Traditional drawback for cationic vinyl polymerization, for example, the instability of the growing

carbocations was overcome by stabilizing carbocationic intermediate with nucleophilic interaction through selecting a proper nucleophilic counteranion or the addition of a Lewis base. A systematic review on the mechanism of the living cationic polymerization was provided by Matyjaszewski and Sigwalt in 1994.<sup>14</sup> These authors proposed that “living/controlled” polymerizations could be explained by the occurrence of equilibrium between two species: a cationic, highly reactive species, being present in very low concentrations, and a dormant (non-propagating) species. The consequence of this equilibrium is that the rate of propagation is slowed down to a value lower than the rate of initiation. Another requisite is that the rate of reaction from active species to the dormant and the reverse reaction are both significantly higher than the overall rate of propagation to achieve a single molecular weight distribution. In general, controlled cationic polymerization can be applied to vinyl monomers with electron donating groups such as vinyl ethers, isobutenes, styrene and its derivatives because on the one hand, the electron cloud density of the double bond is higher compared to normal vinyl monomers, which facilitate the reaction with cationic active species. On the other hand, the carbocations stabilize the electron cloud, which prohibits side reactions.

Group transfer polymerization (GTP) was first announced by DuPont as a method for synthesis of acrylic block polymers.<sup>15</sup> Instead of using costly refrigeration units, the polymerization operates at high enough temperature, which allows reactor cooling by water-cooled reflux condensers. GTP uses 1-methoxy-1-(trimethylsiloxy)-2-methylprop-1-ene (MTS) as initiator and a nucleophilic anion as catalyst. GTP converts

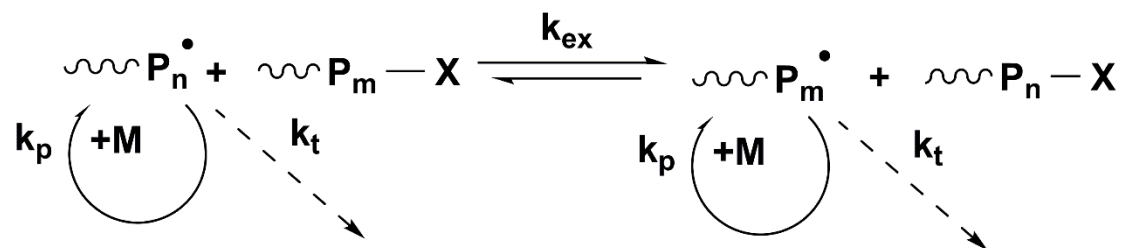
methacrylate monomer to a polymer with trimethylsilyl ketene acetal as the end group. If the initiator contains a vinyl group not reactive to GTP, a macromonomer results, which can be used to prepare block copolymers. GTP operates at temperatures usually between 50 to 80 °C (maximum 100 °C) when catalyzed by weak nucleophiles such as tetrabutylammonium benzoate.<sup>16</sup> Typical molecular weights range around 20,000 Da, however, to achieve a molecular weight higher than 60,000 Da is difficult.<sup>17</sup> The original mechanism proposed by the DuPont workers was that the trimethylsilyl group was transferred to the monomer as it was added to the polymer chain ends and thus named the new procedure Group Transfer Polymerization. However, based on all the evidence now available, this mechanism is almost certainly wrong since there is clear evidence that supports an anionic mechanism, which was first reported by R. Quirk et al.<sup>18</sup>

Living anionic and living cationic polymerizations are widely used but still suffer from a limited monomer scope in particular acrylates and methacrylates can only be polymerized under very specific conditions in a living “controlled” manner with anionic. The ability of polymer chemists to polymerize acrylate and methacrylate in a controlled fashion has changed dramatically in the 1980’s and 1990’s with the advent of controlled radical polymerization techniques. The first example of CRP was reported by Borsig who used diaryl and triaryl protected groups in polymerizations of MMA and observed increase of molecular weights with conversion and also the formation of block copolymers.<sup>19</sup> In 1982 Otsu, for the first time, used the concept “living radical polymerization” to describe a polymerization in the presence of dithiocarbamates.<sup>20</sup>

This system was further studied by Braun, who, however, did not achieve good controllability.<sup>21</sup> The use of nitroxide-mediated radical polymerization (NMP) for producing block and end-functional polymers was first described in a patent application by Solomon et al in 1985. In 1990, Johnson et al<sup>22</sup> described the persistent radical effect and demonstrated the preparation of low dispersity polymers with NMP using an appropriate selection of alkoxyamine and control of reaction conditions.<sup>23</sup> In 1993, Georges reported on the control of bulk radical polymerization of styrene in the presence of TEMPO,<sup>24</sup> which showed good controllability. In consequence, NMP received significant attention in a wider literature. Those systems are limited to styrene and its copolymers, though. The first examples of atom transfer radical polymerization (ATRP) with a good living polymerization character, were reported respectively by Sawamoto,<sup>25</sup> Matyjaszewski<sup>26,27</sup> and Percec<sup>28</sup> in 1995. This technique was developed based on the Kharasch reaction, which allows the addition of halocarbon across alkene double bonds in a radical chain.<sup>29</sup> Since the overall process can be catalyzed by transition metal complexes, it is called atom transfer radical addition (ATRA).<sup>26,30</sup> The mechanism of ATRP can be simplified into a reversible activation–deactivation process. The activation process involves a redox reaction between the polymer end group and the metal complex in its reduced form. In the deactivation process, propagating radicals are trapped by atom or group transfer reaction (most commonly halogen atoms from a metal complex in its higher oxidation state). Another living radical polymerization which was named as reversible addition–fragmentation chain-transfer polymerization (RAFT) was first reported by Chiefari et al in 1998 based on an additional-



system.



**Scheme 1.2.** Radicals participate in reversible transfer degenerative exchange process in CRP system.

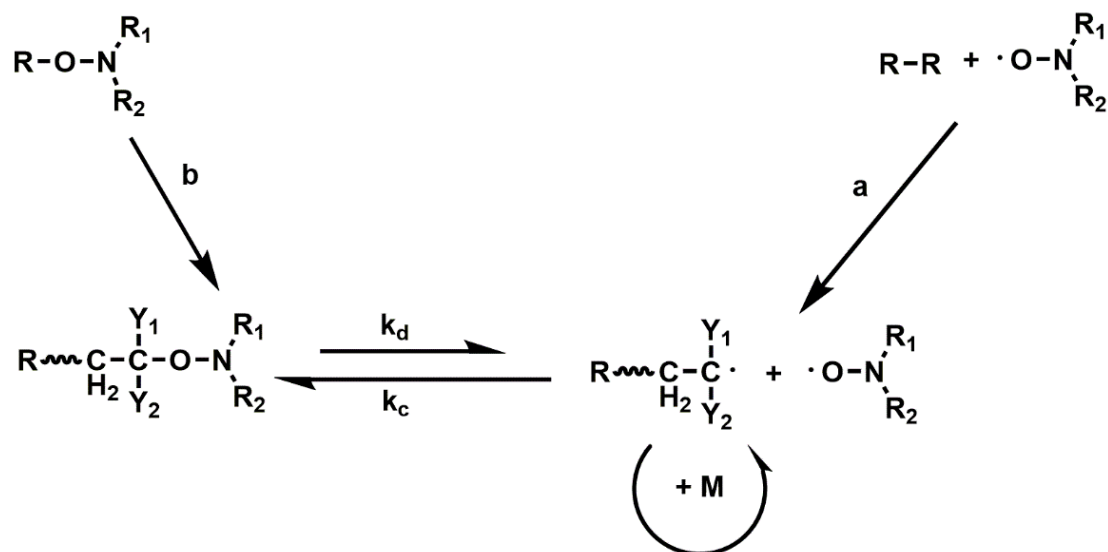
A variety of chemistries have been developed to achieve these conditions, which include ATRP, NMP and RAFT and which will be discussed in more details in the next section. Since they provide fast and quantitative initiation and significantly reduce termination reactions, CRP allows one to prepare polymers with well-defined molecular weights, narrow dispersities as well as controlled functionalities and architectures.

### 1.1.3. Different Types of CRP

This part will discuss the basic principles of different CRP techniques and introduce the selection criteria of monomers, initiators, catalysts and other components.

#### 1.1.3.1. Nitroxide-Mediated Polymerization (NMP)

NMP is one of the earliest and easiest controlled radical polymerizations. It is a technique based on a reversible termination mechanism between the growing propagating radical and the nitroxide to generate an alkoxyamine, as the predominant species. An equilibrium can be established between dormant and active species (activation-deactivation process) upon a judicious design. The general mechanism of NMP, as is illustrated in **Scheme 1.3**, is well known and has been extensively studied.<sup>33</sup>



**Scheme 1.3.** Activation-deactivation equilibrium in NMP. (a) Bicomponent, (b) monocomponent initiation system.

The process involves an initiator, which upon heating dissociates to form radicals that react with the monomer and an excess of the stable radical nitroxide, which caps most of the initiated chains preventing loss of control over the reaction. The NMP is usually carried out at high temperatures ranging from 125 to 135 °C to allow all the polymer chains to initiate at the same time. The C–O bond formed between the propagating radical site and the stable radical is labile in this temperature range so that it can undergo reversible homolytic cleavage to regenerate the stable radical and an active radical site at the end of the polymer chain. The active polymer radical reacts with another nitroxide molecule to reform the dormant polymer chain, or with the monomer to undergo chain extension. Since the reaction equilibrium between dormant and active species strongly favors the dormant site, most polymer chains are in dormant state throughout the reaction. Although some termination is unavoidable during the polymerization,<sup>34</sup> the termination rate decreases as the polymerization proceeds since coupling termination

reaction usually involves at least one short chain.<sup>35</sup> Polymer growth from the initiating species occurs in a controlled way without any side reactions, which generates new chains. Ultimately, the NMP process enables a linear increase in the molecular weight of the polymer chain with monomer conversion, while it yields polymers with very narrow chain distribution.

#### 1.1.3.1.1. Initiators and Mediators

Conventional thermal radical initiators, for example, 2,2-azobisisobutyronitrile (AIBN) or benzoyl peroxide (BPO) can be used in NMP systems, however, their use often requires tuning the system to obtain the optimized ratio of initiator to mediator because the initiation efficiency of various primary initiators differs and any large excess of free nitroxides adversely affects the rates of polymerization.<sup>36</sup> Since the C–O bond of the alkoxyamine is labile and dissociates to form an initiating species and a stable radical mediator upon heating, it can act as an alternative initiator in NMP systems with the addition of an initiator fragment (optional), a monomer and a nitroxide.<sup>37,38</sup>

The preparation of different alkoxyamine initiators that involve the controlled generation and trapping of carbon-centered radicals by stable radicals will be discussed in this paragraph. In general, alkoxyamines are prepared via four routes. Route 1 is using the nucleophilic substitution of the hydroxylamine anion on the corresponding alkyl halide. Route 2 involves the Meisenheimer rearrangement of ally or benzyl amine oxides. Route 3 uses the reaction between an oxoammonium salt and olefin or an enolate and route 4 consists of the in situ generation of an alkyl radical followed by the trapping of a nitroxide. Since route 4 is the most commonly used method, initiators

prepared via route 4 will be mainly discussed. One of the most commonly used alkoxyamine, 2-phenyl-2-(2,2,6,6-tetramethylpiperidine-1-oxy)ethyl benzoate (BST), has been synthesized by the reaction of benzoyl peroxide with styrene in the presence of TEMPO at 80 °C.<sup>39-41</sup> Other alkoxyamine derivatives that do not contain the benzoyloxy moiety can also be synthesized. For example, the reaction between di-tert-butyl peroxide and ethyl benzene generates the corresponding benzylic radical, which further reacts with TEMPO to form the alkoxyamines.<sup>42,43</sup> Another alkoxyamine can be synthesized in the presence of Jacobsen's catalyst. In this reaction a radical intermediate is generated, which can be trapped by a stable nitroxide radical and then reduced to form the corresponding alkoxyamine.<sup>44</sup>

Nitroxide is usually used as a stable radical mediating the polymerization. In order to achieve a controlled polymerization, several requirements have to be met including relative high stability under the reaction conditions and the ability to react with propagating chain in a reversible manner. In addition, it must neither react with itself or with the monomer to initiate new chains nor induce side reactions, such as  $\beta$ -hydrogen atom abstraction. The stability of nitroxides comes from the delocalization of three electrons in the N–O bond. The high delocalization energy ( $\sim 30.4$  kcal/mol) offers a high thermodynamic stability towards the radical center, which as a result prevents the dimerization of two nitroxide radicals. This thermodynamic stability of different nitroxide radicals is strongly influenced by the substituents on the carbons next to the nitrogen. Thus, for example, if all four groups attached to the carbons attached to the nitroxide nitrogen are alkyl, the nitroxide is stable. Replacing one of the alkyl

groups with a hydrogen or attaching a phenyl group directly to nitrogen, however, makes the nitroxide relatively unstable.<sup>45,46</sup>

#### 1.1.3.1.2. Range of Monomers

A wide variety of monomers including styrene and its derivatives, vinylpyridines acrylic esters, acrylonitrile, acrylic acid acrylamide, N-substituted and N,N-disubstituted acrylamides, dienes and cyclic ketene acetals can be polymerized via NMP.<sup>33</sup> Here, two most commonly used monomers will be discussed briefly including styrenes and methacrylates since corresponding polymers have been used in the following chapters of the Thesis.

Styrene and derivatives are most extensively studied in terms of mechanism, kinetics and possible side reactions. Since the rate of polymerization mediated by most cyclic nitroxides is rather slow and high temperatures are required, the use of acyclic nitroxide for example di-tert-butyl nitroxide,<sup>47</sup> 2,2,5-trimethyl-4-fluorophenyl-3-azahexane-3-oxyl<sup>48</sup> and N-tert-butyl-N-[1-diethylphosphono-(2,2-dimethylpropyl)] nitroxide<sup>49</sup> or tuning the steric hindrance of TEMPO derivatives is essential for improving the rate of polymerization.<sup>50</sup> Many styrene derivatives including para-substituted styrenes (F, Cl, Br, CH<sub>3</sub>, OCH<sub>3</sub>, CF<sub>3</sub>, CH<sub>2</sub>Cl ) can be polymerized in the same way not showing significant difference with styrene.<sup>51-53</sup> Many functional styrene derivatives have been prepared using TEMPO-mediated polymerization. In one example, 2, 5-bis [(4-methoxyphenyl)oxycarbonyl]styrene with a mesogenic side group was used to prepare block-copolymers with a liquid-crystal polymer segment.<sup>54,55</sup> In another example, 4-tert-butyl-4-(4-vinylstyryl)-trans-stilbene was incorporated into the PS side chain

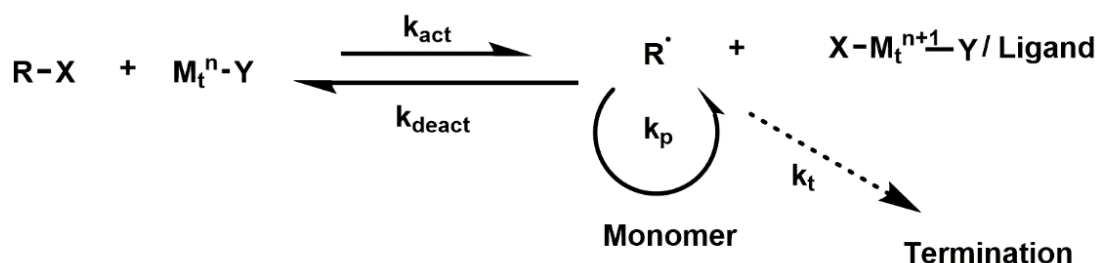
forming a luminescent polymer.<sup>56</sup> 4-(phenylethynyl)styrene and 4-(1-hexynyl)styrene were also polymerized mediated by TEMPO for preparing hybrid polymers or block-copolymers upon interaction with cobalt complexes.<sup>57</sup> Both the N-ethyl-2-vinylcarbazole and 9-(4-vinylbenzyl)-9H-carbazole were successfully polymerized using TEMPO and have been used in organic electronics due to the hole-transporting ability of carbazole group.<sup>58,59</sup> Water soluble monomers are of great importance in preparing amphiphilic block copolymers, with styrene sulfonate (SS) being one of the most important water soluble monomers. By carefully selecting mediators, polymerizing SS directly can be realized either in organic solvents such as ethylene glycol in the presence of TEMPO or in water mediated by 1,1,3,3-tetramethylisindolin-2-oxyl or 1,1,3,3-tetraethylisindolin-2-oxyl with an ionic group for example either a quaternary ammonium or a sulfonate substituent on the aromatic ring.<sup>60-62</sup>

Polymerization of methacrylates via NMP is not as easy as styrene and derivatives. The difficulties arise from two main factors: 1. The recombination reaction between typical nitroxides propagating radicals is slow due to steric hindrance effect from poly(methacrylate) structure. 2. The disproportionation side reactions occurs between poly(methacrylate) radicals and nitroxides.<sup>63-68</sup> Copolymerizing methacrylate monomers with a small amount of a well-behaved monomer such as styrene or acrylonitrile is the most successful approach for controlling polymerization with nitroxides.<sup>69-76</sup> A modeling study suggests that even a low concentration of styrene in NMP of MMA, favors the formation of styryl-alkoxyamine polymer endgroups, which

are more stable and less prone to side reactions compared with methacrylate endgroups.<sup>74</sup> Although, the resulting copolymers are perfectly well-suited for a wide range of applications, and sometimes even better than pure PMMA for other applications, controlling the polymerization of MMA homopolymer via NMP still suffers some difficulties. Developing new nitroxides to minimize the difficulties with NMP of MMA is one way to overcome the difficulties. For example, aryl nitroxides have been proven to be suitable in a moderate controlled polymerization of MMA, even though the conversion is relatively low and the polymerization of styrene cannot be controlled effectively.<sup>70,77,78</sup> Delocalization of the unpaired electron through the aromatic system, which slows recombination of the nitroxide with the propagating radical and the disproportionation side reaction, is the main advantage in the polymerization of methacrylates mediated by aryl nitroxides. Further investigations on related nitroxides in the homopolymerization of methacrylates via NMP are still in need.

#### 1.1.3.2. Atom transfer radical polymerization (ATRP)

The key step of ATRP is to increase of chain lifetime by controlling the equilibrium of the reversible reaction between the propagating radical and dormant species. (**Scheme 1.4**)



**Scheme 1.4.** The mechanism of ATRP.

This equilibrium is mediated by the activator and deactivator forms of catalysts, Cu (I)

$L^+$  and  $X-Cu(II)L^+$ , respectively, in which  $L$  represents a nitrogen-based polydentate ligand. The requirement for the activator  $Cu(I)L^+$  is to be sufficiently active to cleave the  $C-X$  bond in the (macro)alkyl halide initiator, while the  $X-Cu(II)L^+$  deactivator complex must sufficiently trap propagating radicals to generate the  $P_n-X$  dormant species. In the conventional ATRP, the rate of polymerization is described by Equation (1).

$$R_p = \frac{k_p K_{ATRP} [M][RX][Cu^I L_n]}{[Cu^{II} L_n]} \quad (1)$$

Where,  $R_p$  is rate of polymerization,  $k_p$  represent the rate constant of propagation,  $K_{ATRP}$  is the ATRP equilibrium constant. This equation suggests that the rate of polymerization is correlated with the concentration of the involved reagents as well as with the values of the propagation rate constant and ATRP equilibrium constant, which are usually determined by the structure of alkyl halide/monomer and catalyst. Thus, for a given catalyst/alkyl halide system,  $K_{ATRP}$  can be quantified and act as an excellent measure of the catalyst's true activity.<sup>79,80</sup>  $K_{ATRP}$  is the ratio between  $k_{act}$ <sup>81</sup> and  $k_{deact}$ <sup>79,80</sup> so that it can be influenced by many factors including the nature of the ligand, monomer (alkyl halide), as well as reaction conditions (solvent, temperature, pressure).<sup>82</sup> The relationship between polydispersity of the polymer prepared via ATRP and the concentration of initiator ( $RX$ ), deactivator ( $X-Cu(II)L^+$ ),  $k_p$  and  $k_{deact}$ , and monomer conversion ( $p$ ) in the absence of chain termination and transfer reactions is defined by Equation (2).<sup>83,84</sup>

$$\frac{M_w}{M_n} = 1 + \left( \frac{k_p ([RX]_0 - [RX])}{k_{deact} [X-Cu^{II} L]} \right) \left( \frac{2}{p} - 1 \right) \quad (2)$$

To achieve a narrow molecular weight distribution for the same monomer, a catalyst with a higher rate in deactivating the growing chains should be used. Increasing the concentration of deactivator or targeting higher molecular weights are alternative ways to decrease the polydispersity.

#### 1.1.3.2.1. Initiators

The main roles of the initiator is to generate radicals and to determine the number of growing polymer chains. If there is no radical transfer and termination and the initiation rate is high, then the number of growing chains is constant and is equal to the number of the initial initiator molecules. The relationship between theoretical molecular weight or degree of polymerization (DP) and the initial concentration of the initiator can be determined by Equation 3.

$$DP = \frac{[M]_0}{[I]_0} \times \text{Monomer conversion} \quad (3)$$

Here,  $[M]_0$  and  $[I]_0$  are the initial concentration of monomer and initiator, respectively.

In ATRP, alkyl halides (RX) are typically used as the initiator and the rate of the polymerization is first order with respect to the concentration of RX. The basic requisite of the halide group is the rapid and selective migration between the growing chain and the transition-metal complex. Bromides and chlorides have been proved to be the best options for controlling the molecular weight. Iodine can be used to initiate both the polymerization of acrylates via copper-mediated ATRP and styrene using ruthenium and rhenium-based catalyst systems.<sup>85,86</sup> Fluorine is unable to induce polymerization due to the high resistance of C-F bond to homolytic cleavage. Some other compounds which are similiar to halides, for example, thiocyanates and thiocarbamates, have also

been used to initiate the polymerization of acrylates and styrenes.<sup>87</sup> Initiation should be fast and quantitative with a good initiator. Alkyl halides with single activating substituents on the R-C, such as carbonyl, aryl and allyl groups, or polyhalogenated compounds (e.g.  $\text{CHCl}_3$  and  $\text{CCl}_4$ ) or compounds with a weak R-X bond, for example N-X, S-X or O-X can all potentially be used as ATRP initiators.

#### 1.1.3.2.2. Monomers

A number of monomers has successfully been polymerized via ATRP including styrenes, (meth)acrylates, (meth)acrylamides, dienes, acrylonitrile and other monomers.<sup>88,89</sup> Usually those monomers which contain substituents that can stabilize the propagating radicals are compatible with ATRP. The radical propagation rate, however, is usually different due to the intrinsic difference in the structure. Thus, for a specific monomer, the concentration of propagating radicals and the rate of radical deactivation need to be adjusted to maintain a good polymerization control. However, the overall equilibrium does not only depend on the nature of the radical (monomer) and the dormant species, but also on the amount and reactivity of the transition-metal catalyst.

#### 1.1.3.2.3. Catalysts

One key component for ATRP is the catalyst since it determines the position of the ATRP equilibrium and the dynamics of the exchange between the dormant and active species. Several criteria should be considered to find a good catalyst. First, the metal center must have two or more readily accessible oxidation states with one electron difference. Second, the affinity between the metal center and the ligand should be in an appropriate range. Third, the coordination sphere around the metal should be

expandable upon oxidation to selectively accommodate a (pseudo)-halogen. Fourth, the complex coefficient between the ligand and catalyst should be high enough. Eventually, the ATRP equilibrium should be fit to specific systems well.<sup>90</sup>

#### 1.1.3.2.4. Ligands

Ligands may be even more important, to some extent, than metal catalyst, since they can fine-tune selectivity and prohibit the preferred two electron transfer and force the reaction into a single electron transfer process such as in the oxidation and reduction of Ni or Pd complexes. Moreover, they control the solubilities of the metal catalyst in the reaction mixture and ensure stability of the complexes in ATRP solution.<sup>91</sup>

The use of an appropriate ligand enables the polymerization of acidic monomers and monomers which can strongly complex transition metals. An appropriate ligand can shift the equilibrium between the alkyl halide and the transition metal towards the dormant species. This equilibrium will render most of the growing polymer chains dormant and produce a low radical concentration. As a result, the contribution of radical termination reactions to the overall polymerization is minimized. A parameter partition coefficients and their dependence on temperature is always used to determine the efficiency of the catalyst for ATRP. Finally, ligands can help in facilitating the removal and recycling of the catalyst. As a result, this enables the immobilization of the catalyst and also distribution between two phases.<sup>82</sup>

#### 1.1.3.3. Reversible Addition–Fragmentation Chain-Transfer Polymerization (RAFT)

The sequence of addition–fragmentation equilibrium (**Scheme 1.5**) in the RAFT



As is shown in **Scheme 1.5**, the intermediate radical concentration generated by RAFT agent is short-lived and is not lower than in a conventional polymerization process. Thus, around 5 to 10% nonfunctional materials are generated via bimolecular termination events. The controllability of RAFT over molecular weight are imparted when the targeted molecular weight is significantly lower than that, which would be formed under the same conditions but in the absence of the RAFT agent, such that the number of polymer molecules with RAFT agent-derived ends far exceeds the number formed as a consequence of termination.<sup>92-95</sup>

#### 1.1.3.3.1. RAFT Agents

A wide variety of RAFT agents including trithiocarbonate, xanthate and dithiocarbamate has been reported.<sup>31,96</sup> The efficiency of the RAFT agent highly depends on the properties of the free radical leaving group R and the group X which is able to activate or deactivate the thiocarbonyl double bond of the RAFT agent and to tune the stability of the intermediate radicals. There are four criteria for a selection of a RAFT agent for effective polymerization.<sup>97</sup> First, there should be a highly reactive C=S bond in the initial and the polymer RAFT agent. Second, the intermediate radical should fragment rapidly without any side reactions. Third, the intermediate radical should go in favor of the new radical rather than the reverse addition reaction. Fourth, the rate of the initiation rate of the new radical should be higher than the rate of propagation. The equilibrium constants of the RAFT agents associated with radical addition to the thiocarbonylthio compound are the most important parameter in the kinetics study. Since the rates of addition are typically high, a high equilibrium constant generally

implies a low fragmentation rate for the radical adduct and an increased possibility to prevent or decrease side reactions involving this species. However, the values of  $K$  do not provide sufficient information in order to predict the ability of a RAFT agent to control a specific polymerization. To achieve a good controllability, four equilibrium constants are needed to be taken into account:

- $K_P (= k_{addP}/k_{-addP})$  associated with the main equilibrium.
- $K (= k_{add}/k_{-add})$  and  $K_\beta (= k_{-\beta}/k_\beta)$  associated with the pre-equilibrium.
- $K_R (= k_{addR}/k_{-addR})$  associated with the reaction of the expelled radical with the initial RAFT agent

There are also a further reactions that need to be considered involving initiator radical derived RAFT agents. In principle, RAFT agents of differing reactivity might be derived from each radical species present.

#### 1.1.4. The Comparison of NMP, ATRP and RAFT Processes

The common ground of all CRP techniques is to create a dynamic equilibrium between propagating radicals and various types of dormant species. Radicals can propagate and exchange with dormant species and can also terminate and participate in many other organic reactions including transfer, rearrangement and fragmentation.<sup>98</sup> Thus, the chemoselectivity, regioselectivity and stereoselectivity in CRP are similar to conventional radical polymerization. The ability of CRP techniques to control molecular weights and polydispersities as well as to prepare well-defined molecular architectures comes both from fast initiation and from limitation of the concentration of propagating radicals so that other reactions are negligible.

Each CRP technique its advantages and limitations with respect to the other techniques. For example, the advantage of NMP over ATRP is that NMP is applicable to purely organic system without using metal compounds. However, the limitations are also obvious, in particular the need of relatively expensive mediators, the limited control over the polymerization of disubstituted alkenes such as methacrylates and the difficult introduction of end functionality to the polymer. Moreover, other than ATRP with a wide temperature window, relatively high temperatures are generally required in NMP. There are a number of advantages of ATRP, which makes it a versatile technique both in fundamental research and in industry. These advantages include the use of small amounts of transition metal complexes; commercial availability of various initiators including multifunctional and hybrid systems; applicability to almost all monomers; simplicity for end-functionalization; the absence of Trommsdorf effect; a wide range of temperature windows and the ability to polymerize block copolymers in any order (with halogen exchange), which is not possible for other CRP methods. The limitation of ATRP is that the transition metal complex must often be removed from the product. Similar to ATRP, the advantage of RAFT is also applicable to a wide range of monomers. It also allows a smallest perturbation to conventional radical polymerization and is often mediated by purely organic reagent. However, unlike NMP and ATRP, the rate of cross-termination with newly generated short chains is higher than long chains which may result in an increased number of polymer chains. Some other limitations are also existed including the lack of commercially available transfer agents as well as their limited chemical stability, the removal of dithioester and some other end groups after the

polymerization due to their color, toxicity, and potential odor, and the difficulty associated with end-functionalization.

## **2. Swelling-Induced Chain Stretching Enhances Hydrolytic Degrafting of Hydrophobic Polymer Brushes in Organic Media**

### **2.1. Introduction**

Surface-initiated polymerization (SIP) reactions provide access to chain end-tethered polymer assemblies (“polymer brushes”) in which neighboring polymer chains are anchored at intermolecular distances that enforce a stretched chain conformation.<sup>99-114</sup>

The extended chain conformation is an important contributor to e.g. the nonbiofouling<sup>115-125</sup> and lubrication properties<sup>126-136</sup> of hydrophilic polymer brushes prepared by SIP.

Chain stretching in densely grafted polymer brushes also results in a tension that acts on the bonds, which anchor the polymer chains to the underlying substrate. Exposure to a good solvent and swelling of the polymer brush film can amplify this tension. For a number of hydrophilic polymer brushes grown via surface-initiated atom transfer radical polymerization (SI-ATRP) from silicon oxide substrates modified with organosilane functionalized ester or amide based ATRP initiators, incubation in aqueous media results in detachment (degrafting) of the surface-anchored polymer chains.<sup>117,137-</sup>

<sup>144</sup> The degrafting of hydrophilic polymer brushes from silicon oxide surfaces in aqueous media has been attributed to a swelling-induced stretching of the surface-anchored polymer chains and a concomitant amplification of the tension that acts on the siloxane and ester/amide bonds that anchor the chains to the surface.<sup>145,146</sup> The increased tension at the polymer brush-substrate interface has been postulated to

facilitate hydrolysis of the anchoring siloxane and ester/amide bonds resulting in the observed degrafting of the surface-attached polymer chains.

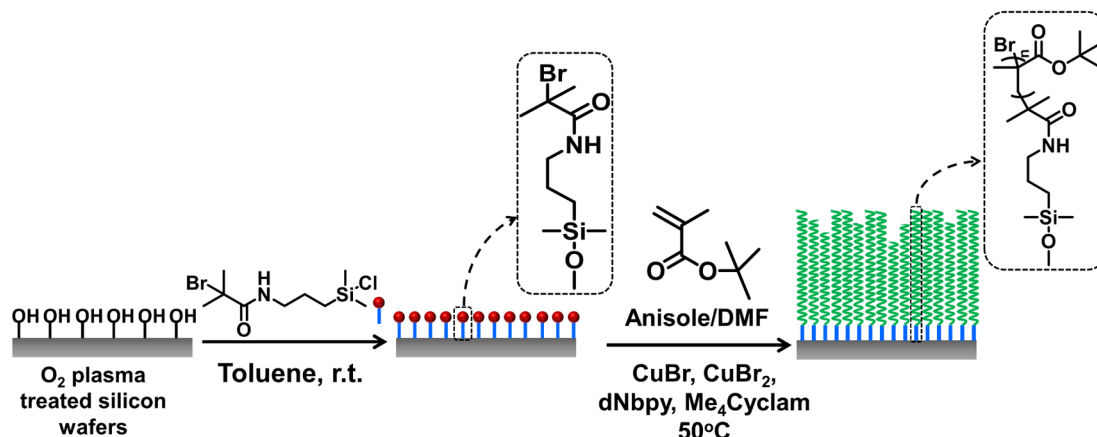
The application of tension on the anchoring points of chain end-tethered polymers by swelling-induced chain stretching represents an alternative method to apply force at the molecular level. Other strategies that have been applied to mechanically activate polymers include the use of ultrasound irradiation<sup>147</sup> and flow fields.<sup>148,149</sup> These methods, however, generate relative strong forces ( $\sim$  nN) that are sufficient to induce scission of carbon-carbon bonds in a polymer backbone. Carbon – carbon bond scission has also been observed upon adsorption of bottlebrush macromolecules on surfaces.<sup>150,151</sup> Swelling-induced stretching of chain end-tethered polymers, in contrast, produces weak forces that do not allow direct scission of covalent bonds but is rather believed to mechanically catalyze reactions, such as for example the hydrolysis of the ester/amide and siloxane bonds that typically anchor polymer brushes grown via SI-ATRP.

While it has been proposed that swelling of a polymer brush and the concomitant stretching of the surface-anchored polymer chains enhances hydrolytic cleavage of bonds at the brush-substrate interface, there is so far no experimental data that show a correlation between the swelling properties of a polymer brush and, for example, the initial rate constant of the degrafting reaction. This manuscript studies the swelling properties and degrafting behavior of poly(tert-butyl methacrylate) (PtBMA) brushes (**Scheme 2.1**) in organic solvents in the presence of small quantities of water. The use of a hydrophobic brush that swells in a water-miscible organic solvent allows to

decouple swelling of the brush and hydrolytic cleavage of the bond(s) at the brush-substrate interface. With hydrophilic brushes in aqueous media this is not possible since in these conditions water simultaneously acts as the solvent that swells the brush and as the reagent that is involved in hydrolytic cleavage. PtBMA brushes can undergo moderate to strong swelling in a range of water-miscible organic solvents. This is attractive as it allows to modulate swelling of the PtBMA brushes, and thus stretching of the surface-grafted polymer chains, at a constant concentration of reagent responsible for the degrafting reaction.

Using the PtBMA brushes as a model system, this manuscript will address several fundamental, open questions related to the degrafting of polymer brushes from silicon oxide substrates. The first question is whether hydrolytic degrafting of polymer brushes occurs exclusively in aqueous media or whether this phenomenon can also be observed in organic media? If degrafting is driven by the increase in tension at the brush-substrate interface as a consequence of chain stretching that results from swelling of the brush, then, in the presence of an appropriate reagent, this process may also occur in organic media (and may also be extended to other cleavage reactions than hydrolysis). Much of the work on the degrafting of polymer brushes points towards swelling of the brush film as the driving force for tension amplification at the brush-substrate interface and concomitant cleavage of the surface-anchored polymer chains. What is not known and has not been demonstrated yet is whether the rate of degrafting of a polymer brush correlates with its swelling behavior and whether the rate of degrafting can be modulated by varying the degree of swelling of the brush. The PtBMA brushes used in

this study are an ideal model system to investigate these questions.



**Scheme 2.1.** Preparation of PtBMA brushes via SI-ATRP.

## 2.2. Experimental section

### 2.2.1. Materials

All chemicals were used as received unless described otherwise. Copper(I)bromide (99.995+%), copper (II)bromide (99.999 %), 2-bromo-2-methylpropionyl bromide, allylamine (98%), trimethylacetyl chloride (99%), ethanol (99.8%) and aluminum oxide were purchased from Sigma-Aldrich. Anisole (99%) and chlorodimethylsilane (98%) were purchased from ABCR. Pt/C (10% Pt) was purchased from Alfa-Aesar. Tert-butyl methacrylate (98%) was purchased from Sigma-Aldrich. Prior to polymerization, the monomer was passed over a basic aluminum oxide column to remove the inhibitor. Sulfuric acid, acetone (99.5%), hydrofluoric acid (38%-40%) and triethylamine (distilled over KOH before use) were purchased from Merck. Dichloromethane, acetone (HPLC grade) and acetone (extra dry) were purchased from Fisher chemicals. The water content in the dry acetone was determined to 4500 ppm, or 0.45 vol%. 4,4'-Dinonyl-2,2'-bipyridyl (dnbpy) and 1,4,8,11-tetramethyl-1,4,8,11-

tetraazacyclotetradecane (Me<sub>4</sub>cyclam) were purchased from TCI. Tetrahydrofuran (THF), dimethylformamide (DMF) and toluene were purified and dried by a solvent-purification system (PureSolv). The water content in the dried DMF was determined to 65 ppm. Toluene with 330 ppm water was prepared by mixing water and toluene (volume ratio 1/50) and shaking overnight at room temperature. Then, the toluene part was used for the degrafting experiments. Deionized water was obtained from a Millipore Direct-Q 5 ultrapure water system. Degrafting experiments were performed on polymer brushes that were grown from 0.8 cm × 1 cm sized rectangular silicon wafers. To determine the molecular weight of the surface grafted polymer before and after degrafting, polymer brushes grown from 2.5 cm × 7 cm sized rectangular silicon wafers were used. All the silicon wafers used in this study are covered by a ~ 2 nm silicon oxide layer.

### **2.2.2. Methods**

X-ray photoelectron spectroscopy (XPS) was carried out using an Axis Ultra instrument from Kratos Analytical equipped with a conventional hemispheric analyzer. The X-ray source employed was a monochromatic Al K $\alpha$  (1486.6 eV) source operated at 100 W and 10<sup>-9</sup> mbar. Static water contact angles (WCA) were determined using a DataPhysics OCA 35 contact angle measurement instrument at ambient conditions. Surfaces were cleaned with a Femto O<sub>2</sub> Plasma system (200 W, Diener Electronic). The water content in organic solvents was measured with a Karl Fischer coulometric titrator (Mettler ToLeDo DL 32). <sup>1</sup>H NMR spectra were recorded on a Bruker AVANCE-400 Ultra Shield spectrometer.

**Ellipsometry (Figure 2.1A-2.1C, S2.3).** A Sopra GES 5E spectroscopic ellipsometer (Sopra SA, France) was used to determine dry film thicknesses. Measurements were recorded at 15 nm intervals from 305 nm to 800 nm at an angle of incidence of 70° under ambient conditions. The ellipsometry data were analyzed using the WINELLI\_II Software (Sopra SA, France) and the calculation method was based on a four-layer silicon/silicon oxide/polymer brush/air model, assuming the polymer brush to be isotropic and homogeneous. The refractive index ( $n$ ) of the PtBMA layer is described by the Cauchy approximation ( $n = A_n + B_n/\lambda^2$ ), where  $A_n = 1.463$ ,  $B_n = -4.3681 \times 10^{-5} \mu\text{m}^2$  and  $\lambda$  is the wavelength of the incident light. Measurements were conducted at three different points on each substrate. All reported dry film thicknesses represent the average  $\pm$  standard deviation (SD) of five substrates.

**Ellipsometry.** The thicknesses of swollen brushes were determined using a SemiLAB (SE2000) ellipsometer with a liquid cell. The swelling ratio of polymer brushes on silicon substrates was determined by calculating the ratio of the swollen film thickness to the dry film thickness in air. Samples were placed on the sample stage and the reflected laser was properly aligned to the detector through the microspot placed on the detection arm. Dry film thicknesses were calculated based on a four-layer silicon/silicon oxide/polymer brush/air model, assuming the polymer brush to be isotropic and homogeneous. To determine the swollen film thicknesses, a gradient model was set up assuming that the polymer brush consists of four layers with different brush-solvent volume ratio.

**AFM (Figure S2.5).** Atomic force microscopy (AFM) was performed on a Veeco CP-II instrument (Digital Instruments, Santa Barbara, CA) controller in contact mode using an MPP-11123-10 (Veeco) cantilever to measure swollen brush thicknesses.

**Gel permeation chromatography (GPC).** GPC analysis was performed using an Agilent 1260 infinity system equipped with a Varian 390-LC refractive index detector, two PLgel 5  $\mu$ m Mixed C (Agilent) columns and a PLgel guard column. The mobile phase was THF (HPLC grade) at a flow of 1.0 mL/min at 40 °C. Samples were filtered prior to analysis and results were calibrated with linear PMMA standards (2200-201000 g/mol, Polymer Standard Service Mainz).

### **2.2.3. Procedures**

Synthesis of the ATRP initiator and functionalization of silicon oxide substrates with the ATRP initiator. The preparation of the ATRP initiator, 2-bromo-2-methyl-N-{3-[chloro(dimethyl)silyl]-propyl}propanamide and the functionalization of silicon oxide surfaces with this initiator were performed following a published protocol.<sup>146</sup> The ATRP inactive, dummy initiator, N-(3-(chlorodimethylsilyl)propyl)pivalamide was synthesized via the same method using trimethylacetyl chloride instead of  $\alpha$ -bromoisobutyryl bromide. Silicon surfaces with different grafting densities were prepared by placing the substrates in anhydrous toluene solutions with 10 mM of the chlorosilanes that contained 20, 50 or 100 mol% of the ATRP active compound. <sup>1</sup>H-NMR spectra of the ATRP initiator and dummy chlorosilane are shown in **Figure S2.9** and **Figure S2.10**. **Figure S2.11** and **Figure S2.12** present the results of the water

contact angle analysis and XPS characterization of the ATRP initiator modified substrates.

Surface-initiated polymerization of tBMA. PtBMA brushes were prepared according to a previously published protocol. Instead of tert-butyl acrylate at a concentration of  $[M] = 3.5$  M, tert-butyl methacrylate ( $[M] = 3.1$  M) was used.<sup>152</sup>

Patterned Polymer Brushes. Patterned polymer brushes were prepared via surface-initiated polymerization from micropatterned substrates, which were obtained by UV irradiation of initiator-modified silicon wafers using a TEM grid as a photomask.<sup>153</sup> A Hamamatsu (Lightningcure L8858, 200 W, wavelength = 360 nm) UV lamp was used as the light source and substrates were irradiated for 8 min. at a distance of 6 cm from the lamp.

Degrafting experiments. Degrafting experiments were performed at room temperature by incubating polymer brush coated substrates in the appropriate medium. The following media have been investigated: toluene, THF + 11 ppm water, toluene + 330 ppm water, THF + 5 vol% water, THF + 20 vol% water, DMF, acetone, DMF + 5 vol% water, acetone + 5 vol% water and pure water. At defined times, the substrates were removed from the medium, washed extensively with ethanol and dried under a flow of N<sub>2</sub>. The degrafting of the polymer brushes was assessed by monitoring the dry film thickness as a function of incubation time.

Cleaving PtBMA brushes from silicon oxide substrates: 3 pieces of PtBMA brush grafted silicon oxide substrates (2.5 × 7 cm) were incubated in a Teflon beaker containing THF (28.5 mL) and 40% hydrofluoric acid (1.5 mL). The mixture was

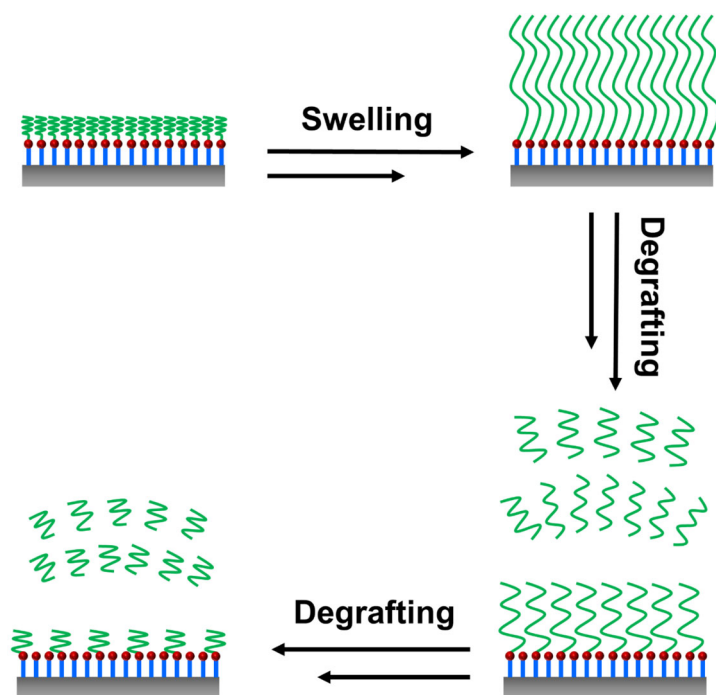
vigorously stirred at 240 rpm for 2 h. After removing the silicon oxide substrates, the content of the Teflon beaker was allowed to evaporate to dryness overnight under ambient conditions in the fume hood. The residual polymer in the beaker was then redissolved in 300  $\mu$ L THF and subjected to GPC analysis. To determine the molecular weight of the remaining surface-tethered polymer after exposure to THF + 5 vol% water for 4 h, cleavage was performed via the same method using 4 pieces of PtBMA brush grafted silicon oxide substrates ( $2.5 \times 7$  cm) instead of 3. (**Figure S2.3**).

### 2.3. Results and Discussion

PtBMA brushes were grown by SI-ATRP of tert-butyl methacrylate (tBMA) from 2-bromo-2-methyl-N-{3-[chloro(dimethyl)silyl]-propyl}propanamide modified silicon oxide substrates as shown in **Scheme 2.1** following a modified literature procedure.<sup>152</sup> Degrafting of the end tethered PtBMA chains via hydrolysis of the siloxane or amide bonds that anchor the polymer to the substrate will result in a gradual decrease in the grafting density of the polymer brush (**Scheme 2.2**). This will lead to a continuous decrease in the dry film thickness of the PtBMA brushes as the degrafting process proceeds. Degrafting is a process that is driven by the entropy gain associated with the cleavage and release of conformationally restricted, surface-tethered polymer chains. The bond tension in chain end tethered, swollen brushes scales with the inverse of the grafting density and has been estimated to 1-10 pN in a dense brush to 0.1-1.0 pN in the mushroom regime.<sup>154</sup> While these tensions are not sufficient to allow direct scission of covalent bonds, the degrafting of polymer brushes observed by us and others<sup>117,137-144</sup> suggests, however, that these may facilitate hydrolytic cleavage of siloxane and/or

amide bonds at the polymer brush – substrate interface. As degrafting progresses, the grafting density, and thus the tension at the interface, continuously decreases. Degrafting proceeds to a limiting, non-zero film thickness where this tension is believed to be reduced to a value that is no longer sufficient to facilitate hydrolytic cleavage.<sup>137</sup>

138



**Scheme 2.2.** Schematic illustration of the swelling and subsequent degrafting of a PtBMA brush, resulting in a gradual decrease in grafting density and dry film thickness.

Ellipsometry was used to characterize the swelling behavior of the PtBMA brushes and to monitor the degrafting process. To describe the swelling properties of the PtBMA brushes in the different media, the swelling ratios were determined, which are defined as the ratio of the swollen and dry film thickness of the initial polymer brush. Degrafting was monitored by determining the dry film thickness of the PtBMA brushes at regular time intervals.

In a first set of experiments, PtBMA brushes with an initial dry film thickness of 160 nm were incubated in THF, toluene and water as well as various THF and toluene-water mixtures. The dry film thickness of the samples was monitored for a period of 7 days. Exposure of the PtBMA brushes to dry toluene, toluene + 330 ppm water, THF + 11 ppm water as well as pure water did not reveal any significant changes in dry film thickness (**Figure 2.1A**). Apparently, although THF and toluene are good solvents for PtBMA and will swell the brush, the water concentration in these media is too low to facilitate hydrolytic cleavage of the bonds at the brush-substrate interface. Similarly, also no changes in dry film thickness were observed when PtBMA brushes were incubated in dry DMF or dry acetone (**Figure S2.1**). Exposure to water was also not found to result in any changes in dry film thickness. Water is a non-solvent for PtBMA. As a consequence, the PtBMA brush does not swell, which limits access of water to the brush-substrate interface and no changes in dry film thickness are observed either. Increasing the amount of water in THF to 5, respectively, 20 vol%, however, results in rapid degrafting (**Figure 2.1B**). This illustrates the presence of water as a necessary requirement for degrafting to occur.

The kinetics of diffusion of the cleaved chains through the surface-grafted polymer film do not seem to influence or limit the degrafting process. This is illustrated in Figure S2, which compares the dry film thickness of a PtBMA brush before and after incubation in THF + 5 vol% water for 4 hours. The dry thickness of the PtBMA film that was taken from the degrafting medium after 4 hours was determined both without any further washing steps as well as after washing the brush with various solvents. The results in

**Figure S2** reveal no significant differences in the dry film thickness that was determined directly after withdrawing the PtBMA film from the incubation medium without further washing and the film thicknesses that were measured after subjecting the brush film to a series of subsequent washing steps using a number of solvents. This indicates that cleavage and subsequent escape of the detached polymer chains is not influenced or limited by diffusion barriers imposed by the remaining, surface-anchored polymer chains.

Gel permeation chromatography (GPC) analysis was used to monitor changes in the molecular weight of the surface-attached polymer chains as degrafting proceeds. Polymer molecular weights were determined by HF-mediated cleavage of the surface-tethered PtBMA, both at  $t = 0$  (before degrafting) as well as after incubation of the brush in THF + 5 vol% water for 4 hours. For a PtBMA brush with an initial dry film thickness of 165 nm, the initial number average molecular weight ( $t = 0$ ) was 248 kDa. After incubation of this brush in THF + 5 vol% water, the molecular weight of the residual, surface-tethered PtBMA was determined to 231 kDa (**Figure S2.3**). This suggests that it is the higher molecular weight fraction that degrafts first, which is in agreement with observations reported in other studies.<sup>144</sup>

As illustrated in **Figure 2.1B**, degrafting is fastest in THF + 5 vol% water and seems to slow down upon increasing the amount of water to 20 vol%. Interestingly, the results in **Figure 2.1B** correlate with the swelling properties of the PtBMA brushes in THF-water mixtures (**Figure 2.1D**). Whereas the swelling ratio of a 160 nm thick PtBMA brush in THF + 5 vol% water is 3.9 (and similar to the swelling ratio of the brush in dry

THF), increasing the water content to 20 vol% is accompanied by a reduction in the swelling ratio to 2.6. The lower swelling ratio of the PtBMA brush in THF + 20 vol% water is consistent with a lower tension at the brush-substrate interface, which concurs with the lower rate of degrafting that is observed in THF + 20 vol% water as compared to THF + 5 vol% water. **Figure 2.1C** shows the evolution of dry film thickness as a function of time (over a period of 2 days) upon incubation of PtBMA brushes with initial dry film thicknesses of 50, 80 and 160 nm in THF + 5 vol% water. Figure S4 shows the change in dry film thicknesses of these brushes over a period of 7 days. The initial swelling ratios of the PtBMA brushes are also included in **Figure 2.1D**. The swelling ratios of PtBMA brushes of different film thicknesses were also determined by AFM analysis of micropatterned samples.<sup>145</sup> The results of these experiments are included in Figure S5 and are in good agreement with the swelling ratios reported in **Figure 2.1D**.

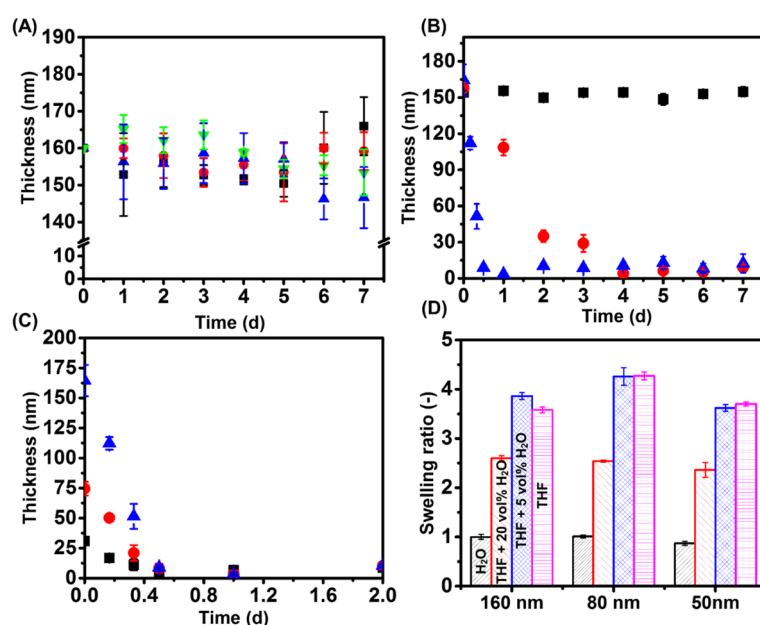


**Figure 2.1.** Ellipsometric dry thickness of PtBMA brushes as a function of incubation time upon exposure to: (A) Toluene (■), THF + 11 ppm water (●), Toluene + 330 ppm

water (▲), pure water (▼); (B) THF + 11 ppm water (■), THF + 5 vol% water (▲), THF + 20 vol% water (●); (C) Evolution of the dry film thickness of PtBMA brushes with initial dry film thicknesses of 160 nm (▲), 80 nm (●) and 50 nm (■) upon incubation in THF + 5 vol% water; (D) Swelling ratios measured by ellipsometry of PtBMA brushes of initial dry film thicknesses of 50, 80 and 160 nm in water (black), THF + 20 vol% water (red), THF + 5 vol% water (blue) and THF (pink).

To quantitatively describe the degrafting of the PtBMA brushes and evaluate the influence of the composition of the solvent and the initial dry film thickness, **Figure 2.1B** and **Figure 2.1C** were replotted as  $\ln(d)$  versus time (Supporting information Figure S6). The  $\ln(d)$  versus time plots reveal 2 linear regimes, suggesting that the degrafting process follows a pseudo-first order kinetics. The slope of the first linear regime was taken as the apparent, initial rate constant ( $k_{ini}$ ) of the degrafting process. **Figure 2.2A** shows  $k_{ini}$  and the initial swelling ratio for a PtBMA brush with an initial dry film thickness of 160 nm in THF, THF + 5 vol% water and THF + 20 vol% water. In **Figure 2.2B**, the  $k_{ini}$  and initial swelling ratios for PtBMA brushes with initial dry film thicknesses of 50, 80 and 160 nm in THF + 5 vol% water are summarized. The results in **Figure 2.2A** suggest a correlation between the swelling ratio, i.e. chain stretching and tension at the bonds at the brush-substrate interface and the  $k_{ini}$ . Upon decreasing the amount of water in THF from 20 vol% to 5 vol%, the initial swelling ratio increases from 2.6 to 3.9. This increase in swelling ratio is accompanied by an increase in  $k_{ini}$  from 0.7 d<sup>-1</sup> to 2.9 d<sup>-1</sup>. As indicated in **Figure 2.2B**, the initial swelling

ratio of PtBMA brushes in THF + 5 vol% water did not significantly change upon varying the dry film thickness from 50 to 160 nm. Consistent with this observation, the  $k_{ini}$  values measured for PtBMA brushes in THF + 5 vol% water were also not found to depend on the initial dry film thickness.

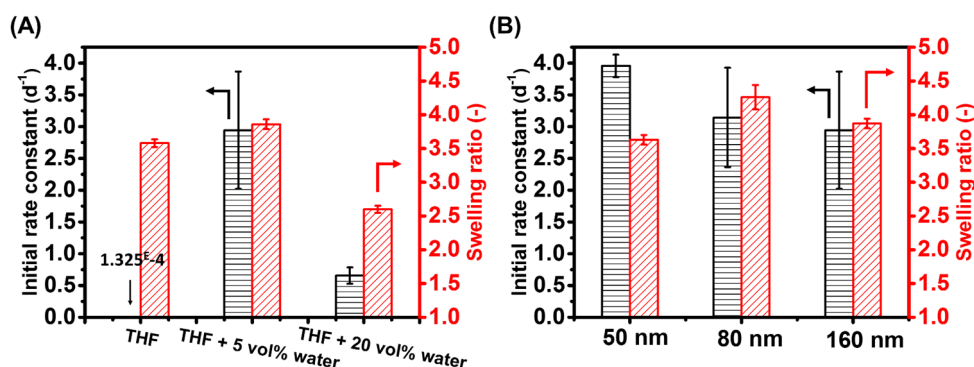


**Figure 2.2.** (A) Initial rate constant of degrafting (left) and initial swelling ratio (right) for PtBMA brushes with an initial dry film thickness of 160 nm upon incubation in THF, THF + 5 vol% water and THF + 20 vol% water; (B) Initial rate constant of degrafting (left) and initial swelling ratio (right) determined for PtBMA brushes with initial dry film thickness of 50, 80 and 160 nm in THF + 5 vol% water.

The results presented in **Figure 2.2** provide a first indication that the  $k_{ini}$ , and thus the putative tension at the brush-substrate interface, correlates with the swelling ratio of the polymer brush. To vary the swelling of the PtBMA brushes in these experiments, the relative amounts of THF and water were varied. To vary the swelling of the PtBMA brush while keeping the water concentration constant, a second series of degrafting experiments with 3 different water-miscible organic solvents, viz DMF, acetone and THF was carried out. For these experiments, PtBMA brush samples with an initial dry film thickness of ~160 nm were used, which were incubated in mixtures of the different

organic solvents that contained 5 vol% water. **Figure 2.3A** shows the evolution of the dry film thickness of the brushes as a function of time upon incubation in the different media. These data were analyzed in the same way as discussed above to determine the  $k_{ini}$  for the degrafting of the PtBMA brushes (Supporting information **Figure S2.7**). **Figure 2.3B** presents  $k_{ini}$  and the initial swelling ratios of the PtBMA brushes in the 3 different media. Upon changing the incubation medium from DMF + 5 vol% water to acetone + 5 vol% water to THF + 5 vol% water,  $k_{ini}$  increased from 0.003 d<sup>-1</sup> to 0.226 d<sup>-1</sup> to 2.944 d<sup>-1</sup>. Swelling of the PtBMA brushes in these media follows the same trend. The swelling ratios of the PtBMA brushes increased from 1.4 in DMF + 5 vol% water to 2.3 in acetone + 5 vol% water to 3.9 in THF + 5 vol% water. These results corroborate those shown in Figure 2 and indicate that  $k_{ini}$ , and thus the putative tension that acts on the bonds at the brush-silicon oxide interface, correlates with the extent of swelling of the surface grafted polymers.

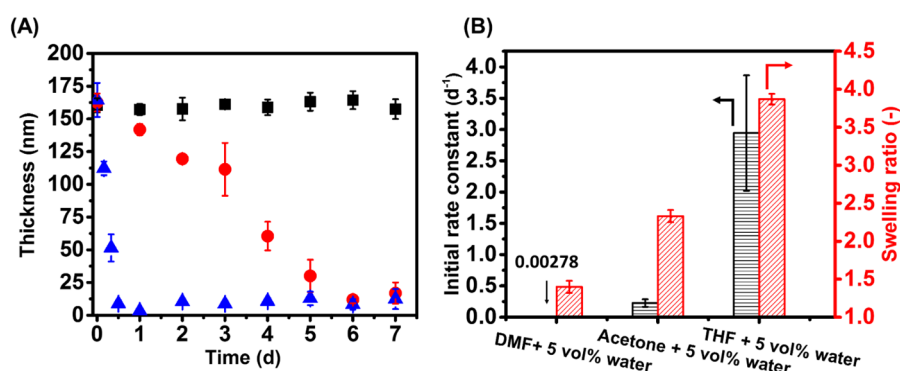


**Figure 2.3.** (A) Evolution of dry film thickness of a PtBMA brush with an initial thickness of 160 nm upon exposure to DMF + 5 vol% water (■), acetone + 5 vol% water (●) and THF + 5 vol% water (▲); (B) Initial rate constant of degrafting (left) and swelling ratio (right) determined for a PtBMA brush with an initial dry film thickness of 160 nm in DMF + 5 vol% water, THF + 5 vol% water and acetone + 5 vol% water.

In a final set of experiments, degrafting of PtBMA brushes with initial grafting densities of 100%, 50% and 20% was investigated. These brushes were prepared by SI-ATRP of tBMA from silicon oxide surfaces that were modified with mixtures of the ATRP active 2-bromo-2-methyl-N-{3-[chloro(dimethyl)silyl]-propyl}propanamide and the polymerization inactive “dummy” N-(3-(chlorodimethylsilyl)propyl)pivalamide, which contained 100 mol%, 50 mol% or 20 mol% of the ATRP initiating organosilane. From these substrates, which present different ATRP initiator surface concentrations, PtBMA brushes were grown using a polymerization time of 0.5 h. For a silicon oxide substrate modified with 100 mol% of the ATRP active chlorosilane this results in a dry film thickness of 160 nm. Degrafting of this series of PtBMA brushes was studied in DMF, acetone and THF, all in the presence of 5 vol% water. The  $k_{ini}$ , which were obtained from the decrease in dry film thickness as a function of incubation time, are summarized in **Figure 2.4A** for brushes of different initial grafting densities and the different degrafting media (Figure S8 presents the corresponding  $\ln(d)$  versus time plots). **Figure 2.4B** compares the ratio of  $k_{ini}$  for degrafting in THF + 5 vol% water and acetone + 5 vol% water for PtBMA brushes of initial grafting densities of 20, 50 and 100%. Upon decreasing the grafting density from 100% to 50% to 20%, the ratio  $k_{ini,THF}/k_{ini,acetone}$  decreases from 13 to 9.6 to 1.6. The observed changes in  $k_{ini,THF}/k_{ini,acetone}$  are a strong indication that the differences in  $k_{ini}$  that are observed in DMF, acetone and THF are not (solely) due to solvent effects, but that chain stretching (and thus tension amplification), in particular at high grafting densities and in good

solvents, is a mechanochemical contributor that accelerates the degrafting process. The increases in  $k_{ini}$  and  $k_{ini,THF}/k_{ini,acetone}$  with increasing grafting density that are shown in **Figure 2.4** are also opposite to what would be expected if access and diffusion of water to the siloxane and amide bonds at the brush – substrate interface would be rate determining.

Results from model studies that have been published on the hydrolysis of tetramethoxysilane (TMOS) and of amides provide further indications for a mechanochemical contribution of swelling-induced chain stretching to the degrafting of polymer brushes grafted from silicon oxide. In experiments, which compared the hydrolysis of TMOS in various solvents, similar reaction rates were observed in a variety of polar, aprotic solvents.<sup>155</sup> Model studies that investigated the base and acid catalyzed hydrolysis of esters and amides have found that reaction rates increase with increasing dielectric constant of the solvent (for the three solvents used in the present study, the dielectric constant is lowest for THF and highest for DMF).<sup>156</sup>

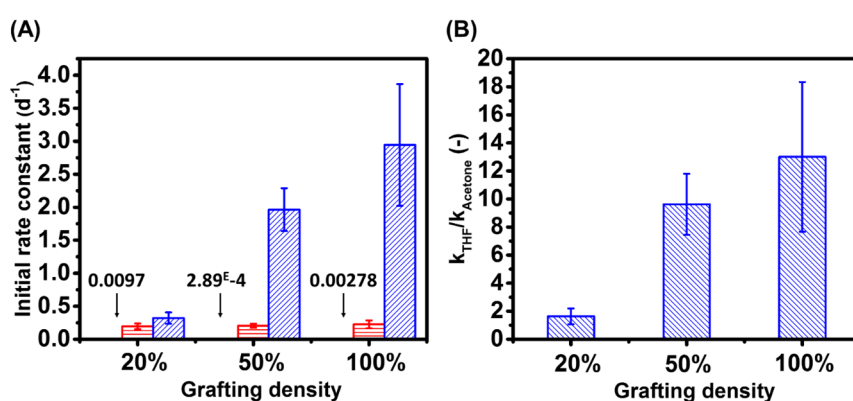


**Figure 2.4.** (A) Initial rate constants of degrafting determined for PtBMA brushes with initial grafting densities of 20%, 50% and 100% in DMF + 5 vol% water (black), acetone + 5 vol% (red) water and THF + 5 vol% water (blue) (as the corresponding  $k_{ini}$

values are very small, the data for DMF + 5 vol% water are not visible); (B) The ratio of  $k_{ini}$  for degrafting in THF + 5 vol% water and acetone + 5 vol% water for PtBMA brushes of initial grafting densities of 20, 50 and 100%.

## **2.4. Conclusions**

The aim of this study was to investigate the swelling-induced, degrafting of hydrophobic polymer brushes grafted by SI-ATRP from planar silicon oxide surfaces in nonaqueous media. The experiments presented here show that in the presence of the appropriate reagent (here: water) degrafting can also be observed for hydrophobic brushes in non-aqueous media. More importantly, the results indicate that degrafting can be modulated by changing the incubation medium and that  $k_{ini}$  of the degrafting process correlates with the swelling ratio of the polymer brush in the degrafting medium. The correlation between  $k_{ini}$  and the swelling ratio supports the hypothesis that the degrafting of polymer brushes is driven by an amplification of tension at the polymer brush-substrate interface that is the consequence of swelling of the surface-grafted polymer film. These insights add to the current understanding of the degrafting of polymer brushes and provide a step forward to unravel the parameters that drive this mechanochemical process. The results of this study, however, are not only of interest from a fundamental point of view, but could also impact the technical use of these polymer films and contribute to the design of more robust polymer brushes or to systems that take advantage of this phenomena and harness degrafting in a productive manner, e.g. towards the development of mechanoresponsive surfaces.<sup>157-159</sup>

## 2.5. Supporting Information

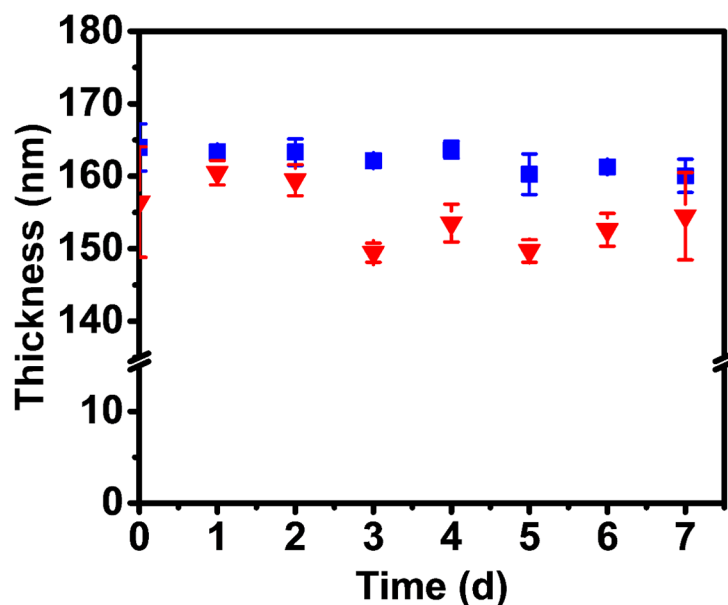


**Figure S2.1.** Ellipsometric dry thickness of PtBMA brushes as a function of incubation time upon exposure to: dry DMF (65 ppm water) (■), dry acetone (0.45 vol% water) (▼).

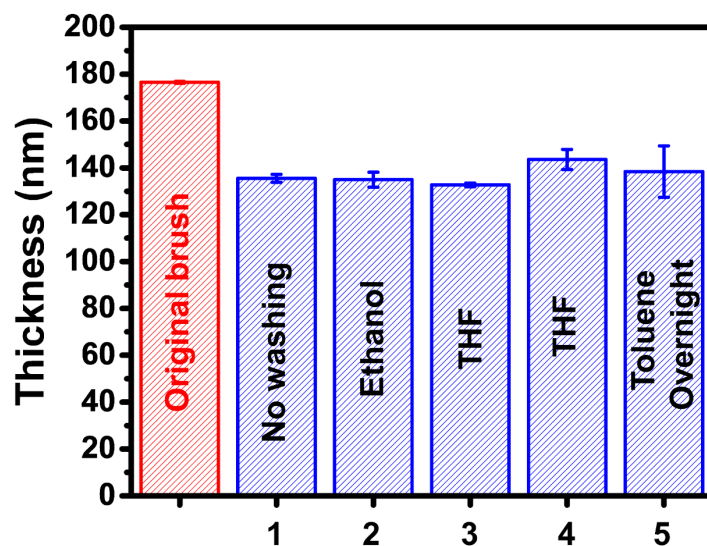


**Figure S2.2.** Comparison of the dry film thickness of a PtBMA brush sample with an initial dry film thickness of 174 nm (red) after incubation in THF + 5 vol% water for 4 hours without further washing (1) as well as after application of several washing steps

(2-5).

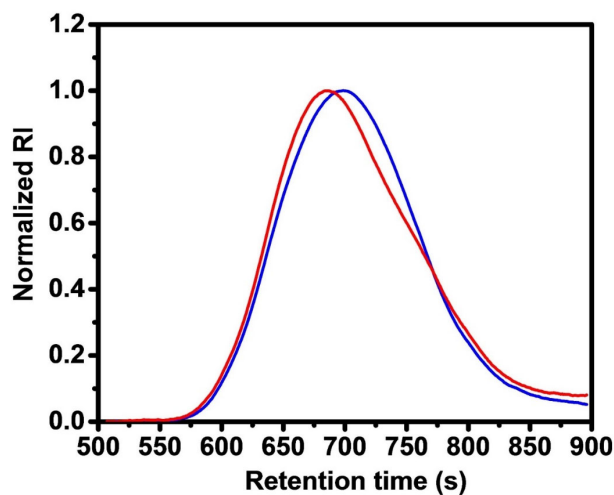


**Figure S2.3.** Normalized GPC traces of PtBMA cleaved from brush coated silicon oxide substrates. Original PtBMA brush (red) (initial dry film thickness = 165 nm),  $M_n$  = 248 kDa,  $M_w$  = 422 kDa and PtBMA brush after 4 h degrafting in THF + 5 vol% water (blue),  $M_n$  = 231 kDa,  $M_w$  = 397 kDa.

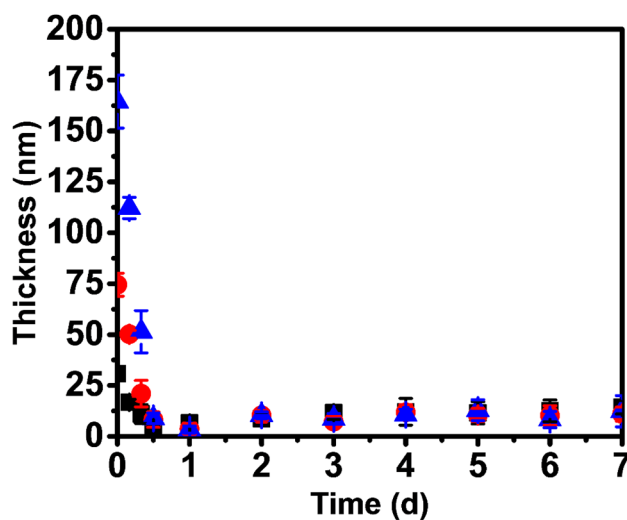


**Figure S2.4.** Evolution of the dry film thicknesses of PtBMA brushes with initial dry film thicknesses of 160 nm ( $\blacktriangle$ ), 80 nm ( $\bullet$ ) and 50 nm ( $\blacksquare$ ) upon incubation in THF + 5 vol% water for 7 days.

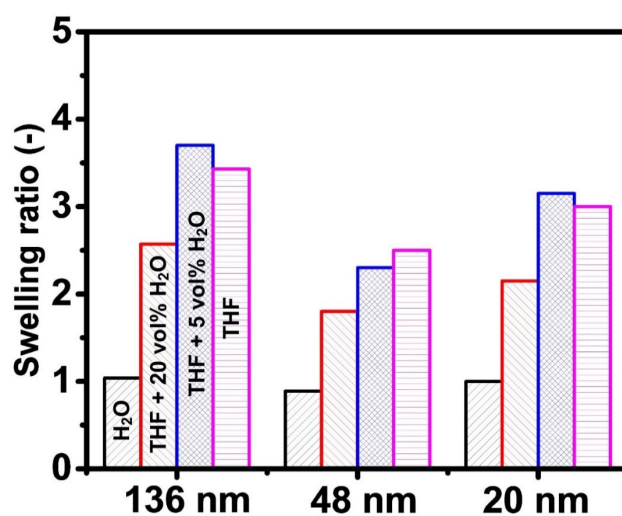


**Figure S2.5.** Swelling ratios of PtBMA brushes with initial dry film thicknesses of 20, 48 and 136 nm in water (black), THF + 20 vol% water (red), THF + 5 vol% water (blue) and THF (pink) as measured by AFM.

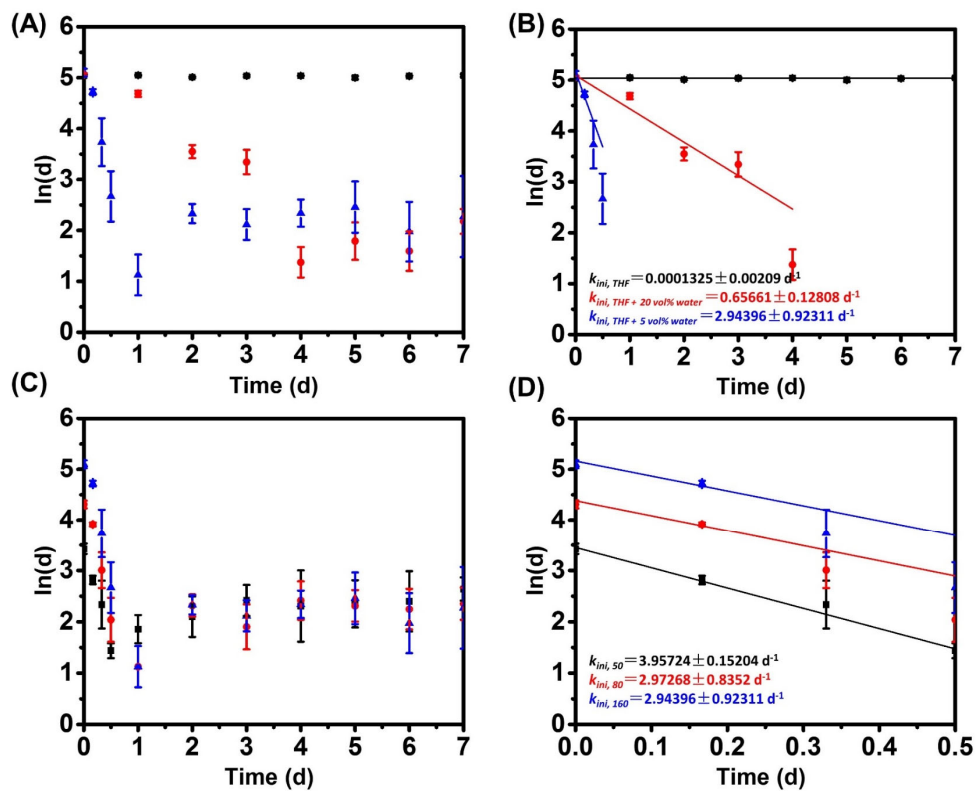


**Figure S2.6.** (A)  $\ln(d)$  ( $d$  = dry film thickness) as a function of time for PtBMA brushes

with an initial dry film thickness of 160 nm upon incubation in THF + 11 ppm water (■), THF + 5 vol% water (▲) and THF + 20 vol% water (●); (B) Determination of the initial rate constant of degrafting for PtBMA brushes with an initial dry film thickness of 160 nm upon incubation in THF + 11 ppm water (■), THF + 5 vol% water (▲) and THF + 20 vol% water (●); (C)  $\ln(d)$  ( $d$  = dry film thickness) as a function of time for PtBMA brushes with initial dry film thicknesses of 50 (■), 80 (●) and 160 nm (▲) upon incubation in THF + 5 vol% water; (D) Determination of the initial rate constant of degrafting for PtBMA brushes with initial dry film thicknesses of 50 (■), 80 (●) and 160 nm (▲) upon exposure to THF + 5 vol% water.

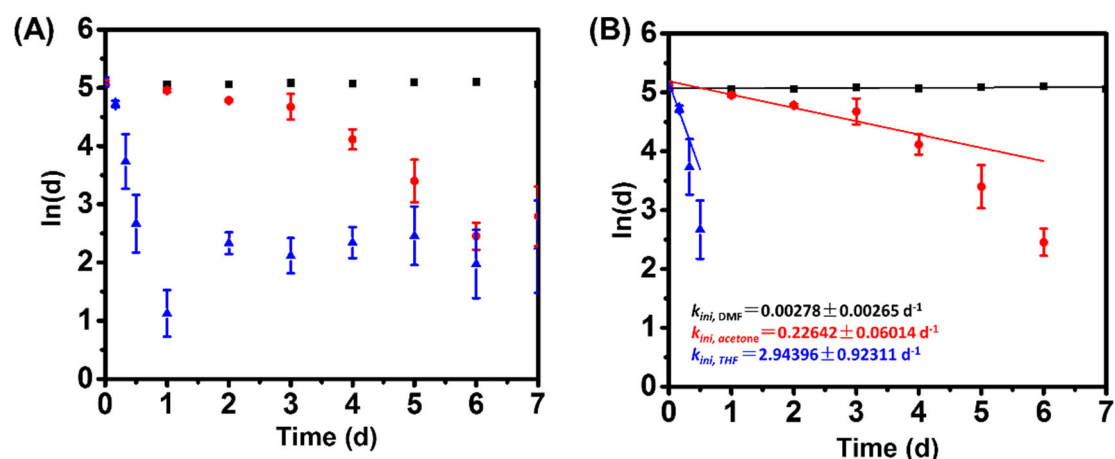


**Figure S2.7.** (A)  $\ln(d)$  ( $d$  = dry film thickness) as a function of time for PtBMA brushes with an initial dry film thickness of 160 nm upon incubation in DMF + 5 vol% water (■), acetone + 5 vol% water (●) and THF + 5 vol% water (▲); (B) Determination of the initial rate constant of degrafting for PtBMA brushes with an initial dry film thickness of 160 nm upon incubation in DMF + 5 vol% water (■), acetone + 5 vol% water (●) and THF + 5 vol% water (▲).

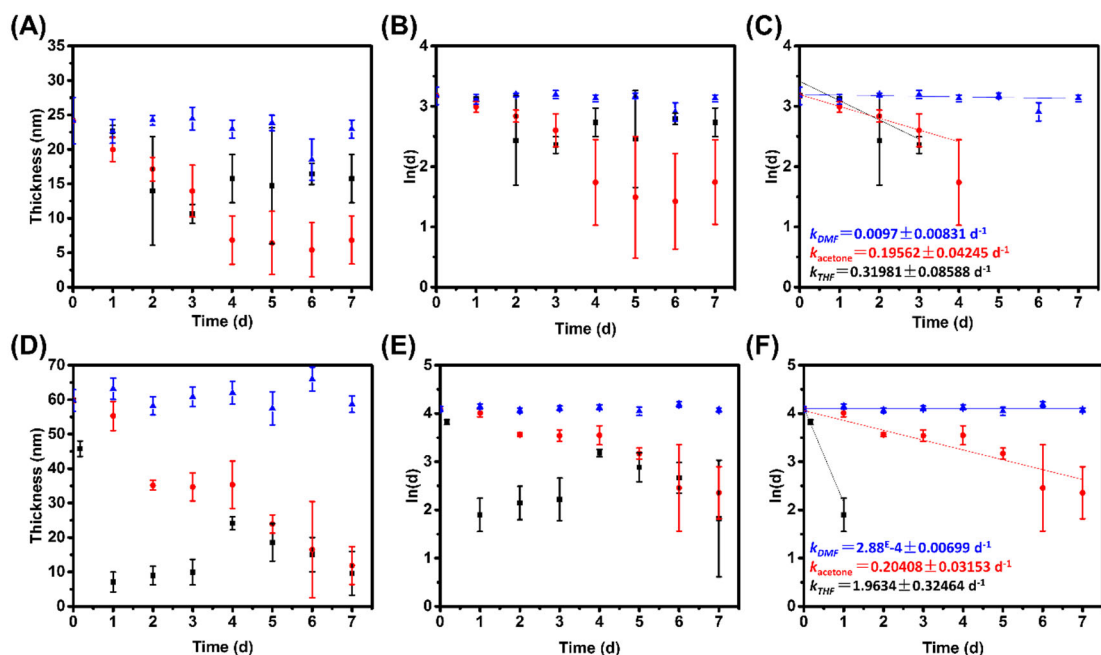


**Figure S2.8.** (A) Ellipsometric dry thicknesses of PtBMA brushes with an initial grafting density of 20% as a function of incubation time upon exposure to in DMF + 5 vol% water ( $\blacktriangle$ ), acetone + 5 vol% water ( $\bullet$ ) and THF + 5 vol% water ( $\blacksquare$ ); (B)  $\ln(d)$  ( $d$  = dry film thickness) as a function of time for PtBMA brushes with an initial grafting density 20% upon incubation in DMF + 5 vol% water ( $\blacktriangle$ ), acetone + 5 vol% water ( $\bullet$ ) and THF + 5 vol% water ( $\blacksquare$ ); (C) Determination of the initial rate constant of degrafting for PtBMA brushes with an initial grafting density of 20% upon incubation in DMF + 5 vol% water ( $\blacktriangle$ ), acetone + 5 vol% water ( $\bullet$ ) and THF + 5 vol% water ( $\blacksquare$ ); (D) Ellipsometric dry thicknesses of PtBMA brushes with an initial grafting density of 50% as a function of incubation time upon exposure to DMF + 5 vol% water ( $\blacktriangle$ ), acetone + 5 vol% water ( $\bullet$ ) and THF + 5 vol% water ( $\blacksquare$ ); (E)  $\ln(d)$  ( $d$  = dry film thickness) as a function of time for PtBMA brushes with an initial grafting density 50% upon incubation in DMF + 5 vol% water ( $\blacktriangle$ ), acetone + 5 vol% water ( $\bullet$ ) and THF + 5 vol% water ( $\blacksquare$ ); (F) Determination of the initial rate constant of degrafting for PtBMA

brushes with an initial grafting density of 50% upon incubation in DMF + 5 vol% water

(▲), acetone + 5 vol% water (●) and THF + 5 vol% water (■).

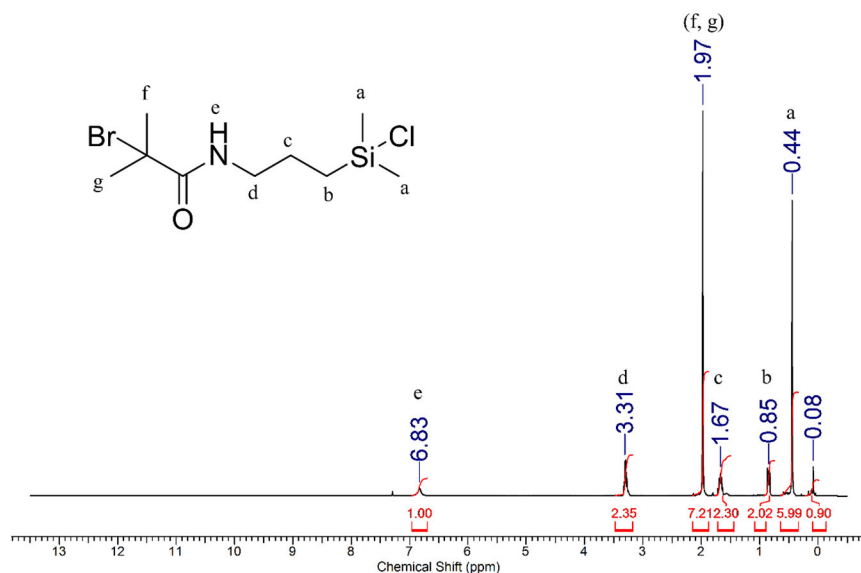


**Figure S2.9.** <sup>1</sup>H-NMR spectrum of 2-bromo-2-methyl-N-{3-[chloro(dimethyl)silyl]propyl}propanamide recorded in chloroform-d<sub>1</sub>.

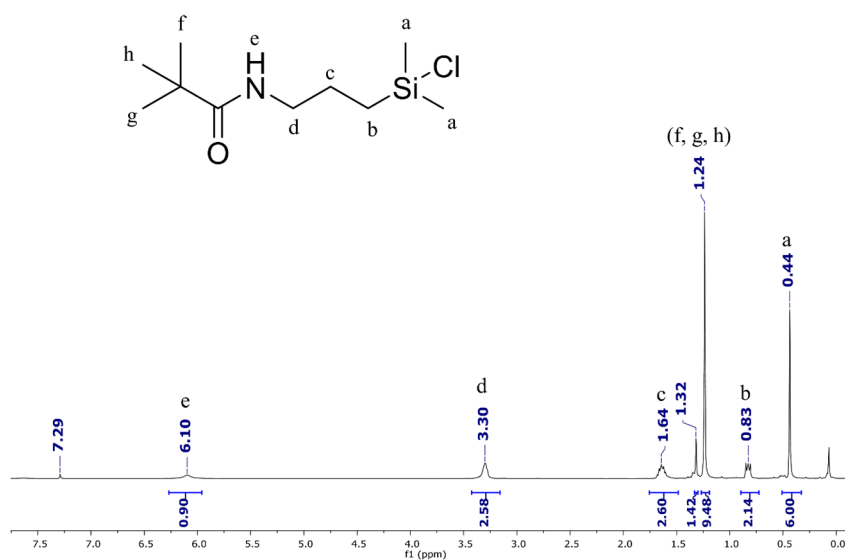


**Figure S2.10.** <sup>1</sup>H-NMR spectrum of N-(3-(chlorodimethylsilyl)propyl)pivalamide recorded in chloroform-d<sub>1</sub>.

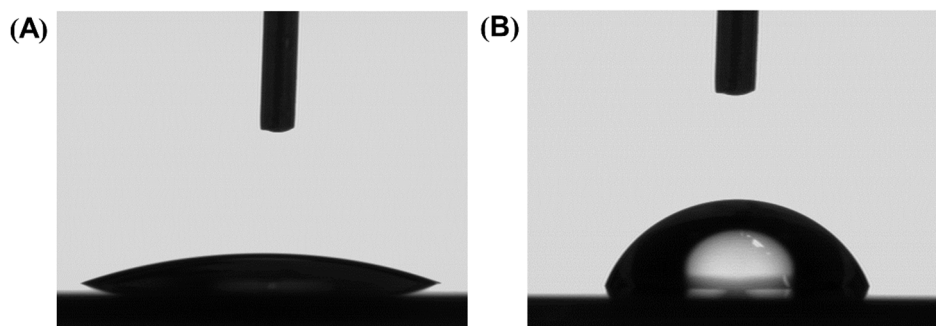


**Figure S2.11.** Water contact angle analysis of (A) an unmodified plasma cleaned silicon oxide surface (46.9°) and (B) a silicon oxide surface modified with 2-bromo-2-methyl-N-{3-[chloro(dimethyl)silyl]-propyl}propanamide (69.2°).

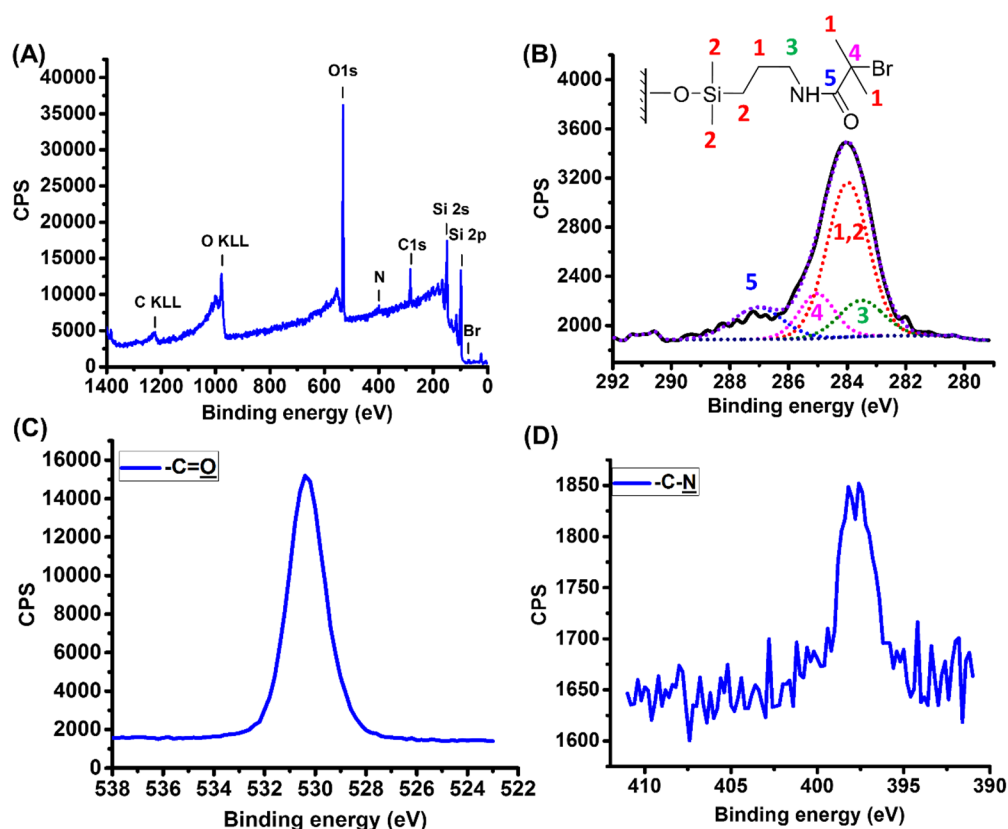


**Figure S2.12.** (A) XPS survey scan; (B) C<sub>1s</sub> high resolution spectrum; (C) O<sub>1s</sub> high resolution spectrum and (D) N<sub>1s</sub> high resolution spectrum of a 2-bromo-2-methyl-N-{3-[chloro(dimethyl)silyl]-propyl}propanamide modified silicon surface.

### **3. Mechanical Acceleration of Hydrolysis in Polymers Incorporating Main Chain Ester Bonds**

#### **3.1. Introduction**

The application of mechanical force represents a powerful strategy to alter the chemical reactivity of polymers.<sup>148,158,160-162</sup> As an example, in solutions of polymers that are subjected to ultrasound irradiation<sup>149,163</sup> or shear forces,<sup>147,149,164,165</sup> stresses typically accumulate near the center of the polymer main chain. For polymers that are composed of an all carbon backbone, this can lead to a sequence of multiple, homolytic carbon-carbon bond scission events. By introducing a defined number of strategically weakened linkages (“mechanophores”) at specific positions along the polymer main chain, the number and location of the scission events can be controlled.<sup>159,166</sup> Over the past decades, a wide variety of mechanophores has been used to design polymers that undergo specific scission events under the influence of a mechanical stimulus. If designed properly, the transformations that mechanophore-containing polymers undergo upon exposure to a mechanical stimulus can be used productively, e.g. to generate color changes, which can be used to report damage, to activate catalysts or to initiate polymerization reactions.<sup>167-169</sup>

Mechanical forces cannot only be harnessed to trigger chemical transformations of specifically designed mechanophores, but may also alter the reactivity of functional groups that are commonly found in synthetic polymers. Ester bonds are one example of such a functional group that is ubiquitous in synthetic polymers. A number of reports in the literature have discussed the effect of mechanical force on ester hydrolysis. On

the one hand, density functional theory calculations together with model experiments on macrocyclic lactones did not point to an acceleration of ester hydrolysis kinetics under the influence of a mechanical force.<sup>170</sup> In contrast, several articles, which explored ultrasound irradiation to trigger release from micelles generated from ester containing block copolymers provide evidence for force accelerated ester hydrolysis.<sup>171-174</sup> The degrafting of densely tethered polymer brushes that are grown via surface-initiated polymerization and anchored via ester containing linkages to a silicon oxide substrate upon exposure to water-containing media is another example suggesting that ester hydrolysis is force sensitive.<sup>140,144-146,175-177</sup>

Ester bonds are omnipresent in a wide range of polymer materials. Examples include degradable hydrogels as well as bioresorbable sutures or screws that are used for wound fixation.<sup>178-181</sup> In many instances, these materials are mechanically challenged in one or several ways during their use. Hydrogels are swollen with water, sutures exposed to tension forces and screws to compression. Given their importance for a variety of biomedical applications, a better understanding of the influence of mechanical load on ester bond hydrolysis could help to improve the design and properties of these materials. Driven by the contradictory findings in the earlier work cited above, the aim of this study was to shed light on the effect of mechanical force on the hydrolysis of ester bonds incorporated in polymers. To this end, a series of polystyrene polymers, which contain two central ester bonds was synthesized and the degradation of these materials upon exposure to ultrasonication studied. The results of these experiments indicate that degradation of these polystyrene polymers proceeds via two concurrent pathways that

involve both homolytic carbon-carbon bond scission as well as ester bond hydrolysis and unambiguously point towards an acceleration of ester bond hydrolysis under the influence of a mechanical force.

## **3.2. Experimental Section**

### **3.2.1. Materials**

All chemicals were used as received unless described otherwise. Copper(I)bromide (99.995+%), ethanol (99.8%), neutral and basic aluminum oxide, pyridine (99.8%), hexadecyltrimethylammonium bromide, 2-butanone (MEK) ( $\geq 99.7\%$ , HPLC grade), N,N,N',N'',N''-pentamethyldiethylenetriamine (PMDETA 99%), tetrahydrofuran (THF) ( $\geq 99.9\%$ ) for matrix-assisted laser desorption/ionization mass spectrometry (MALDI-MS) and imidazole ( $\geq 99\%$ ) were purchased from Sigma-Aldrich. Anisole (99%), 4-(bromomethyl) benzoic acid (97%), hydrobromic acid (48%) and 1,3,5-trioxane were purchased from ABCR. 1,4-Diphenylbutane was purchased from Fluorochem. Thionyl chloride (99%) and diethyl ether were purchased from Fluka. Styrene (99.5%), silver trifluoroacetate (AgTFA) (98%), 1,4-butanediol (99%) and sodium chloride (extra pure) were purchased from Acros. Prior to polymerization, styrene was passed over an aluminum oxide column to remove the inhibitor. 4,4'-Dinonyl-2,2'-bipyridyl (Dnbpy) was purchased from TCI. Triethylamine, glacial acetic acid (100%), sodium bicarbonate and fuming hydrochloric acid (37%) were purchased from Merck. Methanol (analytical grade) and ethanol (analytical grade) were purchased from Fisher chemicals. Petroleum ether was purchased from Thommen-Furter AG. Potassium hydroxide and magnesium sulfate were purchased from Reactolab SA. Trans-2-[3-(4-

tert-butylphenyl)-2-methyl-2-propenylidene]malononitrile (DCTB) was purchased from Santa. Tetrahydrofuran (THF) used in ultrasonication experiments and for GPC analysis and dichloromethane (DCM) were purified and dried using a solvent-purification system (PureSolv). Deionized water was obtained from a Millipore Direct-Q5 ultrapure water system.

### **3.2.2. Methods**

NMR spectra were recorded on a Bruker AVANCE-400 Ultra Shield spectrometer. Atmospheric Pressure Photoionization mass spectrometry (APPI-MS) was performed on an Orbitrap ELITE mass spectrometer (ThermoFisher), which combines a high-field Orbitrap mass analyzer with the dual pressure linear ion trap. Electrospray ionization mass spectra (ESI-MS) were recorded on a Xevo G2-S QToF (Waters) mass spectrometer, which is equipped with the StepWave ion optics and the QuanTof technology for high mass resolution. Matrix-assisted laser desorption/ionization mass spectrometry (MALDI-MS) was performed on a rapifleX MALDI-TOF/TOF instrument (Bruker Daltonik GmbH). Trans-2-[3-(4-tert-butylphenyl)-2-methyl-2-propenylidene]malononitrile (DCTB) was used as the matrix for MALDI MS analysis. AgTFA and THF were used as cationization agent and solvent. The ratio between matrix (20 mg/mL DCTB in THF) and probe (10 mg/mL in THF) is 20: 1. Gel permeation chromatography (GPC) analysis was performed on an Agilent 1260 infinity system equipped with a Varian 390-LC refractive index detector, two PLgel 5  $\mu$ m Mixed C (Agilent) columns and a PLgel guard column. The mobile phase was THF (HPLC grade). Sample analysis was performed at 40 °C at a flow of 1.0 mL/min.

Samples were filtered prior to analysis and polymer molecular weights were analysed using Polymer Standard Service Mainz linear PS standards (1250-277000 g/mol). Ultrasound experiments were performed using a VCX 500 ultrasonic processor (Sonics and Materials) equipped with a 13 mm diameter solid probe from Sonics and Materials.

### **3.2.3. Procedures**

**Butane-1,4-diyl bis(4-(bromomethyl)benzoate) (BDMB) (Supporting Information Scheme S3.1).** Thionyl chloride (15 mL, 206 mmol) was added to 4-bromomethyl benzoic acid (2.15 g, 10 mmol). The suspension was stirred and refluxed at 75 °C for 2 h. The excess thionyl chloride was removed by vacuum distillation. The obtained solid was dissolved in 5 mL anhydrous dichloromethane (DCM). The mixture was cooled to 0 °C and a solution of 0.44 mL (5 mmol) 1, 4-butanediol and 1.6 mL (20 mmol) pyridine in 10 mL dry DCM was added dropwise. The temperature was allowed to rise to room temperature and the reaction mixture stirred overnight. Then, the solution was washed 3 times with 1 M HCl, 3 times with saturated NaHCO<sub>3</sub> and once with brine solution. The organic layer was dried over magnesium sulfate, filtered and dried by rotary evaporation. The crude product was purified by recrystallization from methanol to give white crystals (Yield 60%). <sup>1</sup>H NMR (400 MHz, CDCl<sub>3</sub>, δ): 1.95 (m, 4H, CH<sub>2</sub>), 4.40 (t, 4H, O=C-O-CH<sub>2</sub>), 4.50 (s, 4H, Br-CH<sub>2</sub>-Ar), 4.61 (s, 4H, Cl-CH<sub>2</sub>-Ar), 7.44-7.47 (d, 4H, Ar-H), 8.02-8.04 (d, 4H, Ar-H); <sup>13</sup>C NMR (400 MHz, CDCl<sub>3</sub>, δ): 25.69 (-CH<sub>2</sub>-), 32.33 (Br-CH<sub>2</sub>-Ar), 45.50 (Cl-CH<sub>2</sub>-Ar), 64.73 (O=C-O-CH<sub>2</sub>), 128.65, 129.19, 130.16, 142.44 (-Ar-), 166.19 (O=C-O-). HRMS (ESI m/z) calculated C<sub>20</sub>H<sub>20</sub>O<sub>4</sub>Br<sub>2</sub> 484.2; found 484. <sup>1</sup>H NMR, <sup>13</sup>C NMR and ESI mass spectra are shown in **Supporting Information**

**Figures S3.1, S3.2 and S3.3.** The results of these analyses indicate that the product is a mixture of the corresponding benzyl bromide and benzyl chloride derivatives. The obtained product was used as polymerization initiator without further purification.

**1,4-Bis(4-bromomethylphenyl)butane (BBPB) (Supporting Information Scheme S3.2).** 1,4-Diphenylbutane (2 g, 9.51 mmol) was added to a mixture of 48% aqueous HBr (4.15 mL, 39.9 mmol) and glacial AcOH (50 mL), followed by 1,3,5-trioxane (0.57 g, 6.34 mmol) and hexadecyltrimethylammonium bromide (CTAB) (52 mg, 0.143 mmol). The mixture was well stirred and heated to a gentle reflux for 8 h. After that, the volatiles were removed under reduced pressure and the crude product purified by column chromatography using hexane + 4 vol% diethyl ether as the eluent. The product obtained by column chromatography was further purified by additional recrystallization from petroleum ether. (Yield 10%). <sup>1</sup>H NMR (400 MHz, CDCl<sub>3</sub>, δ): 1.65 (m, 4H, -CH<sub>2</sub>-), 2.62 (t, 4H, Ar-CH<sub>2</sub>-), 4.49 (s, 4H, Br-CH<sub>2</sub>-Ar), 7.12-7.14 (d, 4H, Ar-H), 7.29-7.31 (d, 4H, Ar-H); <sup>13</sup>C NMR (400 MHz, CDCl<sub>3</sub>, δ): 31.00 (-CH<sub>2</sub>-), 33.87 (Br-CH<sub>2</sub>-Ar), 35.63 (Ar-CH<sub>2</sub>-), 129.00, 129.18, 135.31, 143.15 (-Ar-). HRMS (APPI m/z) calculated C<sub>18</sub>H<sub>20</sub>Br<sub>2</sub> 396.2. Instead of at 396.2, two main peaks were found at 327 and 317, which are due to the fragmentation of BBPB under MS conditions. The two peaks can be attributed to C<sub>18</sub>H<sub>20</sub>Br and C<sub>17</sub>H<sub>19</sub>Br. NMR spectra are shown in **Supporting Information Figures S3.4 and S3.5**. The MS spectrum is shown in **Supporting Information Figure S3.6**.

**ATRP of styrene.** 0.15 mL (0.862 mmol) PMDETA and 0.5 mL (4.6 mmol) anisole were dissolved in 10 mL (87.2 mmol) styrene followed by 3 freeze-pump-thaw cycles.

In a separate Schlenk tube, 124.6 mg (0.87 mmol) CuBr was purged with N<sub>2</sub> for 15 min and then the styrene mixture was transferred to the CuBr under N<sub>2</sub> flow and stirred for 20 min until the CuBr was completely dissolved. After that, the initiator (BDMB) was added and the reaction mixture subjected to one freeze-pump-thaw cycle. The monomer to initiator ratio and polymerization time were adjusted to the desired target molecular weight (**Table 3.1**). The solution was then heated to 80 °C for the desired time. Polymerizations with BBPB were performed at 90 °C and used Dnbpy/CuBr = 1/1 instead of PMDETA/CuBr = 1/1. After the reaction, the polymer was precipitated in methanol, dissolved in DMF and passed through a short neutral aluminum oxide column to remove the excess copper. Then, the polymer was precipitated in methanol again and dried under vacuum. Representative <sup>1</sup>H NMR spectra of a **PS(ester)** polymer generated from BDMB and a **PS(carbon)** sample obtained using BBPB are shown in **Supporting Information Figures S3.7** and **S3.8**. MALDI mass spectra of a **PS(carbon)** polymer with *M<sub>n</sub>* 10.9 kDa and a **PS(ester)** polymer with *M<sub>n</sub>* 10.2 kDa are shown in **Supporting Information Figures S3.9** and **S3.10**. These mass spectra confirm the structures of the polymers and the incorporation of the initiator moieties. As reported before, the U series peaks in both spectra corresponds to polystyrene molecules with a terminal double bond by loss of a HBr, the T series peaks corresponds to the reaction product of PS-Br with THF and TFA and the W series peaks can be assigned to the hydrolysis product of PS-Br with water. The presence of these signals and the formation of these products is due to the use of AgTFA in the sample preparation for the MALDI-

TOF analysis.<sup>182</sup> GPC traces of all the polymers prepared in this study are shown in **Supporting Information Figure S11**.

**Calibration of the ultrasonication setup.** The setup that was used is shown in **Supporting Information Figure S3.12**. The output power of the sonicator at amplitudes of 21%, 40% and 70% was calibrated following previously published protocols.<sup>183,184</sup> A four-arm cell was filled with 150 mL Milli-Q water. A thermocouple was introduced into the water. The amplitude on the processor was set to 21%. Sonication was started when the temperature was stabilized at 24 °C for 10 min. The temperature ( $T$ ) of the water was recorded every 120 s for 30 min and the resulting values plotted against time ( $t$ ) to determine  $\Delta T/\Delta t$  by the slope of the line. This procedure was repeated for amplitudes of 40% and 70%. The corresponding calibration curves are shown in **Supporting Information Figure S3.13**. The heat generated from cavitation in Watt ( $q$ ), was determined from the following equation:  $q = \text{specific heat (J.g}^{-1}.\text{°C}^{-1}) \times \text{mass (g)} \times \Delta T/\Delta t (\text{°C/s})$ , with the specific heat of water = 4.179 J.g<sup>-1</sup>.°C<sup>-1</sup>, the mass of water = 150 g and  $\Delta T/\Delta t$  = the slope of the line for the corresponding amplitude (see **Supporting Information Figure S3.13**). The resulting value,  $q$ , was divided by the surface area of the tip (1.5 cm<sup>2</sup>) to afford ultrasound intensities of 1.88, 3.6 and 6.76 W/cm<sup>2</sup> at amplitudes of 21%, 40% and 70%, respectively.

**Ultrasonication experiments.** The polymer solution (1.2 mg/mL in THF or THF + 5 vol% water) was placed in an oven-dried four-arm cell that was inserted into a collar and screwed onto the transducer. A thermocouple was penetrated through a septum on one of the side arms and placed in contact with the solution, ensuring that it did not

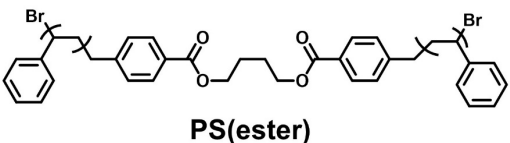
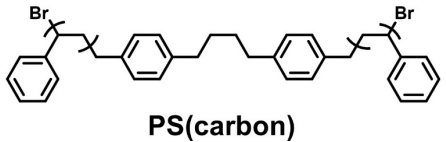
touch the probe. The distance between the probe and the bottom of the cell was 20.0 mm. Prior to each experiment, N<sub>2</sub> was purged for 20 min. The entire system was cooled in an ice water bath to maintain a temperature of 4-9 °C throughout the experiment. The solution was exposed to pulsed ultrasound (1 s on, 2 s off, 20 kHz). At timed intervals, 800 µL of solution was withdrawn from the cell and passed through a syringe filter (pore size 0.22 µm) into a 1 mL sample vial and injected into the GPC. For ultrasonication experiments that were performed in MEK, 9 mL polymer solution was withdrawn from the cell and separated into two portions. One portion, which contained 800 µL of the MEK polymer solution, was passed through a syringe filter and injected into a 1 mL sample vial. MEK was evaporated under reduced pressure at room temperature after which 800 µL THF was added to the 1 mL sample vial and then injected into GPC for  $M_n$  analysis. The other portion, which contained 8.2 mL MEK polymer solution, was dried under reduced pressure at room temperature. The remaining polymer was further dried in vacuum oven at 70 °C for 2 days prior to NMR analysis.

### **3.3. Results and Discussion**

One potential challenge in the study of the effect of mechanical force on ester bond hydrolysis in polymers is that chain degradation upon activation with, for example, ultrasound, may proceed concurrently via homolytic carbon-carbon bond scission as well as ester hydrolysis. When water-soluble polymers are investigated in aqueous solution, these two contributions are hard to distinguish since under these conditions water both acts as solvent and reagent. This study, therefore, has used polystyrene

polymers that can be dissolved in water-miscible organic solvents, such as, for example, THF. In this way, the contributions from homolytic carbon-carbon bond scission and ester hydrolysis can be distinguished by comparing results of ultrasonication experiments in dry THF, which lacks the water that is necessary for ester hydrolysis, with those of experiments in which small quantities of water are added to the THF. To study the effect of mechanical activation on the hydrolysis of ester bonds incorporated in polymers, a series of polystyrene polymers (**PS(ester)**) that contain two ester linkages in the center of the polymer chain was synthesized (**Table 3.1**). As a control, a second series of polystyrene polymers was prepared that was comprised of an all-carbon backbone (**PS(carbon)**, **Table 3.1**). **PS(ester)** and **PS(carbon)** polymers covering a range of molecular weights were obtained via atom transfer radical polymerization (ATRP) of styrene using butane-1,4-diyl bis(4-(bromomethyl)benzoate) (BDMB), respectively, 1,4-bis(4-bromomethylphenyl)butane (BBPB) as the initiator. **Table 3.1** shows the structures of the two polymers and summarizes the molecular weights of the samples that have been prepared. Details on the synthesis of the BDMB and BBPB initiators as well as the **PS(ester)** and **PS(carbon)** polymers are provided in **Supporting Information Scheme S3.1** and **Scheme S3.2**.

**Table 3.1.** Number average molecular weights ( $M_n$ ), number average degrees of polymerization ( $DP$ ) and dispersities ( $\mathcal{D}$ ), all determined by GPC analysis, of the **PS(ester)** and **PS(carbon)** polymers employed in this study.

Polymer	$M_n$ (kDa)	$DP$ (-)	$\mathcal{D}$ (-)
 <p><b>PS(ester)</b></p>	170	1629	1.41
	72	688	1.25
	50	476	1.20
	32	303	1.17
	10.2	98	1.23
 <p><b>PS(carbon)</b></p>	190	1823	1.41
	77	736	1.14
	49	467	1.13
	29	275	1.14
	10.9	100	1.20

The effect of mechanical force on the hydrolysis of the ester bonds in the **PS(ester)** polymers was investigated using dilute polymer solutions that were subjected to ultrasound irradiation. For these experiments, polymers were dissolved at a concentration of 1.2 mg/mL in either THF or a THF + 5 vol% water mixture. This sample concentration was selected to be well below the overlap concentration of polystyrene for the range of molecular weights indicated in **Table 3.1**.<sup>185</sup> To distinguish chain degradation events that are the result of direct homolytic C-C backbone scission from those that are the consequence of ester bond hydrolysis (which requires water), ultrasonication experiments were performed on solutions of the polymer both in THF and in THF containing 5 vol% water. Chain degradation was monitored by GPC analysis of samples that were subjected to ultrasonication for different periods of time.

**Figure 3.1A** illustrates the decrease in molecular weight that is observed upon exposure of a **PS(ester)** polymer with an initial number-average molecular weight ( $M_n$ ) of 170 kDa to pulsed ultrasound at a power density of 1.88 W/cm<sup>2</sup> for 120 min. From the change in  $M_n$ , an apparent rate constant ( $k'$ ) for the chain degradation reaction can be obtained using **Equation 1**:

$$\frac{1}{M_t} = \frac{1}{M_i} + k't \quad (1)$$

where  $M_t$  is the number-average molecular weight of the sonicated sample at time  $t$  and  $M_i$  is the initial number-average molecular weight of the polymer.<sup>186-190</sup> Rate constants are obtained by least square linear regression analysis of the slope of plots of  $(1/M_t - 1/M_i)$  versus time, as illustrated in **Figure 3.1B** for the **PS(ester)** sample with  $M_i = 170$  kDa.

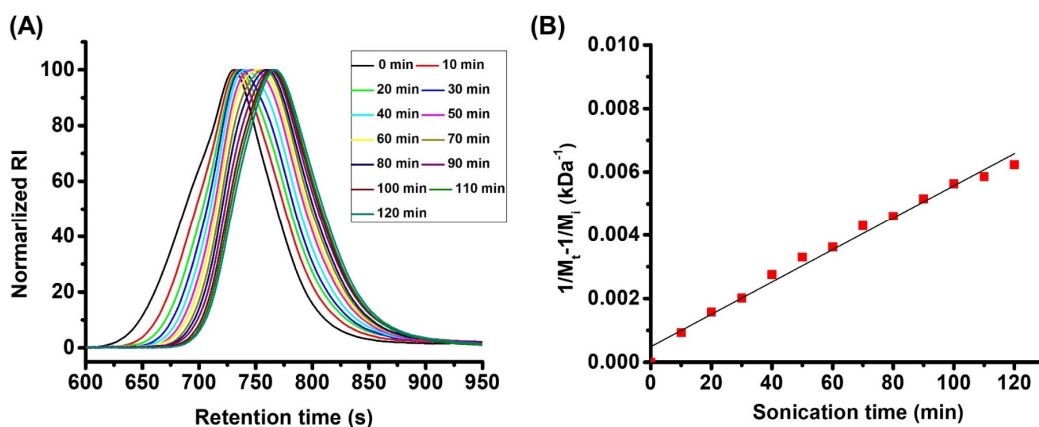


**Figure 3.1.** (A) GPC traces of a **PS(ester)** sample with an initial number-average molecular weight ( $M_n$ ) of 170 kDa upon ultrasonication in THF + 5 vol% water at a power density of 1.88 W/cm<sup>2</sup>; (B) Plot of  $(1/M_t - 1/M_i)$  for a **PS(ester)** sample with  $M_n = 170$  kDa as a function of sonication time in THF + 5 vol% water at a power density of 1.88 W/cm<sup>2</sup>.

**Figure 3.2.** summarizes the results of all the ultrasonication experiments that were carried out with the **PS(ester)** samples and the **PS(carbon)** control polymers. In a first series of experiments, the effect of polymer molecular weight on the degradation of the **PS(ester)** samples at a power density of  $1.88 \text{ W/cm}^2$  was studied. For the **PS(ester)** sample with an initial  $M_n$  of 10.3 kDa, no degradation was observed in THF and THF + 5 vol% water under these conditions (**Supporting Information Figure S3.14**). This reflects that a certain threshold polymer molecular weight is required for the polymer main chain to experience a force that is sufficient for chain degradation to occur.<sup>183,191-</sup>  
<sup>193</sup> For all the other polymers, chain degradation was observed. **Figure 3.2A** plots the rate constants of degradation for the **PS(ester)** polymers that were determined from ultrasonication experiments that were performed in THF and in THF + 5 vol% water. As is commonly observed upon ultrasonication of polymers in solution, the rate constants for the degradation reaction increase with increasing initial polymer molecular weight.<sup>183,184,187,192,194-198</sup> For a given initial polymer molecular weight, **Figure 3.2A** indicates an increase in the rate constant of degradation in THF + 5 vol% water as compared to those determined in THF, which is consistent with a contribution of ester bond hydrolysis to chain degradation in the water-containing medium. GPC analysis of ultrasonication experiments on a **PS(ester)** sample with an initial  $M_n$  of 170 kDa in THF, THF + 2.5 vol% water and THF + 5 vol% water revealed an increase in the rate constant for degradation with increasing water concentration in the THF solution (**Supporting Information Figure S3.15**). In **Figure 3.2B**, the apparent

degradation rate constants determined for 3 **PS(carbon)** samples in THF and THF + 5 vol% water solutions are shown and compared with those measured for **PS(ester)** samples of similar molecular weight in (dry) THF. **PS(carbon)** polymers with initial number average molecular weights of 10.9 and 29 kDa were not found to undergo chain degradation under these conditions. **Figure 3.2B** reveals no significant difference between the degradation rate constants for **PS(carbon)** and **PS(ester)** samples of comparable molecular weight in THF. Since degradation of the **PS(carbon)** polymers can only proceed via homolytic scission of backbone carbon-carbon bonds, this indicates that the degradation of the **PS(ester)** polymers in THF also involves homolytic carbon-carbon bond scission. **Figure 3.2B** further shows that the degradation rate constants for the **PS(carbon)** samples do not change in the presence of 5 vol% water. This is further evidence indicating that the increase in the degradation rate constants that is observed for the **PS(ester)** samples upon addition of 5 vol% water (**Figure 3.2A**) can be attributed to the contribution of ester bond hydrolysis to the chain degradation process. **Figure 3.2C** presents the apparent rate constants for ester bond hydrolysis, which were obtained by subtracting the degradation rate constants in THF + 5 vol% water and those measured in THF for the **PS(ester)** samples reported in **Figure 3.2A**. The data in **Figure 3.2C** indicate an increase in the apparent rate constant for ester hydrolysis with increasing polymer molecular weight.<sup>183,184,187,192,194-198</sup> The apparent rate constants for ester hydrolysis do not only increase with increasing initial polymer molecular weight, but also with increasing ultrasonication power, i.e. mechanical force, as illustrated in **Figure 3.2D**. **Figure 3.2D** compares the apparent

rate constants for ester hydrolysis that were measured for a **PS(ester)** polymer with an initial molecular weight of 32 kDa at power densities of 1.88 and 3.6 W/cm<sup>2</sup>. The molecular weight and power density dependence of the hydrolysis rate constants are characteristic for ultrasonication mediated polymer degradation processes.<sup>184,199-202</sup> The observed increase in degradation rate constant upon the addition of 5 vol% water (**Figure 3.2A**) and the increase in the apparent rate constant of hydrolysis with increasing polymer molecular weight (**Figure 3.2C**) and power density (**Figure 3.2D**) are strong indications that point towards a mechanical acceleration of ester bond hydrolysis.

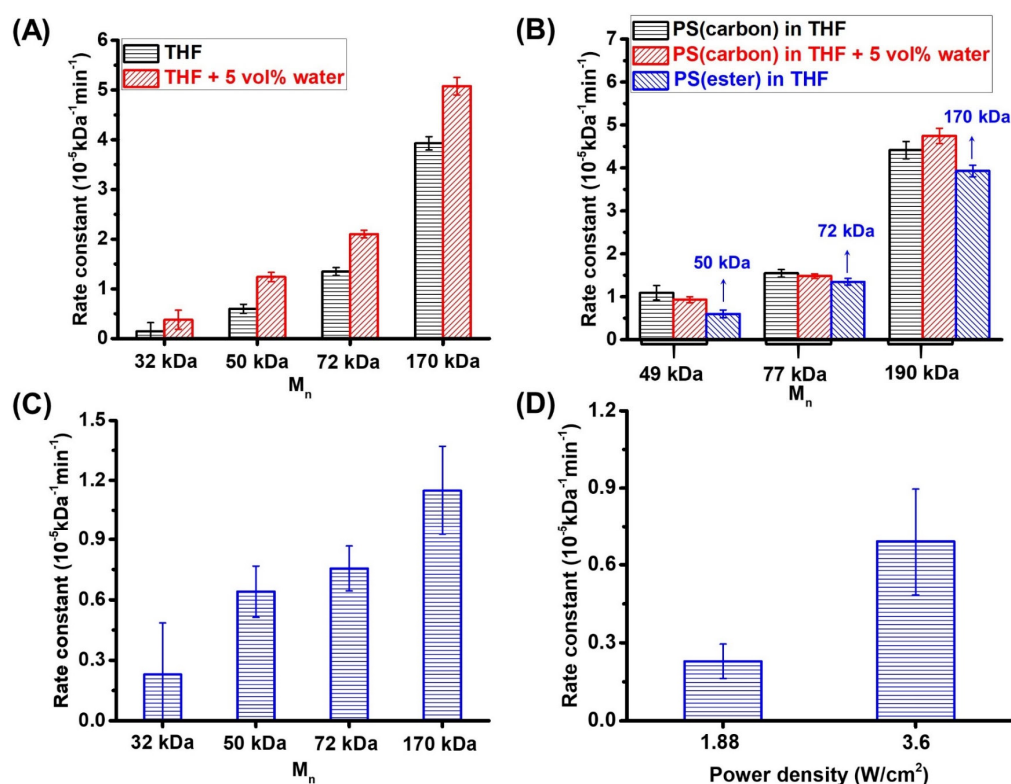


**Figure 3.2.** (A) Rate constants of degradation determined for **PS(ester)** samples with initial  $M_n$  = 32 kDa, 50 kDa, 72 kDa and 170 kDa upon ultrasonication in THF (black) and THF + 5 vol% water (red) at a power density of 1.88 W/cm<sup>2</sup>; (B) Rate constants of degradation determined for **PS(carbon)** polymers with an initial  $M_n$  of 49 kDa, 77 kDa

and 190 kDa ultrasonicated in THF (black) and THF + 5 vol% water (red) as well as for **PS(ester)** samples with an initial  $M_n$  of 50 kDa, 72 kDa and 170 kDa ultrasonicated in THF (blue) at a power density of 1.88 W/cm<sup>2</sup>; (C) Rate constants of ester hydrolysis determined for **PS(ester)** polymers with initial  $M_n$  = 32 kDa, 50 kDa, 72 kDa and 170 kDa at a power density of 1.88 W/cm<sup>2</sup>; (D) Rate constants of ester hydrolysis determined for a **PS(ester)** polymer with an initial  $M_n$  of 32 kDa at power densities of 1.88 and 3.6 W/cm<sup>2</sup>.

Ultrasonication of the **PS(ester)** polymers was further analyzed by FTIR and NMR spectroscopy. **Figure 3.3A** compares FTIR spectra of a **PS(ester)** sample with an initial  $M_n$  = 32 kDa before and after ultrasonication at a power density of 3.6 W/cm<sup>2</sup> for 4 hours. The spectra indicate the appearance of a broad peak at 3400 cm<sup>-1</sup> upon ultrasonication that can be assigned to O-H stretching vibrations of carboxylic acid residues and which indicates that ester bond hydrolysis contributes to the observed decrease in molecular weight.

To monitor degradation of the **PS(ester)** samples by <sup>1</sup>H NMR spectroscopy, ultrasonication experiments were performed in MEK and MEK + 2 vol% water solutions instead of THF. For these experiments, MEK was chosen, since trace amounts of THF that were found difficult to remove resulted in NMR signals that overlap with key NMR resonances of the **PS(ester)** polymer samples. First, chain degradation of a 50 kDa  $M_n$  **PS(ester)** sample upon ultrasound irradiation at 1.88 W/cm<sup>2</sup> in MEK and MEK + 2 vol% water for **200** min was monitored by GPC. The

degradation rate constants obtained from these experiments are summarized in **Figure 3.3B**. These rate constants are comparable to those obtained in THF and THF + 5 vol% water solutions (**Figure 3.2A**), indicating that changing the solvent to MEK does not significantly alter chain degradation. The results in **Figure 3.3B** also confirm the earlier observed increase in rate constant of degradation in the presence of water, which reflects the contribution of ester hydrolysis to chain degradation in the presence of water. **Figure 3.3C** and **Supporting Information Figure S3.16** present  $^1\text{H}$  NMR spectra of a **PS(ester)** sample (initial  $M_n = 50$  kDa) and the BDMB initiator and highlight the key resonances that were used to monitor polymer degradation via NMR spectroscopy. To assess the contribution of ester hydrolysis to chain degradation, the ratio of the integrals of signal “a”, which is due to the aromatic protons of the styrene repeat units of polymer, was compared with that of signal “b”, which is attributed to the BDMB initiator. **Figure 3.3C** shows  $^1\text{H}$  NMR spectra of this polymer both before and after ultrasonication for 200 min at  $1.88\text{ W/cm}^2$ . Additional  $^1\text{H}$  NMR spectra of this **PS(ester)** sample recorded after sonication in MEK as well as in MEK + 2 vol% water for 200 min at  $1.88\text{ W/cm}^2$  are included in **Supporting Information Figures S3.17** and **S3.18**. From the  $^1\text{H}$  NMR analyses, the ratio of integrals  $(a'/b') / (a/b)$  was taken as a measure of the rate of main chain ester bond hydrolysis. **Figure 3.3D** compares these integral ratios for ultrasonication experiments conducted in MEK and in MEK + 2 vol% water. For the ultrasonication experiments conducted in MEK, the ratio  $(a'/b') / (a/b)$  is equal to one, consistent with the absence of ester bond hydrolysis and hydrolytic chain degradation

in the absence of water. In the presence of 2 vol% water, however,  $(a'/b') / (a/b) > 1$ , which confirms the contribution of ester hydrolysis to chain degradation.

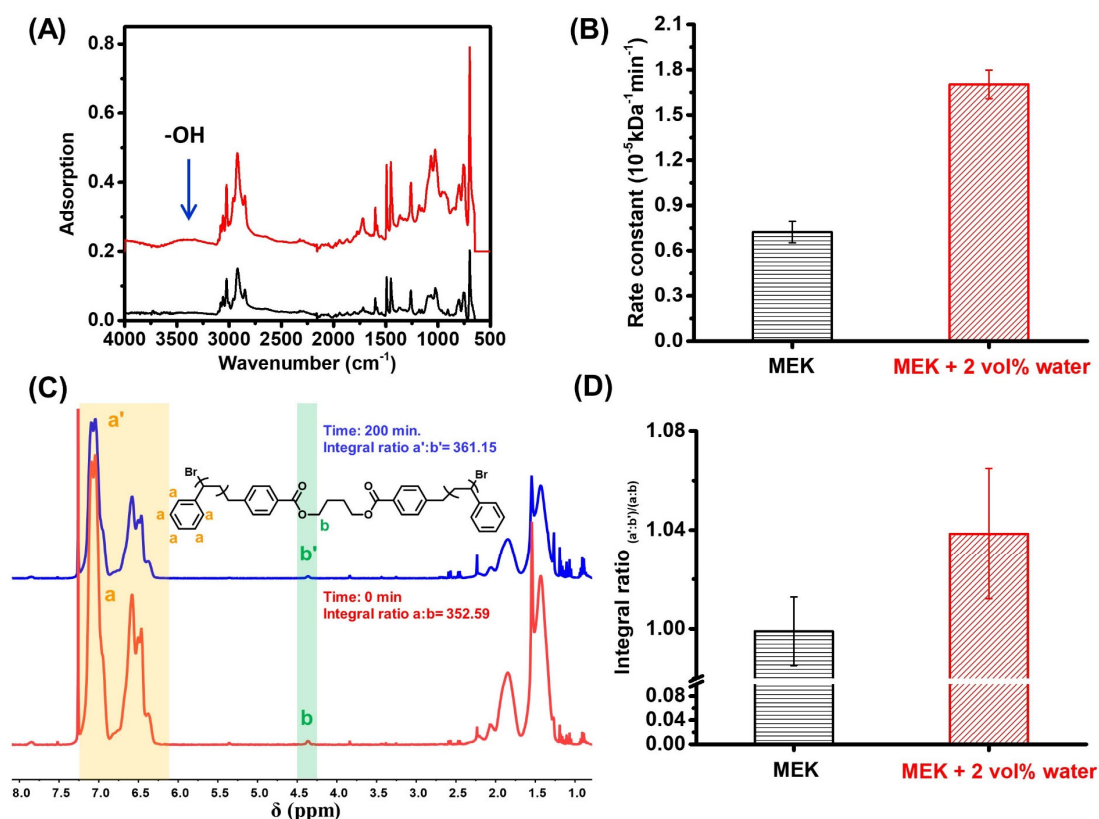


**Figure 3.3.** (A) FTIR spectra of a **PS(ester)** sample with an initial  $M_n$  of 32 kDa before (black) and after 4 h ultrasonication (red) in THF + 5 vol% water at power density 3.6 W/cm<sup>2</sup>; (B) Rate constant of degradation determined for a **PS(ester)** polymer with an initial  $M_n$  = 50 kDa upon ultrasonication in MEK (black) and MEK + 2 vol% water (red) at power density 1.88 W/cm<sup>2</sup>; (C) <sup>1</sup>H NMR spectra of a **PS(ester)** polymer with an initial  $M_n$  = 50 kDa before (0 min) and after (200 min) ultrasonication in MEK + 2 vol% H<sub>2</sub>O at power density 1.88 W/cm<sup>2</sup>; (D) Integral ratio  $(a'/b') / (a/b)$  determined from the <sup>1</sup>H NMR spectra of a **PS(ester)** polymer with an initial  $M_n$  = 50 kDa before and after 200 min ultrasonication in MEK (black) and MEK + 2 vol% water (red).

To further corroborate that ester hydrolysis contributes to the ultrasound induced degradation of the **PS(ester)** samples, an experiment was performed in which a 170 kDa **PS(ester)** sample was subjected to 1.88 W/cm<sup>2</sup> ultrasound irradiation in the presence of imidazole, which is a catalyst known to accelerate ester hydrolysis.<sup>203</sup> **Figure 3.4** presents the degradation rate constants determined for ultrasonication of a 170 kDa **PS(ester)** sample in THF, THF + 5 vol% water as well as THF + 5 vol% water and 0.1 M imidazole. For comparison, **Figure 3.4** also shows the rate constants of degradation determined for ultrasonication of a **PS(carbon)** sample of  $M_n = 49$  kDa in the same three media. The results in **Figure 3.4** reveal a significant increase in the rate constant of degradation of the **PS(ester)** sample upon the addition of 0.1 M imidazole, which is further evidence that ester hydrolysis contributes to the observed chain degradation. In contrast, no significant differences between the degradation rate constants for **PS(carbon)** were observed when a 49 kDa sample was subjected to 1.88 W/cm<sup>2</sup> ultrasonication in the same three media. As a control experiment, the **PS(ester)** polymer was dissolved in THF + 5 vol% water together with 0.1 M imidazole and analyzed by GPC after 24 h (without the application of ultrasound). **Supporting Information Figure S3.19** compares the GPC trace of this sample with that of the original polymer as well as that of the same polymer after 120 min ultrasonication at 1.88 W/cm<sup>2</sup> in the same medium. While ultrasonication in THF + 5 vol% water in the presence of 0.1 M imidazole results in chain degradation, no changes in polymer molecular weight were observed when the sample was incubated in this same medium

without the application of ultrasound. This underlines the importance of mechanical activation for ester bond hydrolysis to occur in these polymers.

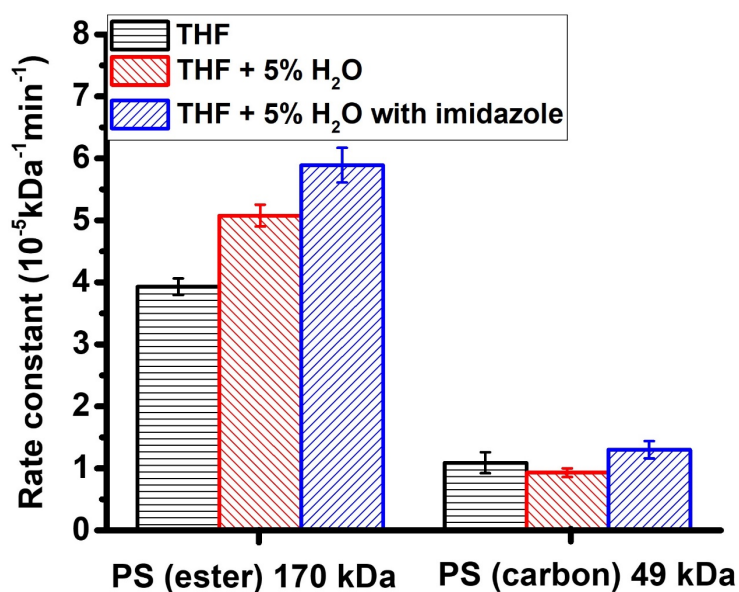


**Figure 3.4.** Rate constants of degradation of a **PS(ester)** sample with an initial  $M_n$  of 170 kDa upon exposure to ultrasonication at a power density of  $1.88 \text{ W/cm}^2$  in THF (black), THF + 5 vol% water (red) and THF + 5 vol% water with 0.1 M imidazole (blue) as well as for a **PS(carbon)** polymer with  $M_n$  of 49 kDa in THF, THF + 5 vol% water and THF + 5 vol% water with 0.1 M imidazole.

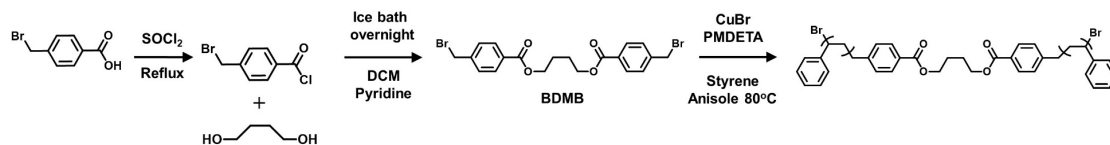
To confirm that the observed degradation of the **PS(ester)** polymers is a mechanochemical rather than a sonochemical process, a final experiment was conducted in which a **PS(ester)** sample with  $M_n = 10.2 \text{ kDa}$  was subjected to ultrasound irradiation in THF + 5 vol% water at an even higher intensity of  $6.76 \text{ W/cm}^2$ . This sample was selected since ultrasonication at  $1.88 \text{ W/cm}^2$  did not result in any degradation of this polymer (**Figure S3.14**). GPC analysis revealed that ultrasonication of this **PS(ester)** sample at an ultrasound intensity of  $6.76 \text{ W/cm}^2$  for a duration of 120

min did not result in any significant chain degradation (**Supporting Information Figure S3.20**). This observation confirms that the observed chain degradation is indeed a mechanochemical and not a sonochemical process.

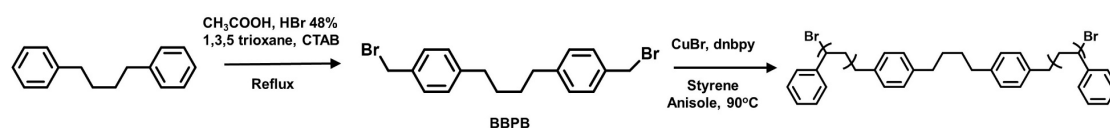
### **3.4. Conclusions**

In contrast to the mechanochemical degradation of all carbon backbone polymers or the activation of specially designed mechanophores that are embedded in polymers, not much is known about the impact of mechanical force on the reactivity of functional groups, such as ester bonds, which are a ubiquitous component of the backbone of many important classes of synthetic polymers. Using a series of polystyrene polymers that incorporate two central ester linkages, this study has elucidated the effect of mechanical force on the hydrolysis kinetics of ester bonds incorporated in the polymer backbone. GPC and NMR analyses of solutions of these polymers that were subjected to ultrasound irradiation unambiguously revealed that ester bond hydrolysis contributes to the degradation of these polymers in water containing media and further demonstrates that hydrolysis of these ester bonds is a mechanically-accelerated process.

### 3.5. Supporting Information



Scheme S3.1. Synthesis of PS(ester).



Scheme S3.2. Synthesis of PS(carbon).

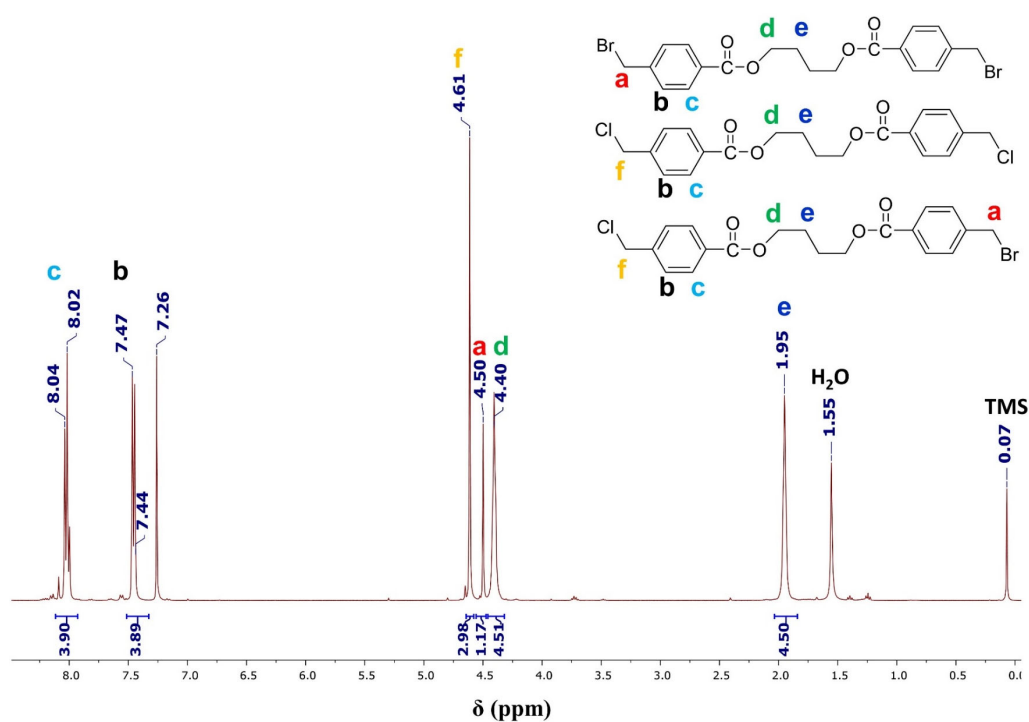


Figure S3.1.  $^1\text{H}$  NMR spectrum of BDMB recorded in  $\text{CDCl}_3$ .

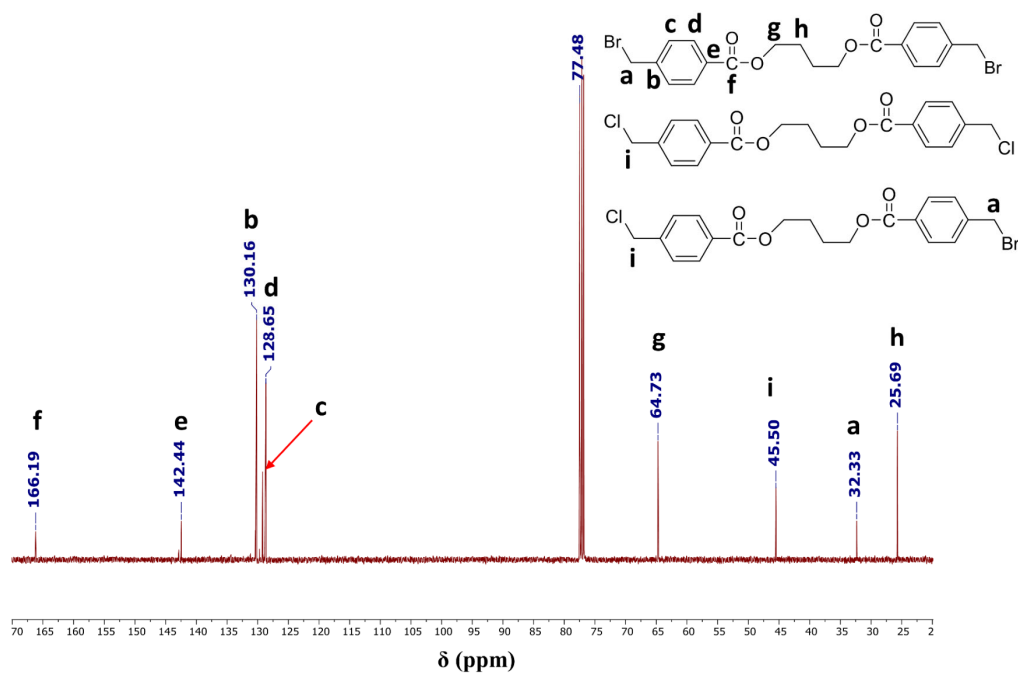


Figure S3.2. <sup>13</sup>C NMR spectrum of BDMB recorded in CDCl<sub>3</sub>.

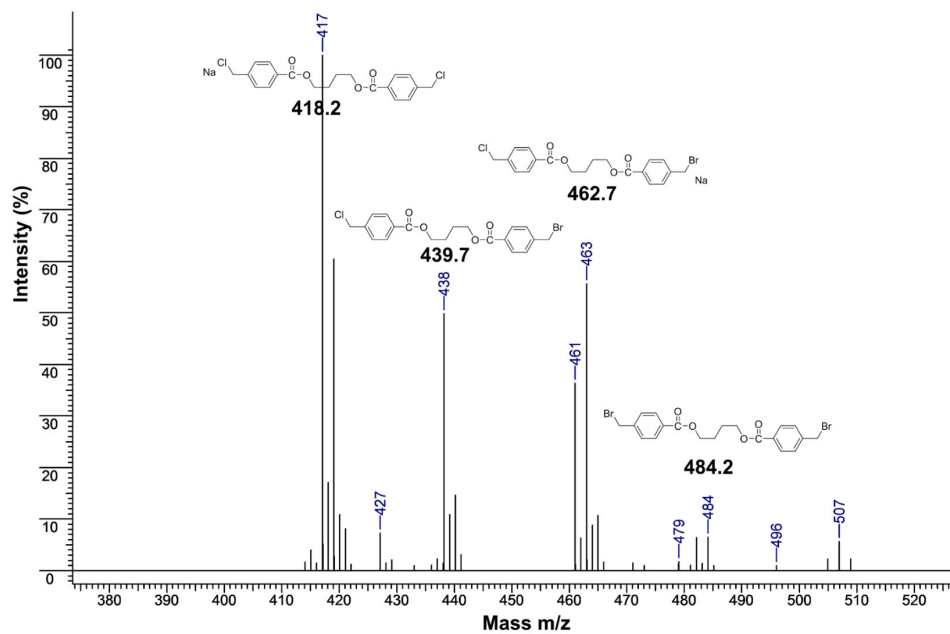


Figure S3.3. ESI MS spectrum of BDMB.

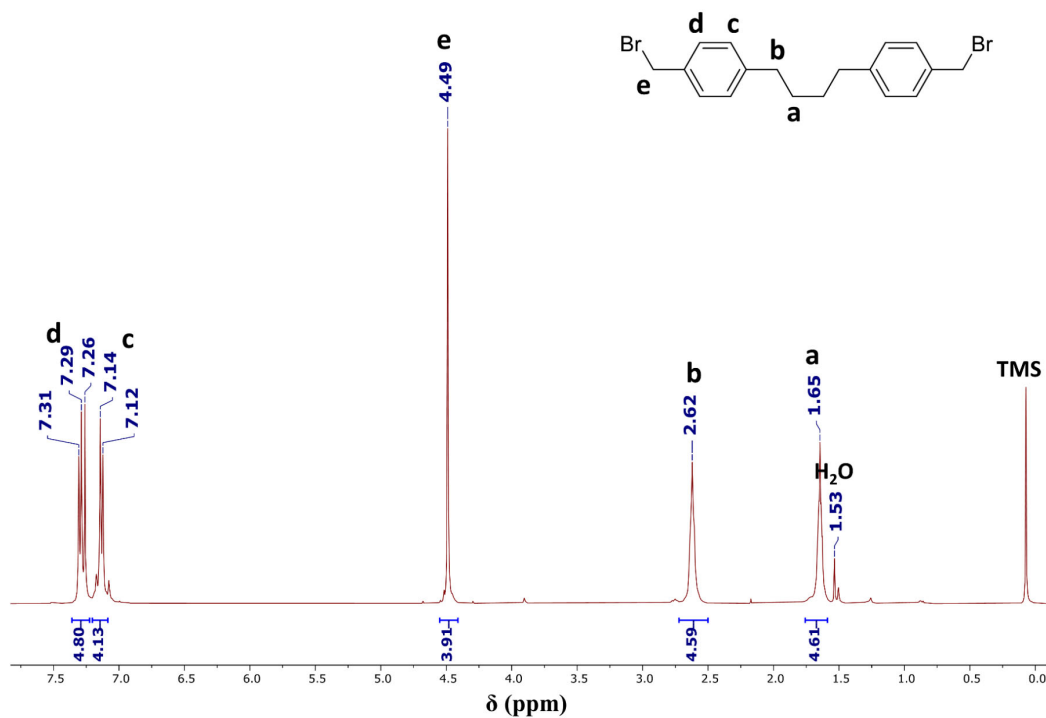


Figure S3.4. <sup>1</sup>H NMR spectrum of BBPB recorded in CDCl<sub>3</sub>.

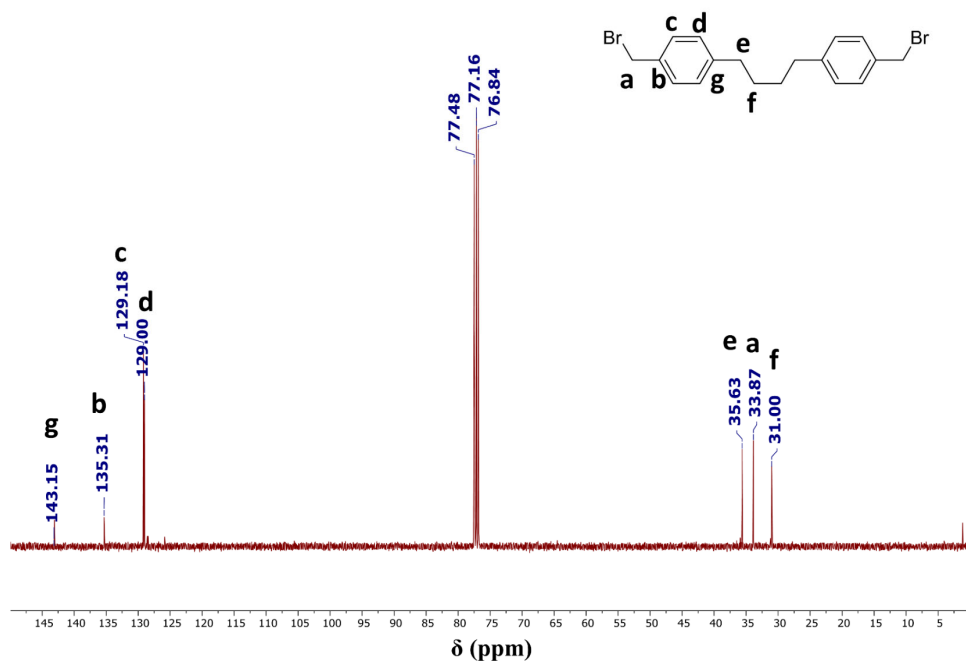


Figure S3.5. <sup>13</sup>C NMR spectrum of BBPB recorded in CDCl<sub>3</sub>.

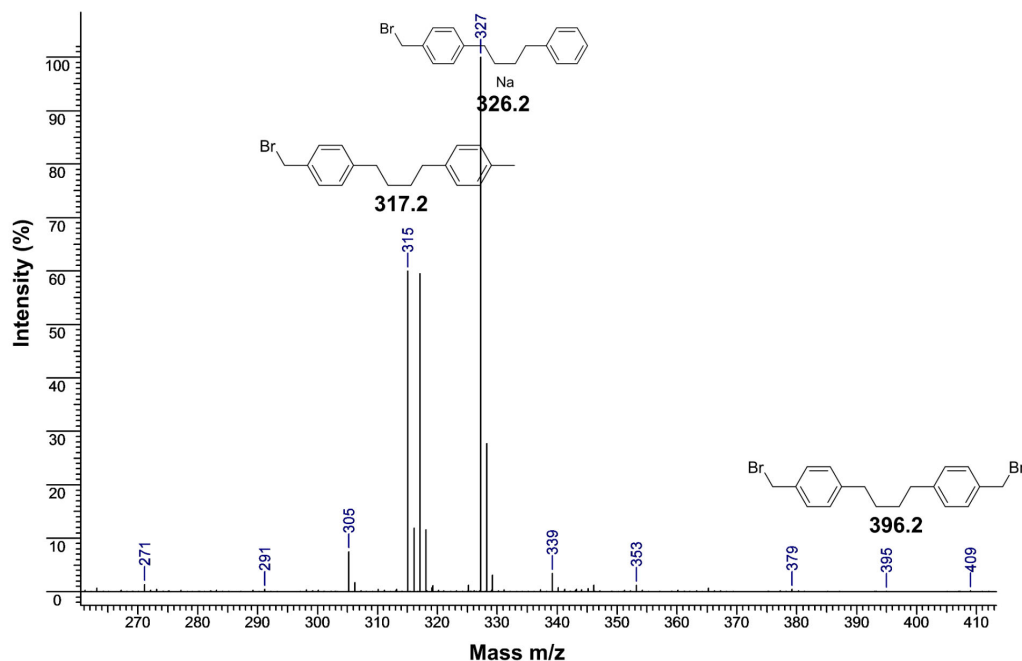


Figure S3.6. APPI-MS spectrum of BBPB.

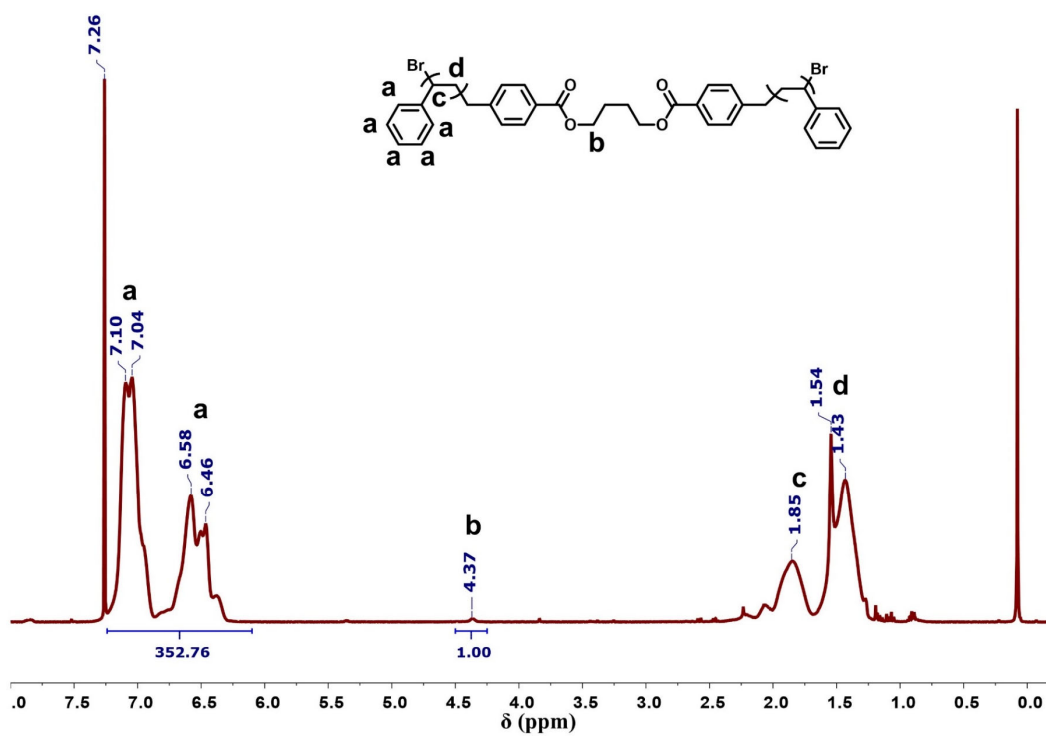


Figure S3.7.  $^1\text{H}$  NMR spectrum of a PS(ester) sample with  $M_n = 50$  kDa.

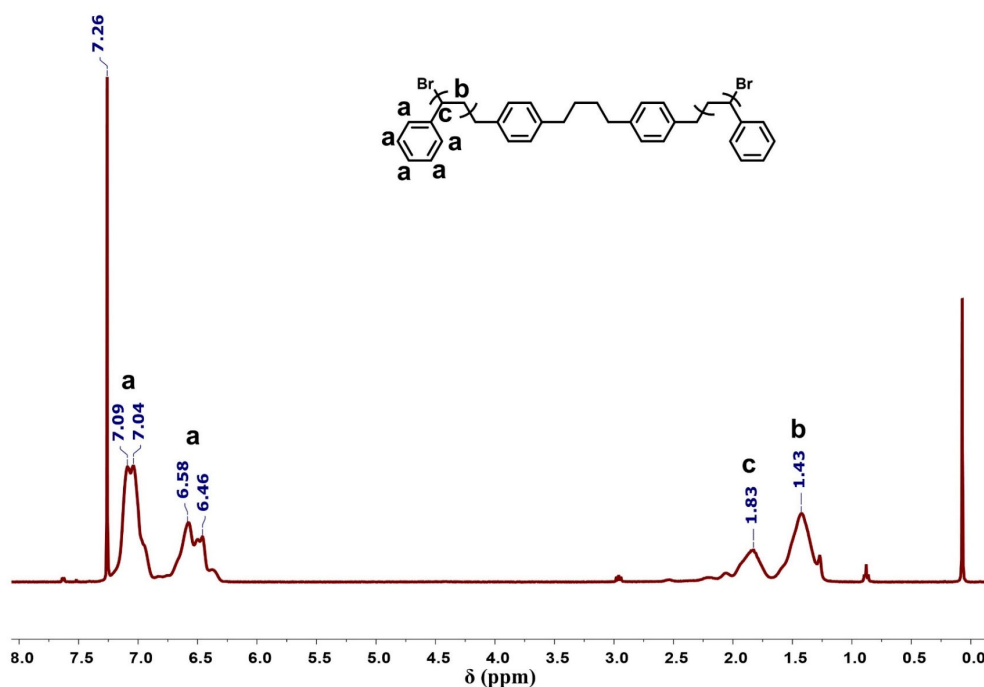


Figure S3.8.  $^1\text{H}$  NMR spectrum of a PS(carbon) sample with  $M_n = 29$  kDa.

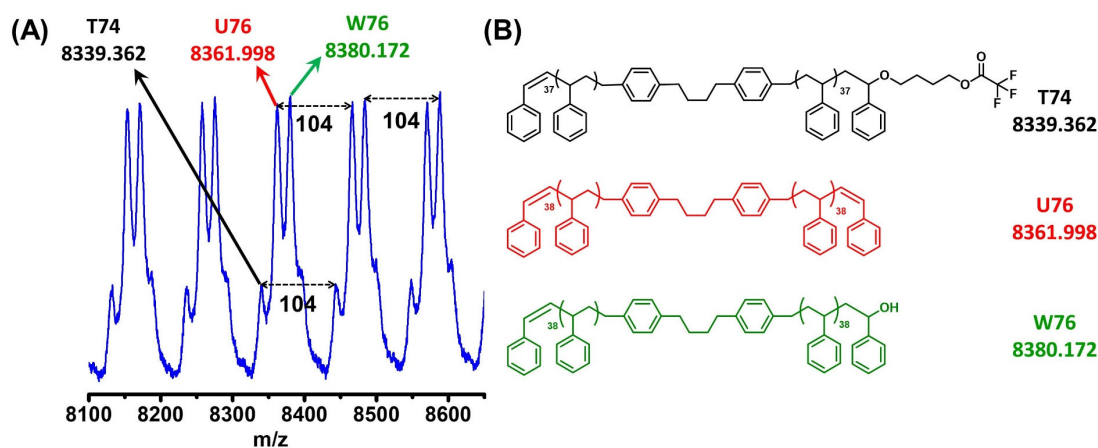
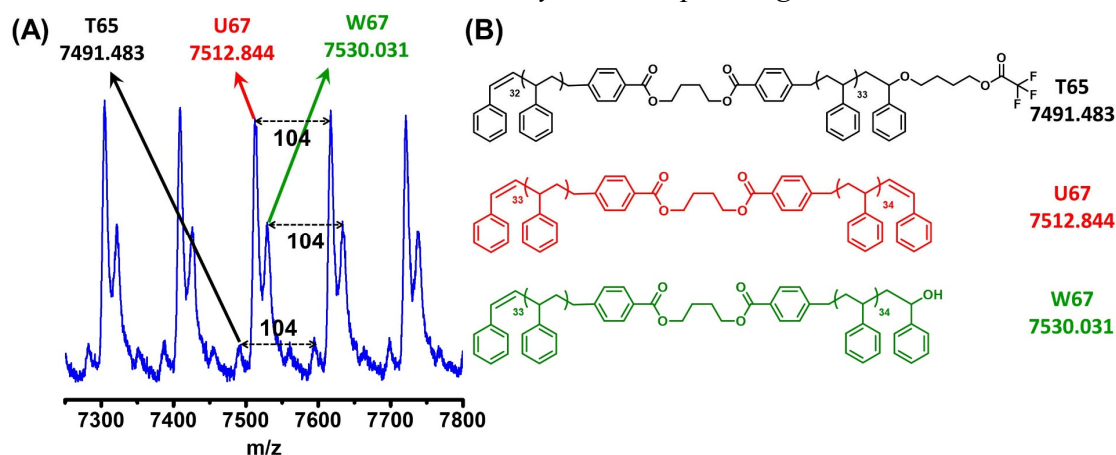
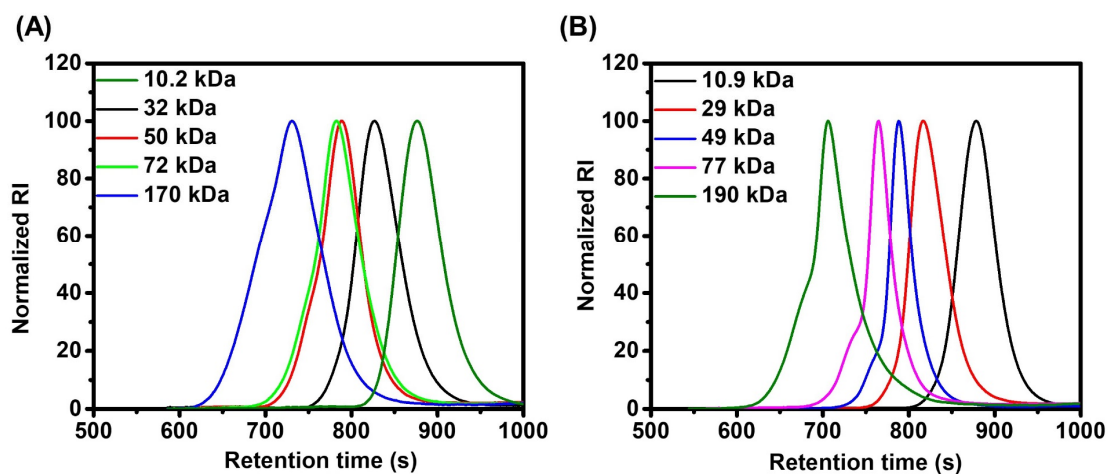


Figure S3.9. (A) MALDI TOF mass spectrum of a PS(carbon) polymer with  $M_n = 10.9$  kDa; (B) Chemical structures of the three most intense series of peaks: U series (U76, degree of polymerization = 76); T series (T74, degree of polymerization = 74) and W series (W76, degree of polymerization = 76).



**Figure S3.10.** (A) MALDI TOF mass spectrum of a **PS(ester)** polymer with  $M_n = 10.2$  kDa; (B) Chemical structures of the three most intense series of peaks: U series (U67, degree of polymerization = 67); T series (T65, degree of polymerization = 65) and W series (W67, degree of polymerization = 67).



**Figure S3.11.** GPC traces of (A) **PS(ester)** polymers with  $M_n = 10.2$  kDa (olive), 32 kDa (black), 50 kDa (red), 72 kDa (green) and 170 kDa (blue); (B) **PS(carbon)** polymers with  $M_n = 10.9$  kDa (black), 29 kDa (red), 49 kDa (blue), 77 kDa (pink) and 190 kDa (olive).

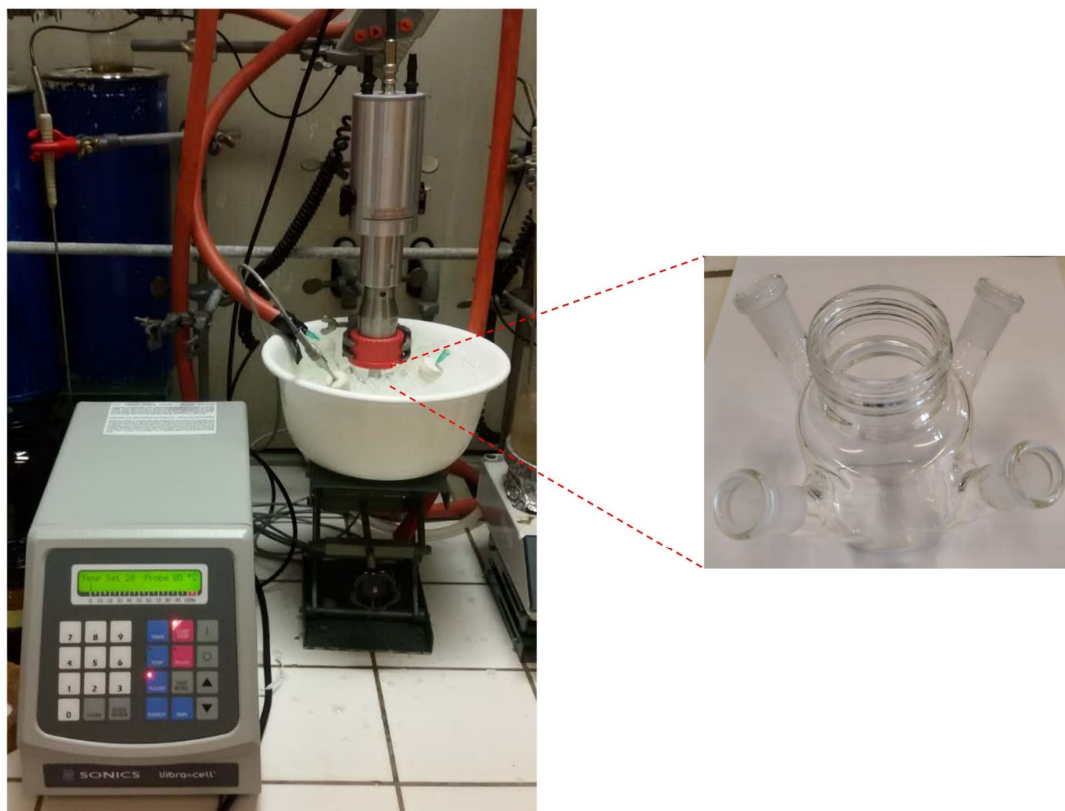


Figure S3.12. Setup that was used for the ultrasonication experiments.

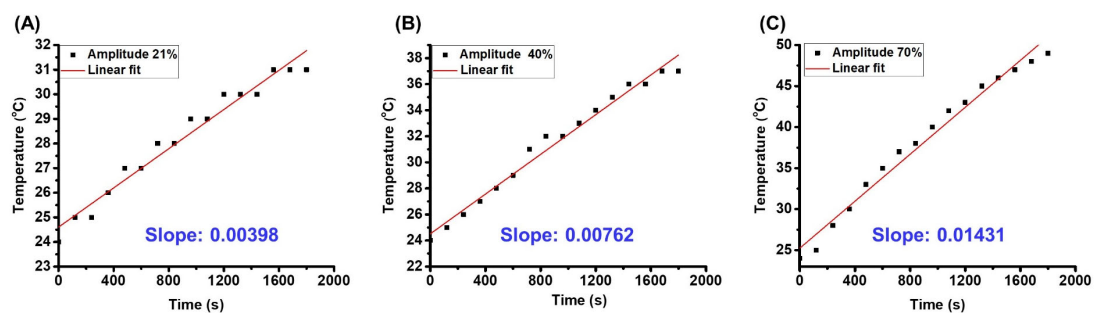
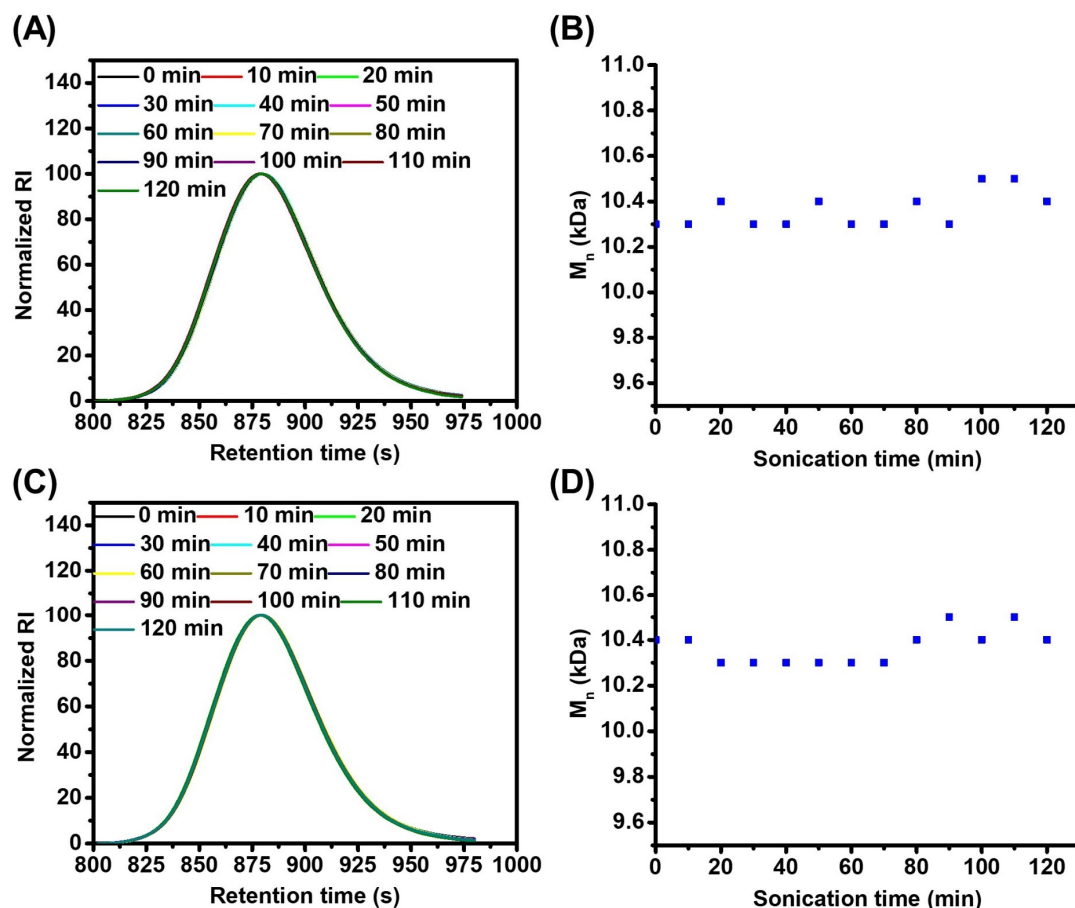
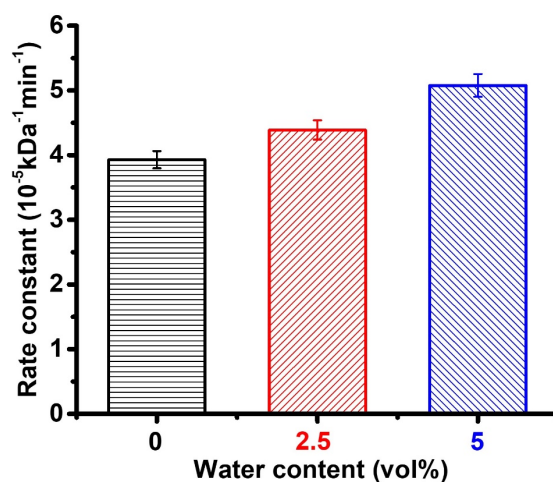


Figure S3.13. Temperature of water as a function of sonication time at amplitudes of:

(A) 21%; (B) 40% and (C) 70%. The slope of the linear fit was used as  $\Delta T/\Delta t$ .



**Figure S3.14.** (A) GPC traces of a **PS(ester)** sample with an initial  $M_n = 10.3$  kDa upon ultrasonication in THF for different times at a power density of  $1.88 \text{ W/cm}^2$ ; (B)  $M_n$  as a function of sonication time for a **PS(ester)** sample with an initial  $M_n = 10.3$  kDa in THF at a power density of  $1.88 \text{ W/cm}^2$ ; (C) GPC traces of a **PS(ester)** sample with an initial  $M_n = 10.4$  kDa upon ultrasonication THF + 5 vol% water for different times at a power density of  $1.88 \text{ W/cm}^2$ ; (D)  $M_n$  as a function of sonication time for a **PS(ester)** sample with an initial  $M_n = 10.4$  kDa in THF + 5 vol% water at a power density of  $1.88 \text{ W/cm}^2$ .



**Figure S3.15.** Rate constants of degradation determined for a **PS(ester)** sample with an initial  $M_n$  of 170 kDa upon ultrasonication in THF and THF + 2.5 and 5 vol% water at power density  $1.88 \text{ W/cm}^2$ .

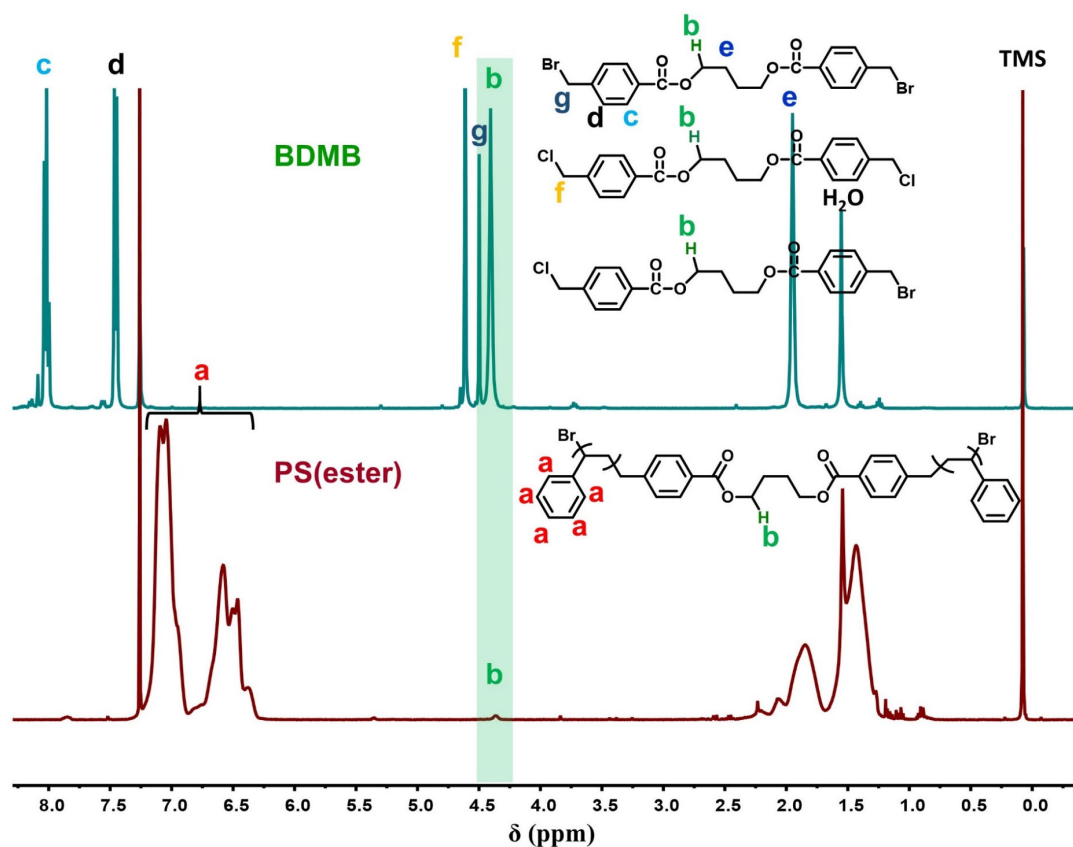


**Figure S3.16.**  $^1\text{H}$  NMR spectra of a **PS(ester)** sample with an initial  $M_n$  of 50 kDa (bottom) and BDMB (top) recorded in  $\text{CDCl}_3$ .

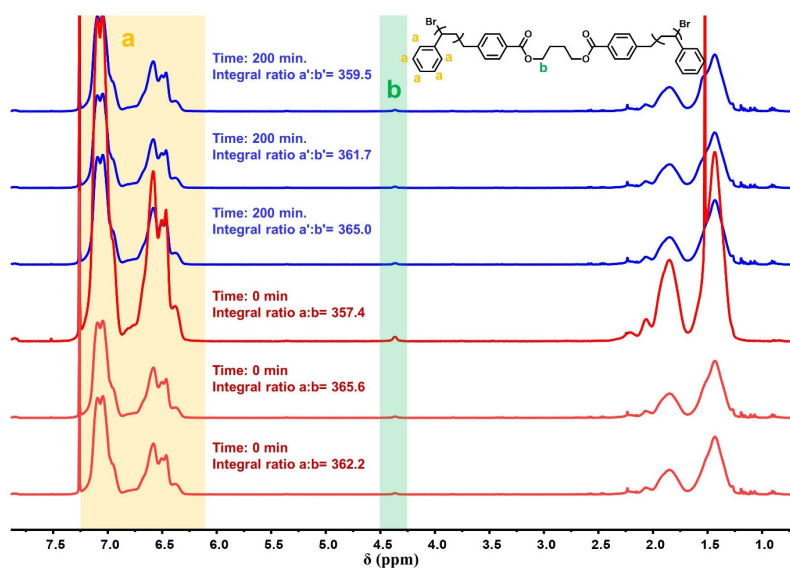


**Figure S3.17.**  $^1\text{H}$  NMR spectra of a PS(ester) sample with an initial  $M_n$  of 50 kDa before (0 min) and after 200 min ultrasonication in MEK at power density  $1.88 \text{ W/cm}^2$ . Three replicates from each time point were collected and analyzed independently.

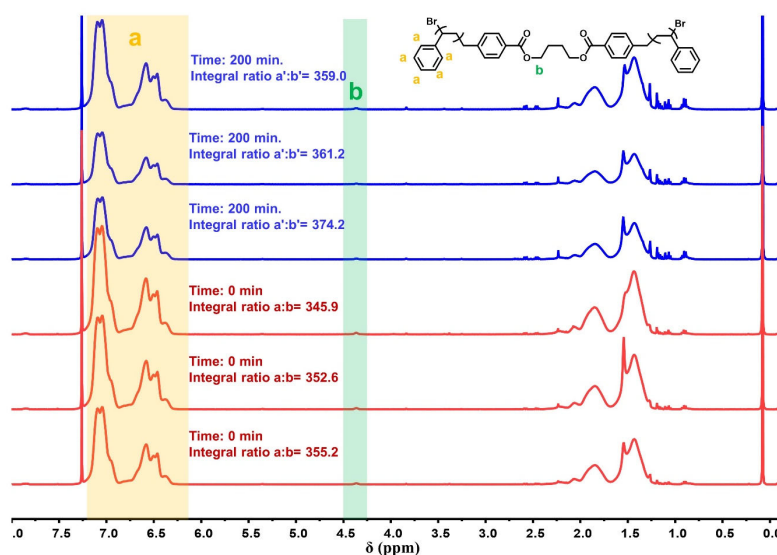


**Figure S3.18.**  $^1\text{H}$  NMR spectra of a PS(ester) sample with an initial  $M_n$  of 50 kDa before (0 min) and after 200 min ultrasonication in MEK + 2 vol% water at power density  $1.88 \text{ W/cm}^2$ . Three replicates from each time point were collected and analyzed independently.

density  $1.88 \text{ W/cm}^2$ . Three replicates from each time point were collected and analyzed independently.

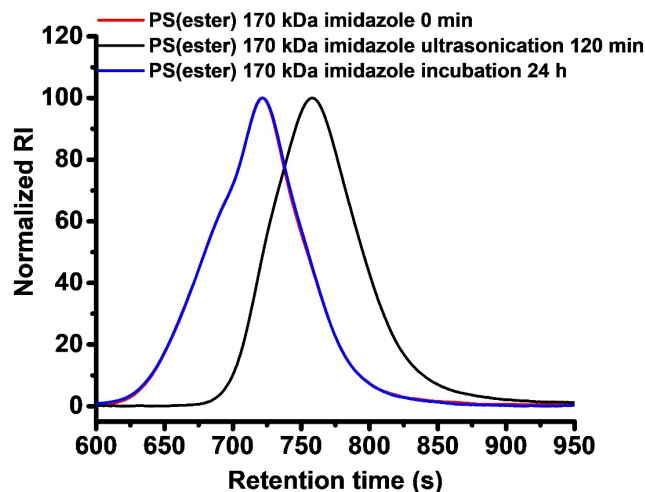


**Figure S3.19.** GPC traces of a **PS(ester)** polymer with an initial  $M_n$  of 170 kDa (red), of the same polymer after ultrasonication in THF + 5 vol% water with 0.1 M imidazole for 120 min at power density of  $1.88 \text{ W/cm}^2$  (black) as well as after incubation in THF + 5 vol% water with 0.1 M imidazole for 24 h with no ultrasonication (blue).

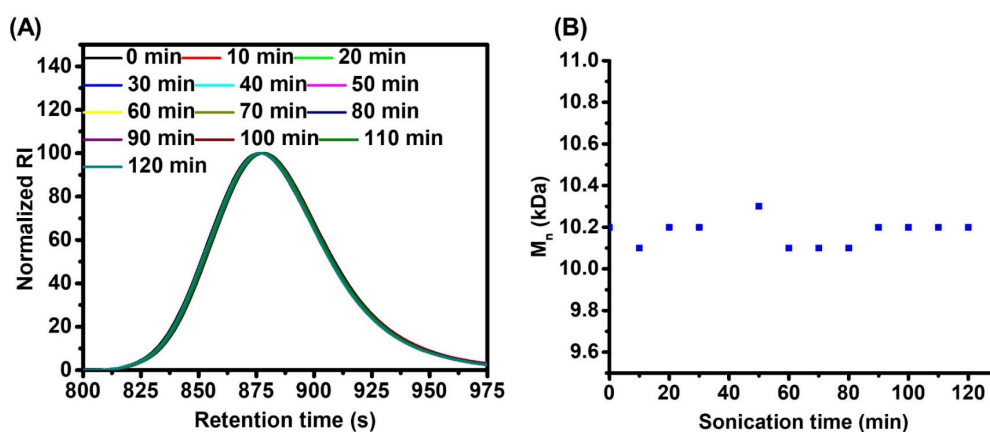


**Figure S3.20.** (A) GPC traces of a **PS(ester)** sample with an initial  $M_n = 10.2 \text{ kDa}$  upon ultrasonication in THF + 5 vol% water for different times at a power density of  $6.76$

W/cm<sup>2</sup>; (B)  $M_n$  as a function of sonication time for a **PS(ester)** sample with an initial

$M_n = 10.2$  kDa in THF + 5 vol% water at a power density of 6.76 W/cm<sup>2</sup>.

## **4. Light-Activated, Bioadhesive Poly(2-Hydroxyethyl Methacrylate) Brush Coatings**

### **4.1. Introduction**

Rapid adhesion between tissue interfaces or between tissue and synthetic materials is sought after clinically to accelerate wound healing and facilitate the integration of implantable medical devices and biosensors. Sutures and staples are widely used to mediate tissue fixation. The use of these mechanical techniques, however, can damage surrounding tissue and lead to scar formation. One way to overcome these drawbacks is the use of bioadhesive materials that can form (covalent) chemical bonds with the tissue.<sup>204-206</sup>

A number of bioadhesive materials platforms, which can chemically mediate tissue adhesion has been developed.<sup>207-213</sup> These include both synthetic polymeric materials, most notably cyanoacrylates but also PEG-based systems, as well as biological polymers such as fibrin. Each of these systems has distinguished advantages but also specific limitations. Cyanoacrylate based adhesives, for example, provide relatively high adhesion strengths, but are brittle and relatively inflexible. Fibrin and PEG-based adhesives, in contrast, provide a soft interface, but generally only provide limited adhesive strength.

Most of the adhesive materials discussed above are applied as one or two component formulations in the form of a viscous liquid. This only provides limited control over the amount of material that is applied, and thus over the thickness of the adhesive layer. In case of two-component formulations, specialized delivery syringes are required that

allow to mix the two components immediately before application. Another challenge with many bioadhesives is that network formation and interfacial bonding set in as soon as the two components of the adhesive are mixed and brought into contact with the tissue. As a consequence, precise control of the activation of the adhesive is limited, which makes it difficult to reposition or readjust the tissue–tissue or tissue–device interface after application of the adhesive. One way to overcome this limitation is to use external stimuli to trigger interfacial bonding. Light is an attractive and powerful stimulus as it potentially allows to control adhesion in time and space. A number of reports has been published that describe light activated tissue adhesives.<sup>214-222</sup> Often, UV light is used to initiate network formation and interfacial bonding.<sup>215-218,221,222</sup> In other cases, UV-irradiation has been used to convert non-reactive, non-adhesive functional groups such as diazirines, into carbene moieties that can react to form covalent bonds with the tissue.<sup>214,219,220,223,224</sup>

Most of the light activated adhesives that have been reported so far are applied as a gel or as a liquid formulation. One interesting exception is a study in which photoreactive diazirine moieties were attached to amine-functionalized PLGA substrates.<sup>214</sup> Upon photoirradiation, diazirines generate carbenes that can insert in C-H, N-H and O-H bonds present in tissue. While this work demonstrated the feasibility of the diazirine motif to photochemically mediate the formation of robust, covalent bonds with tissue, the specific system also suffers from a number of limitations. One drawback is the relatively hydrophobic nature of the PLGA film, which impedes effective wetting of the tissue. Another limitation is the rigid nature of the PLGA substrate, which hampers

the establishment of close, interfacial contact between the tissue and the synthetic material. One possible, general strategy to alleviate these challenges is to modify the substrate of interest with a thin, water-swellaable and soft polymer thin film, which provides conformal contact with the tissue surface and is modified with functional groups that can be transformed on-demand using, for example, light from non-adhesive to tissue reactive, and thus adhesive. This article explores the feasibility of this strategy, using thin, chain-end tethered polymer coatings, polymer brushes, prepared via surface-initiated atom transfer radical polymerization (SI-ATRP) as a model system. SI-ATRP is an attractive method to prepare these systems as it provides relatively good control over the molecular weight of the surface grafted polymer (and thus film thickness) as well as the chemical composition and functionality of the resulting polymer films.<sup>104,225</sup> The polymer brushes investigated in this study were obtained by SI-ATRP of 2-hydroxyethyl methacrylate (HEMA). This monomer was selected since polymer brushes containing side chain ethylene glycol functional groups such as PHEMA and poly(poly(ethylene glycol methacrylate)) (PPEGMA) are well known for their ability to prevent non-specific adsorption of proteins, cells, bacteria as well as fungi.<sup>115,121,226-228</sup> PHEMA brushes as, a consequence, thus represent an attractive, non-bioadhesive model polymer coating. To convert these non-bioadhesive PHEMA brushes into tissue-binding coatings, two light-mediated strategies have been explored. A first strategy involves direct irradiation of a PHEMA brush film with UV-light. The second strategy uses PHEMA brushes that have been post-modified to introduce photo-reactive diazirine moieties. For each of these two classes of photoactive brush coatings, this

manuscript presents the synthesis and characterization of the brush films as well as their evaluation as bioadhesive coatings in experiments that use bovine meniscus tissue.

## **4.2. Experimental Section**

### **4.2.1. Materials**

All chemicals were used as received unless described otherwise. Copper(I)chloride (99.999%), copper(II)bromide (99.999%), copper(I)bromide (99.995+ %), 2,2'-bipyridyl (bpy) (99%), 2-bromo-2-methylpropionyl bromide, chlorodimethylsilane (98%), dimethyl sulfoxide (DMSO, 99.5%), aniline (99.5%), N,N'-dicyclohexylcarbodiimide (DCC, 99%), 4-(dimethylamino)pyridine (DMAP, 99%), 2-hydroxyethyl methacrylate (HEMA) (97%) and 2-methacryloyloxyethyl phosphorylcholine (MPC, 97%) were purchased from Sigma Aldrich. Before use, MPC was washed with cold acetonitrile to remove the inhibitor, filtered and dried under vacuum. HEMA was freed from the inhibitor by passing through a column of activated, basic aluminum oxide and distilling prior to use. Aniline was distilled before use. 4-[3-(Trifluoromethyl)-3H-diazirin-3-yl]benzoic acid (TFMDA, 98%) was purchased from TCI. Acetic anhydride was purchased from Fluka. The ATRP initiator (6-(2-bromo-2-methyl)propionyloxy)hexyldimethylchlorosilane was synthesized as previously reported.<sup>229</sup> Methanol (MeOH) was purchased from Alfa Aesar. Triethylamine was purchased from Aldrich and distilled over KOH before use. Dichloromethane (DCM) and toluene were purified and dried using a solvent-purification system (PureSolv). Deionized water was obtained from a Millipore Direct-Q5 water purification system. For adhesion studies, polymer brushes were grown from fused silica wafers, which had

been cut into rectangular slides of  $\sim 1.5 \text{ cm} \times 1.5 \text{ cm}$ . Ellipsometry and X-ray photoelectron spectroscopy (XPS) analyses were performed on polymer brushes, which were prepared using  $0.8 \text{ cm} \times 1 \text{ cm}$  rectangular silicon substrates. Samples for UV-vis analysis were grafted from  $0.8 \text{ cm} \times 1 \text{ cm}$  rectangular fused silica substrates. Tissue specimens were harvested from mature bovine knee joints procured from the local abattoir shortly after slaughter of the animals (12-18 months of age). Before sample preparation, the isolated tissue was washed in PBS, which was obtained from Thermo Fisher Scientific.

#### **4.2.2. Methods**

XPS was carried out using an Axis Ultra instrument from Kratos Analytical equipped with a conventional hemispheric analyzer. The X-ray source employed was a monochromatic Al K $\alpha$  (1486.6 eV) source operated at 100 W and  $10^{-9}$  mbar. Surfaces were cleaned with a Femto O<sub>2</sub> Plasma system (200 W, Diener Electronic). Dry film thicknesses were determined using a SemiLAB (SE2000) ellipsometer and calculated based on a four-layer silicon/silicon oxide/polymer brush/air model, assuming the polymer brush to be isotropic and homogeneous. A Hamamatsu Lightningcure L8858-02, 200 W UV lamp was used as the light source. The spectral characteristics of this UV lamp, which has a center wavelength of 365 nm, are included in Supporting Information Figure S4.1. For some experiments, a Mercury Line Bandpass Filter with a center wavelength of  $365 \pm 2 \text{ nm}$  was used to block lower wavelength UV light (in particular the  $\sim 250 \text{ nm}$  wavelength band). UV-Visible absorbance spectra were recorded using a Varian Cary 100 Bio UV-Visible spectrophotometer at room

temperature. Attenuated total reflectance Fourier transform infrared (ATR-FTIR) spectroscopy was carried out on a Nicolet 6700 FT-IR spectrometer from Thermo Scientific.

#### **4.2.3. Procedures**

Preparation of ATRP initiator modified silica and fused silica surfaces. Silica and fused silica surfaces were first sonicated in ethanol, water and acetone (5 minutes each). The substrates were dried under a flow of nitrogen and exposed to oxygen plasma for 20 minutes. After that, the substrates were transferred immediately to a reactor containing a 10 mM solution of (6-(2-bromo-2-methyl)propionyloxy)hexyldimethylchlorosilane in dry toluene under nitrogen atmosphere. The reaction was allowed to proceed for 16 hours at room temperature after which the modified surfaces were removed and washed extensively with toluene, ethanol and DCM. All substrates were dried under a flow of nitrogen and subsequently transferred to a reactor for SI-ATRP.

Surface-initiated atom transfer radical polymerization of 2-hydroxyethyl methacrylate (HEMA). Surface-initiated atom transfer radical polymerization of HEMA was carried out following an established protocol.<sup>230</sup>

Surface-initiated atom transfer radical polymerization of 2-methacryloyloxyethyl phosphorylcholine (MPC). MPC (6.65 g, 22.5 mmol) was placed in a Schlenk tube under nitrogen atmosphere. The Schlenk tube was subsequently evacuated and filled with nitrogen three times. Then, 2,2'-bipyridyl (bpy) (140.5 mg, 0.9 mmol), CuBr<sub>2</sub> (10.05 mg, 0.045 mmol) and a methanol/water solution (4:1, v:v, 15 mL) were added into another Schlenk tube. After three freeze/pump/thaw cycles, the solution was frozen.

Then, CuBr (64.5 mg, 0.45 mmol) was added under nitrogen flow and the frozen solution was thawed. The molar ratio of MPC/CuBr/CuBr<sub>2</sub>/bpy in the reaction mixture was 50:1:0.1:2. The mixture was stirred under nitrogen and briefly sonicated to completely dissolve the CuBr. After an additional freeze/pump/thaw cycle, the resulting ATRP solution was cannula transferred to a Schlenk tube containing the MPC powder. After complete dissolution of MPC, the reaction mixture was cannula transferred to nitrogen-purged glass vials containing an initiator-functionalized substrate. After 15 h, the substrate was removed from the ATRP solution, extensively rinsed with methanol, water and ethanol and finally dried under a flow of N<sub>2</sub>.

**Albright-Goldman oxidation of PHEMA brushes.** The post-polymerization oxidation of PHEMA brushes was performed following a previously published protocol.<sup>231</sup>

**Aniline labeling of the aldehyde-functionalized PHEMA brushes.** Aniline labeling of aldehyde-functionalized PHEMA brushes was performed following a previously published protocol with slight modifications.<sup>232</sup> Instead of poly(poly(ethylene glycol) methacrylate) (PPEGMA) brush coated substrates and a reaction time of 24 h, aldehyde functionalized PHEMA brushes were used, which were incubated in 10 mL of an ethanol solution containing 1 mL of aniline for 5 h.

**Post-polymerization modification of PHEMA brushes with TFMDA.** Post-polymerization modification of PHEMA brushes with TFMDA was performed by using a previously published protocol with slight modifications.<sup>233</sup> In a typical experiment, 92 mg (0.08 mmol) TFMDA and 107.2 mg (0.88 mmol) DMAP were dissolved in 24 mL

dry DCM. The resulting solution was transferred to a nitrogen purged reaction vessel containing the PHEMA modified surfaces in 16 mL of a DCM solution containing 91.2 mg (0.44 mmol) DCC. After stirring the reaction solution at 0 °C for 5 min and subsequently 1 or 16 h at room temperature, substrates were washed extensively with DCM and ethanol and dried under a flow of nitrogen. TFMDA concentrations ( $[c]$ ) were calculated according to the Beer-Lambert law,  $A = \epsilon \cdot l \cdot [c]$ , where “ $A$ ” is the measured absorbance, “ $\epsilon$ ” is the calculated molar extinction coefficient and “ $l$ ” is the polymer brush thickness.

**Adhesion Testing.** The adhesive performance of the brush-coated substrates was evaluated in tensile mode, as schematically illustrated in **Figure S4.2**, against fresh bovine meniscus tissue. Cylindrical discs with a diameter of 6.8 mm were cut in the circumferential direction from the central region of bovine lateral meniscus and then glued onto a metal support using cyanoacrylate glue (LOCTITE® 401). The brush coated fused silica samples were placed on top of the tissue surface and then exposed to UV illumination with an intensity of 17.3 mW/cm<sup>2</sup> at 365 nm for a defined period. Directly after illumination, the samples were mounted into an Instron E3000 linear mechanical testing machine (Norwood, MA, United States) equipped with a 50 N load cell. Tests were performed with a constant speed of 0.5 mm·s<sup>-1</sup> at room temperature and the applied force was recorded. The adhesion strength was determined by dividing the maximum detected force by the surface area of the meniscus. As an example, Figure S4.3 illustrates this experiment using a PHEMA brush with a dry thickness of 145 nm that was exposed to UV light for 3 minutes. Tests were performed until failure at the

polymer brush–tissue interface. Each test was performed with at least 5 replicates. For adhesion tests on PHEMA coated substrates, which were activated by Albright-Goldman oxidation, the brush-modified substrates were placed on top of and in contact with the tissue for 3 min without UV irradiation.

**Statistical Analysis.** Tensile adhesion data are presented as means  $\pm$  standard deviation across samples. Statistical analysis was performed using one-way ANOVA. A p-value  $< 0.05$  was considered statistically significant.

### **4.3. Results and Discussion**

The manuscript investigates the feasibility of two light-activated polymer brush-based bioadhesive coatings. First, the preparation, characterization and bioadhesive properties of coatings obtained by direct UV-irradiation of PHEMA brushes will be presented. After that, a second approach towards light-activated polymer brushes, which are obtained by post-polymerization modification of PHEMA films with photo-reactive diazirine moieties will be discussed.

#### **Direct UV-activation of PHEMA Brushes**

The first strategy towards light-activated polymer-based bioadhesive surfaces is based on the direct UV-irradiation of PHEMA brushes (**Figure 4.1**). PHEMA, and other side chain ethylene glycol substituted polymethacrylate brushes are well-known for their ability to prevent the non-specific adsorption of proteins, cells, bacteria and fungi.<sup>121,226-</sup>

<sup>228</sup> It has also been shown that irradiation of PPEGMA brushes, as well as oligo(ethylene glycol) terminated self-assembled monolayers with  $\sim 250$  nm UV light generates functional groups, presumably aldehydes, which have been used to covalently

bind proteins.<sup>234-239</sup> Covalent immobilization of proteins on aldehyde surfaces involves the formation of imine bonds that are generated by reaction between aldehyde groups and amine groups in proteins. As tissue extracellular matrix is rich in amine groups, this suggests that the photochemical reactivity of PHEMA or PPEGMA brushes may not only be explored to allow light-controlled protein immobilization, but may possibly also be harnessed to create on-demand light activated tissue-adhesive thin polymer interfaces. To explore the feasibility of this concept, PHEMA brushes with a dry film thickness of 145 nm were grown from silicon wafers or fused silica substrates via SI-ATRP as outlined in **Scheme 4.1**. As a control, putatively non-photoreactive control coating, poly(2-methacryloyloxyethyl phosphorylcholine) (PMPC) brushes with a dry film thickness of 154 nm were used, which were also produced via SI-ATRP. PMPC brushes are also very effective non-biofouling surface coatings,<sup>240-242</sup> but in contrast to PHEMA brushes, do not produce tissue reactive groups upon UV-irradiation (*vide infra*).

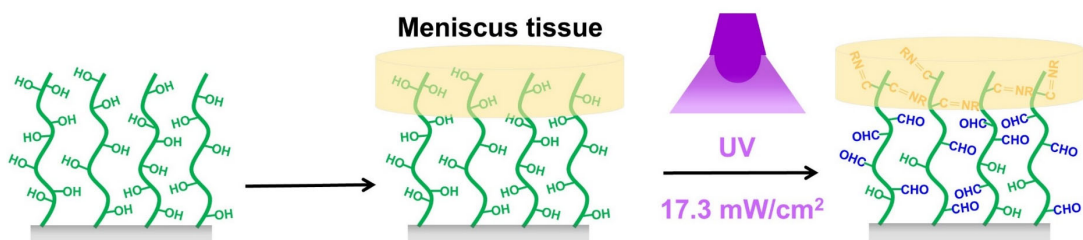
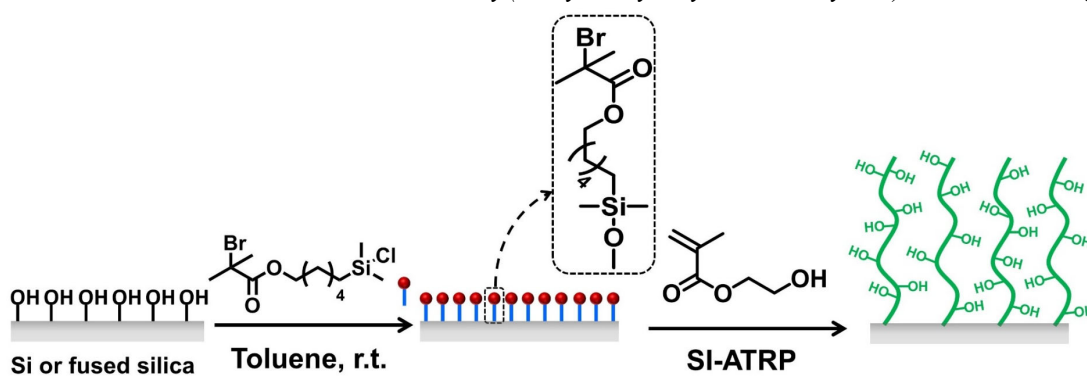


**Figure 4.1.** Schematic illustration of the UV-activation of PHEMA brushes and subsequent adhesion to meniscus tissue.



**Scheme 4.1.** Synthesis of PHEMA brushes via SI-ATRP

The ability of the PHEMA brushes to act as on-demand, light-activated adhesive coatings was investigated using meniscus tissue. Details of the experimental set-up are provided in **Figure S4.2**. PHEMA brushes with a dry film thickness of 145 nm grown from fused silica substrates were placed in contact with the meniscus tissue and subsequently irradiated with UV light for a defined period of time. After that, adhesion strengths were determined at room temperature using a 50 N load at a constant speed of 0.5 mm.sec<sup>-1</sup>. The adhesive properties of the UV-activated PHEMA brushes were compared with those of 154 nm thick PMPC brushes that were subjected to UV-irradiation under the same conditions. As a second control, PHEMA brushes with a dry film thickness of 191 nm were used, which were not activated by UV-irradiation, but instead were treated with DMSO/acetic anhydride before being put in contact with the meniscus tissue. The use of DMSO/acetic anhydride (“Albright–Goldman oxidation”) represents a wet-chemical strategy that has been used previously to convert hydroxyl side chain functional groups of PHEMA brushes into aldehyde moieties.<sup>231</sup>

**Figure 4.2** compares the adhesion strengths that were measured on untreated PHEMA brushes with those exposed to UV-irradiation for 1 or 3 min as well as on the PMPC

and wet-chemically oxidized PHEMA brush control samples. The results summarized in **Figure 4.2** show that the adhesion strengths of the PHEMA brushes increase upon UV-light irradiation and that increasing the duration of the UV treatment leads to a further, significant increase of the adhesion strength. The adhesion strengths that were measured on the UV-activated PHEMA brush films compare well with those that have been reported for fibrin glue and synthetic polymer adhesives, which were applied in a conventional way as a liquid/gel formulation on meniscus tissue.<sup>243-245</sup> The adhesion strengths recorded on the non-irradiated, control PHEMA brushes were comparable to those measured on the PMPC brushes. UV-irradiation of the PMPC brushes did not result in a change in the adhesion strength. Finally, the adhesion strengths measured on PHEMA brushes, which were subjected to UV-irradiation for 3 min were comparable to those determined on PHEMA brush films that were activated via Albright-Goldman oxidation. This last observation is consistent with the formation of aldehyde groups upon UV-irradiation of the PHEMA brushes.

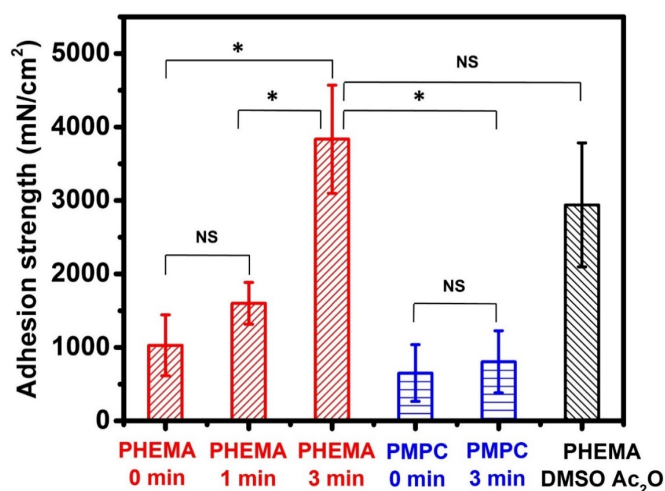


**Figure 4.2.** Adhesion strengths of PHEMA brush coated substrates ( $d = 145$  nm) treated with UV light for 0, 1 and 3 min (red), PMPC brush coated substrates treated with UV

light for 0 and 3 min (blue) and DMSO Ac<sub>2</sub>O activated PHEMA brush coated substrates (black). Asterisks indicate statistically significant differences whereas NS represent not significant difference between two conditions. Significant at \*  $p < 0.05$ .

Next, a number of experiments was carried out to elucidate the effect of UV-irradiation on the chemical composition and structure of the PHEMA brushes. First, a 145 nm thick PHEMA brush grafted from a silicon substrate was subjected to UV-irradiation for 3 min and subsequently analyzed by XPS and ellipsometry. **Figure 4.3A** compares the XPS C<sub>1s</sub> high resolution scans that were recorded on the brush prior to and after 3 min irradiation time. Most prominent is the decrease in the intensity of the shoulder at 285.9 eV, which is indicative of changes in the chemical composition of the brush upon UV-irradiation. Ellipsometric analysis of the PHEMA brush revealed a decrease in film thickness from 145 nm to 75 nm indicating that these changes in chemical structure are accompanied by partial photodegradation of the brush film. The observed changes in chemical composition as well as the partial photodegradation are in agreement with the results of previous work in which 250 nm wavelength UV-laser light was used to generate protein-patterned PPEGMA brushes.<sup>234-239</sup> In contrast, when the PHEMA brush was subjected to UV light using a bandpass filter that removes the lower wavelength band around 250 nm, no changes in the C<sub>1s</sub> high resolution XPS scans were observed (**Figure S4.4**) and the film thickness remained constant. This indicates that it is the lower wavelength, UV-C part of the light spectrum of the light source that is responsible for the photoactivation and degradation of the PHEMA brushes.

**Figure 4.3B**, **C** and **D** show XPS high-resolution scans and FTIR spectra recorded on PHEMA brush samples that were activated by Albright-Goldman oxidation. To illustrate the reactivity of the activated brushes towards amines, these films were also treated with aniline, which served as a model amine. Comparison of the C<sub>1s</sub> high resolution scans taken from PHEMA brushes before and after Albright-Goldman oxidation (**Figure 4.3B**) reveals changes that are similar to those in **Figure 4.3A**, which is a further indication that UV-irradiation of PHEMA brushes results in the formation of tissue-reactive aldehyde groups. **Figure 4.3C** and **Figure 4.3D** show N<sub>1s</sub> high-resolution XPS scans and FTIR spectra of aldehyde functionalized PHEMA brushes generated via Albright-Goldman oxidation before and after reaction with aniline. The N<sub>1s</sub> high-resolution XPS scan recorded after the reaction reveals a signal at 398.9 eV, which is consistent with the formation of an imine bond upon reaction of aniline with the side chain aldehyde groups in the brush (**Figure 4.3C**).<sup>246,247</sup> Furthermore, the FTIR spectra in **Figure 4.3D** indicate the appearance of a small, new peak at 1600 cm<sup>-1</sup> after aniline labeling, which can be assigned to the C-C stretching vibrations of the aromatic aniline ring. In addition to the PHEMA brushes, also the influence of UV-irradiation on the PMPC control samples was studied. As for the PHEMA brushes, UV-irradiation was found to result in partial photodegradation. For the PMPC brushes, 3 min UV-irradiation resulted in a decrease in film thickness from 154 nm to 32 nm. **Figure S4.5**, finally, compares XPS spectra of the PMPC brushes before and after UV-irradiation. In contrast to the PHEMA brushes, these spectra do not indicate any changes in the chemical composition of the PMPC brushes.

Taken together, the results presented above indicate that direct UV-irradiation of PHEMA brushes provides a way to convert these polymer films, which are generally considered non-biofouling, into tissue-reactive adhesives. The model studies discussed in the previous paragraph indicate that the UV-irradiation generates aldehyde groups and that it is the lower wavelength part of the UV-spectrum that is responsible for these photochemical changes.

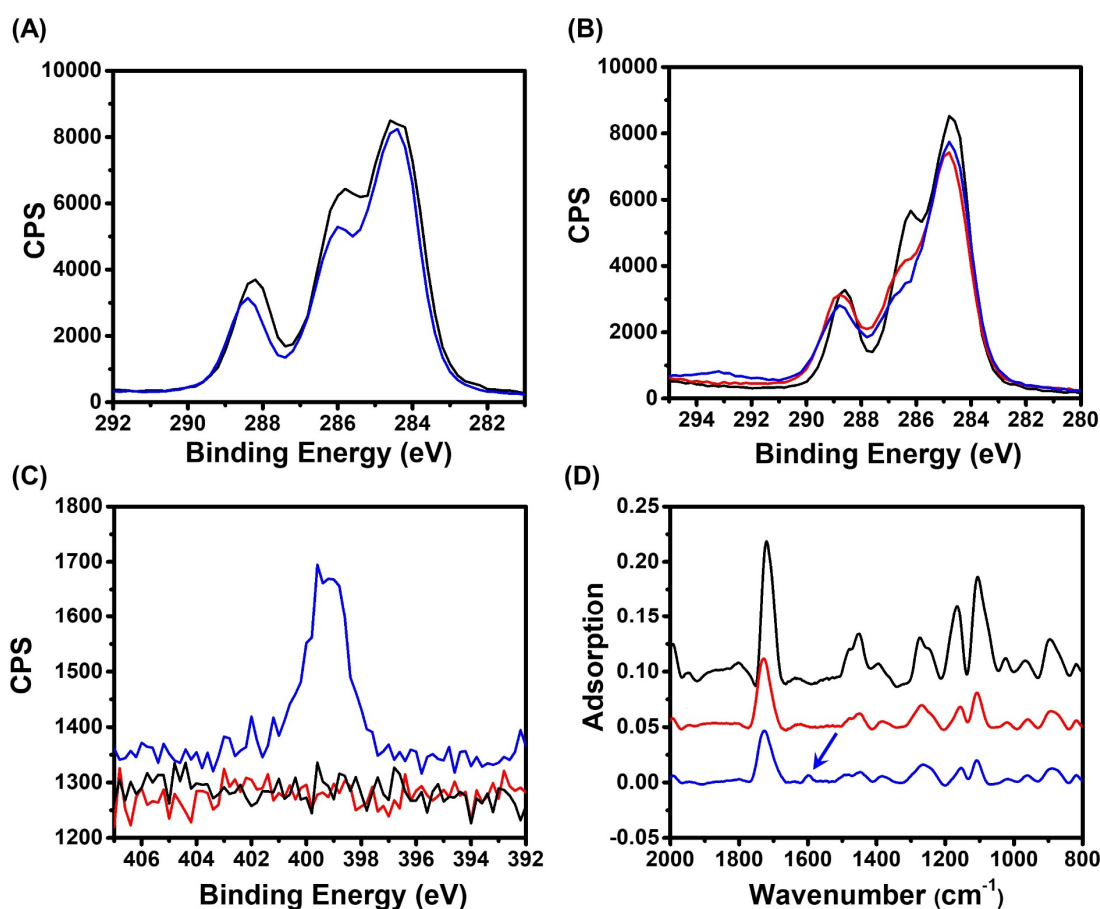


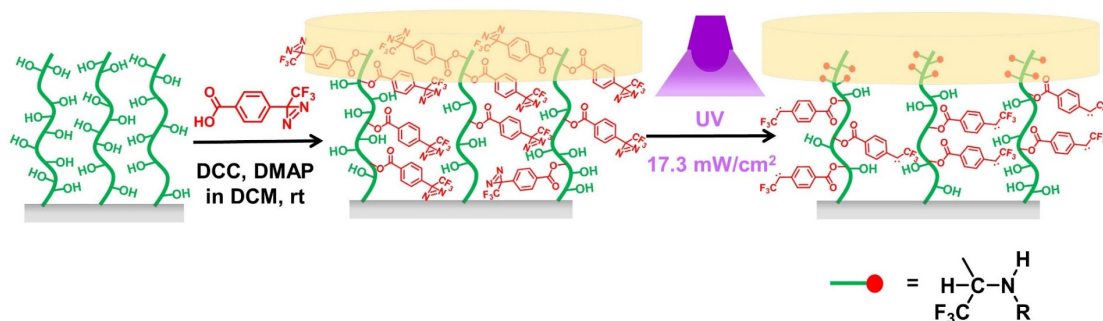
**Figure 4.3.** (A)  $C_{1s}$  high resolution XPS spectra of a PHEMA brush coated substrate before (black) and after treated with UV irradiation for 3 min (blue), (B)  $C_{1s}$  and (C)  $N_{1s}$  high resolution XPS scans of a PHEMA brush coated substrate (black), a DMSO/Ac<sub>2</sub>O activated PHEMA brush coated substrate (red) and an aniline labeled aldehyde functionalized PHEMA brush coated substrate (blue). (D) FTIR spectra of a

PHEMA brush coated substrate (black), a DMSO/Ac<sub>2</sub>O activated PHEMA brush coated substrate (red) and an aniline labeled aldehyde functionalized PHEMA brush coated substrate (blue).

### **UV-Activation of Diazirine Functionalized Brushes**

The work described above demonstrates that direct UV-irradiation of PHEMA brushes allows to introduce amine-reactive groups into these polymer thin films and transforms these otherwise non-fouling coatings into bioadhesive surfaces. While the data presented in **Figure 4.2** show that this approach allows to facilitate adhesion with meniscus tissue, there are also several limitations to this strategy. The most significant drawback of the approach presented above is that the generation of tissue reactive aldehyde groups requires the use of short wavelength (~ 250 nm) UV-C type light, which does not only help to transform the polymer brush side chain functional groups, but, as discussed above, also leads to extensive photodegradation of the polymer brush. In addition, this part of the UV light spectrum is also the region that is most harmful to tissue and cells.<sup>248,249</sup> Another potential limitation of the direct UV-irradiation of PHEMA brushes is that the aldehyde groups that are generated react with amine groups present in the tissue to form imine bonds, which in principle are reversible in aqueous media.<sup>250</sup> Alternative chemistries may allow to facilitate the application of these coatings in wet environments. As an alternative bioadhesive coating platform, PHEMA brushes containing side chain diazirine moieties were investigated (**Figure 4.4**). Diazirines are attractive photoreactive groups to generate bioadhesives since they can be activated with relative long wavelength UV-light<sup>251</sup> and upon irradiation generate

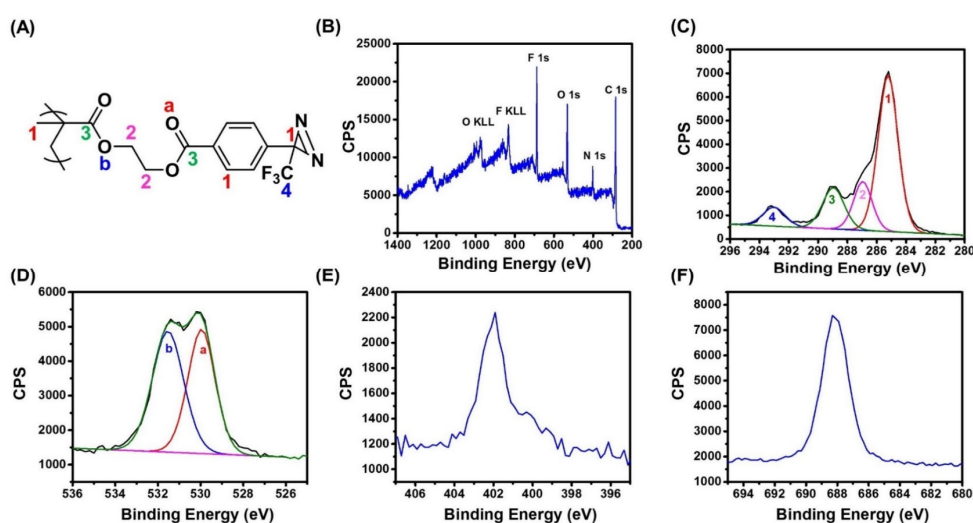
carbene groups that can insert in C-H, N-H and O-H bonds.<sup>252-254</sup> The diazirine functionalized brushes investigated in this study were prepared by DCC/DMAP mediated coupling of TFMDA to PHEMA precursor brushes with thicknesses of 110 nm and 218 nm.



**Figure 4.4.** Post-polymerization modification of a PHEMA brush coated substrate with TFMDA and subsequent photoactivation and adhesion to meniscus tissue.

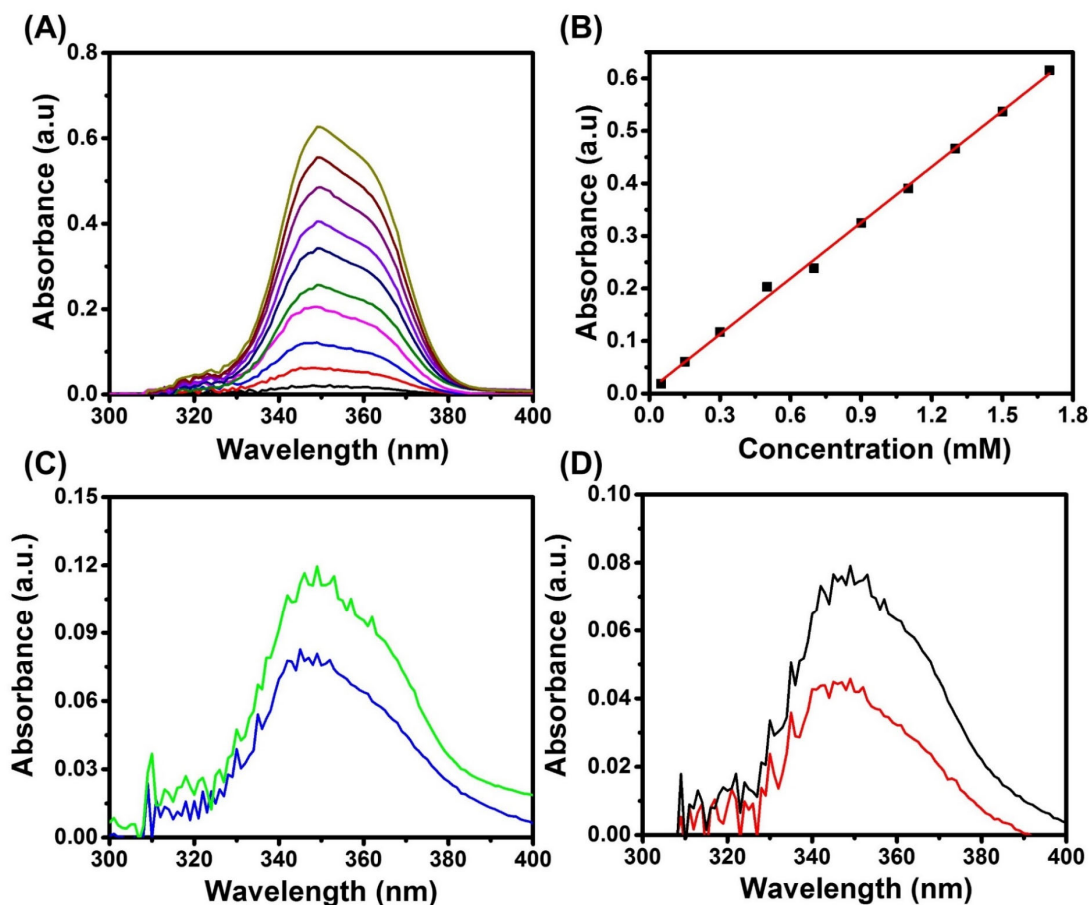
The introduction of the TFMDA side chain functional groups was monitored with XPS, UV-Vis and FTIR spectroscopy. **Figure 4.5** shows the XPS survey scan as well as C<sub>1s</sub>, O<sub>1s</sub>, N<sub>1s</sub> and F<sub>1s</sub> high resolution scans recorded on a PHEMA brush with an initial film thickness of 218 nm, which was reacted with TFMDA in the presence of DCC and DMAP for 16 h. The C, O and F atom percentages determined by XPS analysis of the post-modified brush, which are listed in Supporting Information **Table S4.1**, indicate quantitative substitution of the PHEMA side chains with TFMDA groups. The XPS N percentage, however, is lower than expected, which is attributed to partial degradation of the diazirine groups during the XPS analysis.<sup>255</sup> Since XPS only probes the top 10 - 20 nm of the brush film, UV-Vis spectroscopy was used to estimate the total concentration of TFMDA moieties in the brushes. The TFMDA concentration in the

polymer brushes was estimated using a calibration curve that was constructed using a series of TFMDA solutions in DCM with concentrations ranging from 0.05 mM to 1.7 mM (**Figure 4.6A** and **Figure 4.6B**). To determine the TFMDA concentration, brushes grown from fused silica substrates were analyzed. **Figure 4.6C** and **Figure 4.6D** show UV-Vis spectra of PHEMA brushes with initial film thicknesses of 218 nm (**Figure 4.6C**) and 110 nm (**Figure 4.6D**), which were reacted with TFMDA for 1 and 16 h. The TFMDA concentrations and percentages of conversion of HEMA side chain functional groups that were obtained from those spectra are summarized in **Table 4.1**. The results in **Table 4.1** indicate that a reaction time of 16 h resulted in complete conversion of the HEMA side chain functional groups with TFMDA moieties in the thinner brush ( $d = 110$  nm). Shortening the reaction time for the modification of the 110 nm thick polymer brush from 16 h to 1 h decreases the conversion to 65%. For the thicker (218 nm) PHEMA brush, conversions of 55%, respectively, 78% were determined after reaction times of 1 and 16 h.



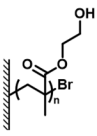
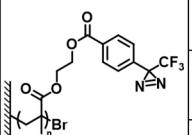
**Figure 4.5.** (A) Chemical structure of a TFMDA functionalized PHEMA brush; (B) XPS survey scan; (C) C<sub>1s</sub> high resolution spectrum; (D) O<sub>1s</sub> high resolution spectrum;

(E) N<sub>1s</sub> high resolution spectrum and (F) F<sub>1s</sub> high resolution spectrum of a TFMDA functionalized PHEMA brush coated substrate.



**Figure 4.6.** (A) UV-vis absorbance spectra of DCM solutions of TFMDA with concentrations of: 0.05 mM (black), 0.15 mM (red), 0.3 mM (blue), 0.5 mM (pink), 0.7 mM (olive), 0.9 mM (navy), 1.1 mM (violet), 1.3 mM (purple), 1.5 mM (wine) and 1.7 mM (dark yellow). (B) Experimental data and linear fitting curve of absorbance vs. TFMDA concentration. (C) UV-vis absorbance spectra of 218 nm thick PHEMA brush coated fused silica substrates incubated in TFMDA DCM solution for 1 h (blue) and 16 h (green). (D) UV-vis absorbance spectra of 110 nm thick PHEMA brush coated fused silica substrates incubated in TFMDA DCM solution for 1 h (red) and 16 h (black).

**Table 4.1.** Ellipsometric film thicknesses and side chain conversions of TFMDA functionalized PHEMA brushes.

PHEMA Brush	Dry film thickness (nm)	PHEMA-TFMDA Brush	Reaction time (h)	Dry film thickness (nm)	Amount of TFMDA groups (nmol)	Estimated amount of HEMA units (nmol) <sup>[a]</sup>	HEMA conversion (%)
	110.3±1.5		1	143.7±0.7	101	155	65%
			16	181.8±2.8	169	155	100%
	217.8±2.7		1	262.9±2.8	178	306	55%
			16	334.1±1.7	238	306	78%

<sup>[a]</sup> Calculated using the dry film thickness of the PHEMA brush,  $\rho = 1.15 \text{ g/cm}^3$  and the molecular weight of the HEMA repeating unit (130 g/mol).

The adhesion of the TFMDA functionalized brushes towards meniscus tissue was studied using samples that were obtained from PHEMA brushes with initial film thicknesses of 110 or 218 nm, which were post-modified with TFMDA for 1 or 16 h. **Figure 4.7A** reports and compares the adhesion strengths of these 4 samples before and after UV irradiation for 3 min. Prior to UV-activation, the adhesion strengths of the TFMDA modified brushes are comparable to those of non-modified PHEMA brushes before UV-irradiation (see **Figure 4.2**). UV-irradiation results in a significant increase in the adhesion strength. The adhesion strengths that are reported in **Figure 4.7A** are comparable to the results summarized in **Figure 4.2**. The results shown in **Figure 4.7A**, however, do not reveal any significant effects of the initial brush thickness or TFMDA concentration on the measured adhesion strength. This suggests that it is probably only

the top-most layer of the TFMDA functionalized brush, where all of the HEMA repeating units are modified with TFMDA moieties according to the XPS analysis, which is involved in the formation of adhesive bonds with the meniscus tissue. It is important to note that the light source that was used to activate the brushes for the experiments that are summarized in **Figure 4.7A** extends into the UV-C region and contains a small band around 250 nm as well. As a consequence, the application of this range of UV wavelengths most likely leads to simultaneous generation of carbene moieties by photo-decomposition of the diazirine groups as well as the formation of aldehyde groups by direct activation of the PHEMA brush. The adhesion strengths that are determined in these experiments thus reflect the contributions of both the carbene and the aldehyde groups. In a second experiment, in order to avoid direct activation of the PHEMA brush and to exclusively mediate adhesion using carbene moieties, the TFMDA functionalized brushes were exposed to UV light using a bandpass filter that removes the 250 nm band and allows for exclusive activation with only 365 nm light. **Figure 4.7B** compares the adhesion strengths that were measured on a non-modified PHEMA brush and two TFMDA functionalized brushes that were UV-activated under these conditions for 3 min. The adhesion strength of the non-modified PHEMA brush that is measured is comparable to those of the non-irradiated samples shown in **Figure 4.2**. This indicates that 365 nm UV-light does not lead to direct formation of tissue reactive groups in PHEMA brushes. In contrast, activation of the TFMDA modified brushes with 365 nm UV light results in an increase in the adhesion strength with the meniscus tissue. The covalent bonds that are formed and which contribute to tissue

adhesion in this case are exclusively due to reaction of carbene moieties that are the product of the photodegradation of the diazirine groups.

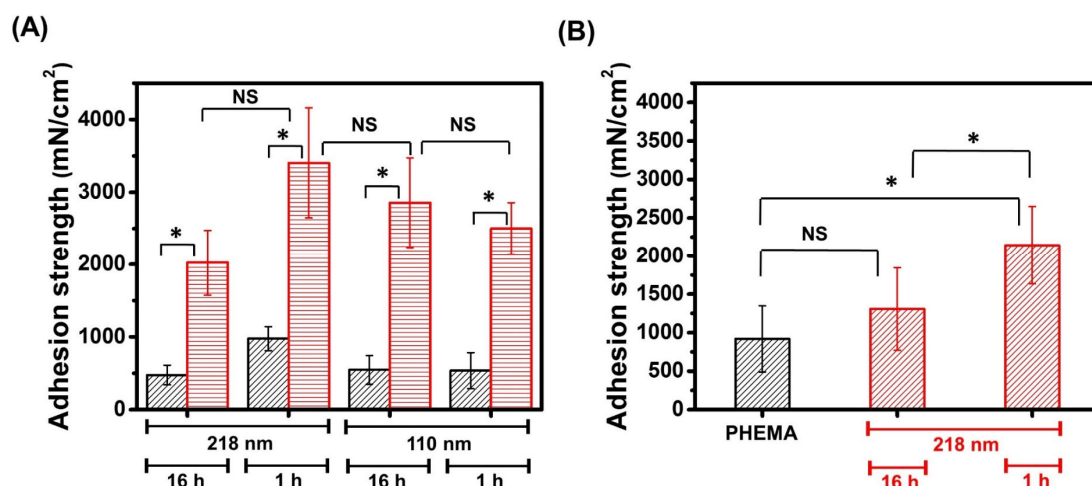


**Figure 4.7.** Adhesion strengths of (A) TFMDA functionalized PHEMA brush coated substrates with various thicknesses before (black) and after UV irradiation for 3 min (red). (B) PHEMA brush (black) and TFMDA functionalized PHEMA brush coated substrates (red) treated with UV irradiation using a bandpass filter, which removes the 250 nm and allows for activation with only the 365 nm band, for 3 min. Asterisks indicate statistically significant differences whereas NS represent not significant difference between two conditions. Significant at \*  $p < 0.05$ .

#### 4.4. Conclusions

Surface-initiated atom transfer radical polymerization has been used to produce thin, PHEMA brush coatings that can be transformed on-demand, using UV-light as a trigger, from a non-adhesive to a tissue reactive state. Two strategies have been explored for the photochemical activation of the PHEMA brushes. A first strategy is based on direct

UV-irradiation of PHEMA brush films, whereas the second approach involved the post-polymerization modification of the PHEMA side chain hydroxyl functional groups with 4-[3-(trifluoromethyl)-3H-diazirin-3-yl]benzoic acid. Adhesion experiments with meniscus tissue demonstrated that both polymer brush platforms upon UV-irradiation were able to create adhesive bonds with the tissue surface. While the direct irradiation of PHEMA brushes is very straightforward from an experimental point of view, this strategy relies on the 250 nm wavelength part of the UV spectrum. This short wavelength UV light unfortunately, not only generates the tissue reactive aldehyde groups, but also leads to extensive photodegradation of the polymer brush film. The diazirine containing brushes are comparably effective in terms of forming adhesive bonds with meniscus tissue. The activation of the diazirine groups, however, can be achieved using 365 nm wavelength UV light that does not lead to photodegradation. The proof-of-concept experiments presented in this manuscript have used silicon wafers and fused silica substrates as model surfaces. The versatility of SI-ATRP (and related grafting-from chemistries), however, will allow to apply this concept to a broader range of biomedically relevant surfaces.

#### 4.5. Supporting Information

**Table S4.1.** Experimental (determined by XPS) and expected atomic concentrations of C, N, O and F for a 218 nm thick PHEMA brush after reaction with TFMDA solution for 16 h.

	C <sub>1s</sub>	N <sub>1s</sub>	O <sub>1s</sub>	F <sub>1s</sub>
<b>Atomic concentration (XPS)</b>	<b>62.97</b>	<b>4.29</b>	<b>17.96</b>	<b>14.78</b>
<b>Atomic concentration (theory)</b>	<b>62.5</b>	<b>8.3</b>	<b>16.7</b>	<b>12.5</b>

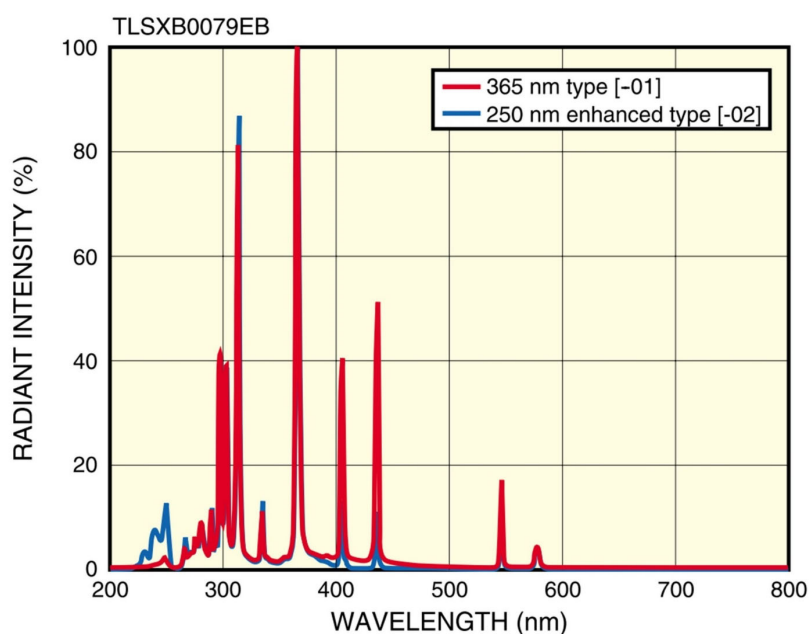


**Figure S4.1.** Radiant spectral distribution of the HAMAMATSU L8858-02 UV lightening source. For the experiments in this study, a [-02] type source that possesses a band at 250 nm (blue curve) was used (from: <https://www.digchip.com/datasheets/parts/datasheet/190/L8858-02-pdf.php>).

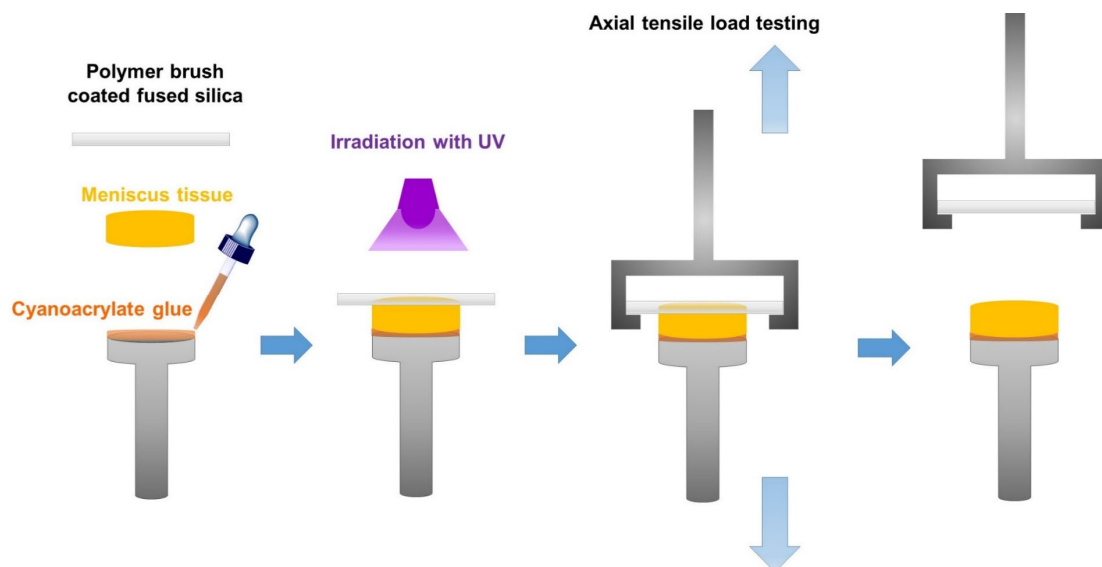


**Figure S4.2.** Schematic illustration of the setup that was used for the adhesion tests.

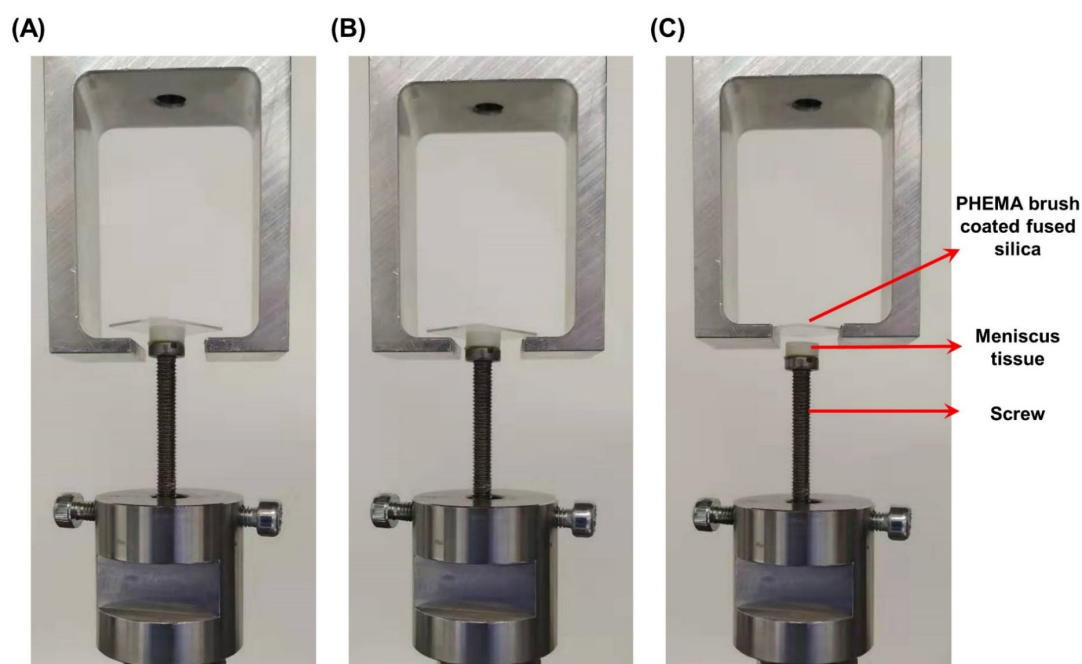


**Figure S4.3.** Images of an axial tensile stress measurement on a PHEMA brush coated substrate ( $d = 145$  nm; irradiation time = 3 min) at different time points during the experiment. (A) Before the start of the experiment; (B) after 1 s and (C) after 2 s. Load was applied along the interface.

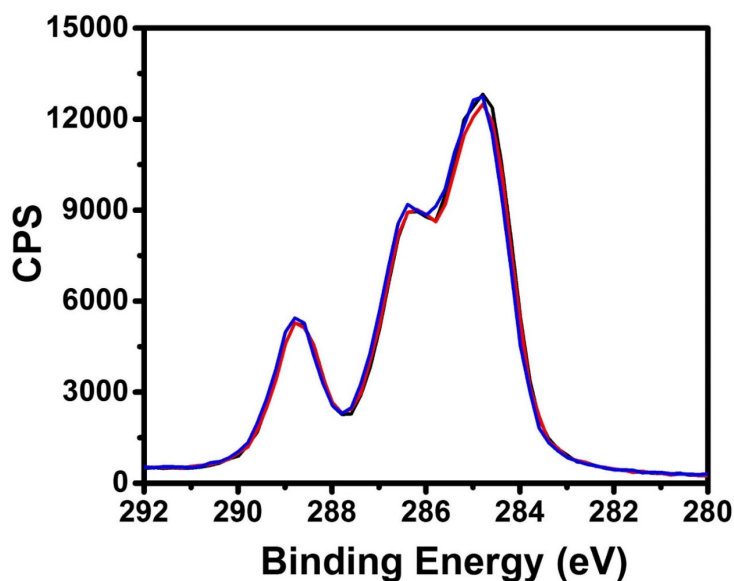


**Figure S4.4.** C<sub>1s</sub> high resolution spectra XPS of a PHEMA brush coated substrate ( $d = 145$  nm) before (black) after UV irradiation with a band-pass filter under dry (red) and wet (blue) conditions.

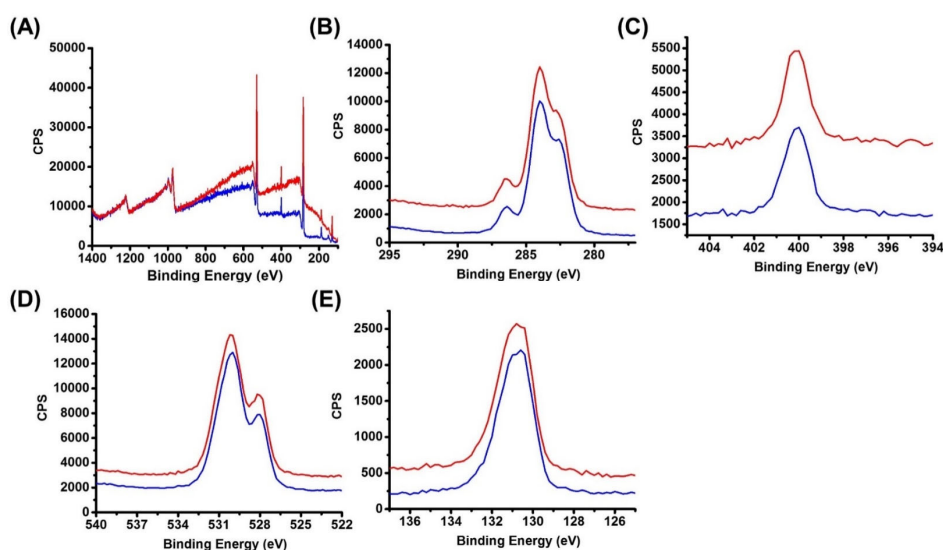


**Figure S4.5.** (A) XPS survey scan; (B) C<sub>1s</sub>; (C) N<sub>1s</sub>; (D) O<sub>1s</sub> and (E) P<sub>1s</sub> high resolution XPS spectra of a PMPC brush before (blue) and after (red) UV irradiation.

## **5. Pyroelectric Properties of Polyelectrolyte Brushes**

### **5.1. Introduction**

Polyelectrolyte (PE) brushes are charged polymer chains with one end tethered to a surface. The most significant character of PE brushes is the strong confinement of the counterions within the brush layer, which leads to many important research both in fundamental science and commercial product development. For example, the study on the effect of counterion on the lubricity of PE brushes,<sup>256-258</sup> the fabrication DNA brush based gene chips,<sup>259,260</sup> the preparation of anti-fogging and anti-freezing surfaces<sup>261</sup> and the fabrication of stimuli-responsive surfaces<sup>262</sup> are all rely on the presence of charges of the PE brushes. However, although a large amount of studies have focused on how counterions influence the structural change of polymer backbone<sup>263</sup> and how use this effect to tune the lubrication and antifouling properties of PE brushes, the intrinsic structure of PE brushes especially the counterion distribution along the brushes remains unknown. It is commonly believed that the counterion should distributed along the brush chain evenly to keep an electrical neutral state in dry condition. However, our observations suggest a counterintuitive conclusion that some of the PE brushes are not in electrical neutral state.

At the beginning of the polymerization, the strong electrolyte monomer in solution is always in a dissociation state and with the polymerization goes on, only part of the counterions will condense on the polymer backbone based on Manning theory.<sup>264</sup> Thus, we hypothesized that after polymerization during the washing step, some of the counterions was washed away from the brushes, whereas the polymer chains which are

fixed on the substrate will remain at the interfaces, which makes the dry brushes a non-electrical neutral state. This non-neutral state result in a net charge within the brushes, will generate a permanent dipole moment inside the thin film, which make the PE brushes pyroelectric materials.

In this chapter, a series of PE brushes including PMETAC, PSPMA, PMPC were prepared to test this hypothesis. PMETAC and PSPMA are strong PE brushes with chloride and potassium as counterions while PMPC are zwitterionic brushes with no counterions. The pyroelectric and piezoelectric properties as well as the surface potential and atom surface concentration of these brush films will be studied.

## **5.2. Experimental Section**

### **5.2.1. Materials**

All chemicals were used as received unless described otherwise. Copper(I)chloride (99.999%), copper(II)chloride(99.999%) copper(II)bromide (99.999%), copper(I)bromide (99.995+%), 2,2'-bipyridyl (bpy) (99%), 2-bromo-2-methylpropionyl bromide, [2-(methacryloyloxy)ethyl]trimethylammonium chloride (METAC) solution 80 wt% in H<sub>2</sub>O, 3-sulfopropyl methacrylate, potassium salt (SPMA) (98%), 2-hydroxyethyl methacrylate (HEMA) (97%), ethanol (99.8%), basic aluminum oxide and 2-methacryloyloxyethyl phosphorylcholine (MPC, 97%) were purchased from Sigma Aldrich. Before use, MPC was washed with cold acetonitrile to remove the inhibitor, filtered and dried under vacuum. HEMA was freed from the inhibitor by passing through a column of activated, basic aluminum oxide and distilling prior to use. The ATRP initiator (6-(2-bromo-2-methyl)propionyloxy)hexyldimethylchlorosilane

was synthesized as previously reported.<sup>229</sup> Dichloromethane was purchased from Fisher chemicals. Methanol (MeOH) was purchased from Alfa Aesar. Isopropanol (99%) was purchased from Reactolab SA. Triethylamine was purchased from Aldrich and distilled over KOH before use. Dichloromethane (DCM) was purified and dried using a solvent-purification system (PureSolv). Deionized water was obtained from a Millipore Direct-Q 5 water purification system. Pyroelectric measurement was performed on polymer brushes, which were grown from 0.8 cm × 1 cm rectangular fused silica substrates. Samples for piezoelectric force microscopy (PFM) and scanning kelvin probe microscopy (SKPM) analysis were grafted from 0.8 cm × 1 cm rectangular boron doped silicon substrates.

### **5.2.2. Methods**

XPS was carried out using an Axis Ultra instrument from Kratos Analytical equipped with a conventional hemispheric analyzer. The X-ray source employed was a monochromatic Al K $\alpha$  (1486.6 eV) source operated at 100 W and 10<sup>-9</sup> mbar. Surfaces were cleaned with a Femto O<sub>2</sub> Plasma system (200 W, Diener Electronic). Dry film thicknesses on silicon samples were determined using a SemiLAB (SE2000) ellipsometer and calculated based on a four-layer silicon/silicon oxide/polymer brush/air model, assuming the polymer brush to be isotropic and homogeneous. Piezoelectric force microscopy and scanning kelvin probe measurements were carried out using Cypher VRS, Oxford Instrument.

### **5.2.3. Procedures**

**Preparation of ATRP initiator modified silica and fused silica surfaces.** Silica and

fused silica surfaces were modified following a previously published protocol.<sup>265</sup>

**Surface-initiated atom transfer radical polymerization of [2-(methacryloyloxy)ethyl]trimethylammonium chloride (METAC).** 2,2'-bipyridyl (bpy) (351.4 mg, 2.25 mmol), CuCl<sub>2</sub> (6.725 mg, 0.05 mmol) were dissolved in a mixture of 80 wt% aqueous solution of METAC (15.6 g, 60 mmol) and isopropanol (12.5 mL). After three freeze/pump/thaw cycles, CuBr (178.75 mg, 1.25 mmol) was added under nitrogen flow. The molar ratio of METAC/CuBr/CuCl<sub>2</sub>/bpy in the reaction mixture was 48:1:0.04:1.8. The mixture was sonicated to completely dissolve the CuBr. After an additional freeze/pump/thaw cycle, the resulting ATRP solution was cannula transferred to a nitrogen purged flask containing initiator-functionalized substrate at room temperature. After a certain period of time, the substrates were removed from the ATRP solution and rinsed with water and ethanol extensively and dried under a flow of N<sub>2</sub>.

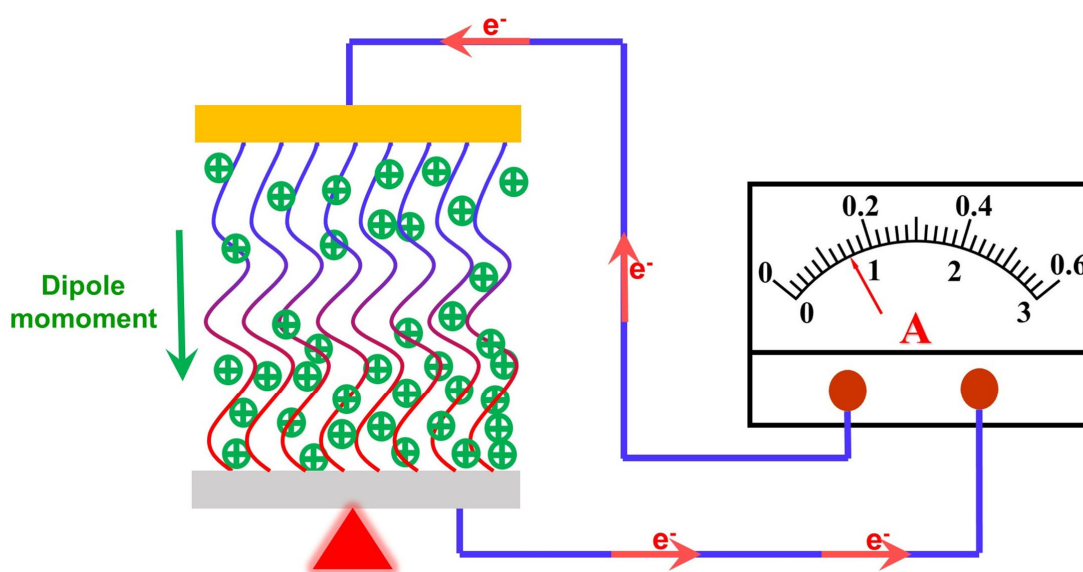
Surface-initiated atom transfer radical polymerization of SPMA,<sup>266</sup> MPC<sup>265</sup> and HEMA<sup>230</sup> were carried out following established protocols.

**Atom transfer radical polymerization of METAC.** The polymerization of METAC in solution have been done following the SI-ATRP of METAC protocol with a slight modification. Instead of putting initiator modified surfaces, (6-(2-bromo-2-methyl)propionyloxy)- hexyldimethylchlorosilane initiator (0.07 mL 0.24 mmol, monomer/initiator = 250:1) was mixed with METAC, isopropanol, CuCl<sub>2</sub> and bpy before freeze-pump-thaw cycles. After polymerization at room temperature for 3 h, the polymer solution passed through neutral Al<sub>2</sub>O<sub>3</sub>. The polymer was partially precipitated

in methanol and dried under vacuum overnight for further use. The molecular weight is 27.5 kDa with PDI 1.37. The GPC curve was shown in **Figure S5.13A**.

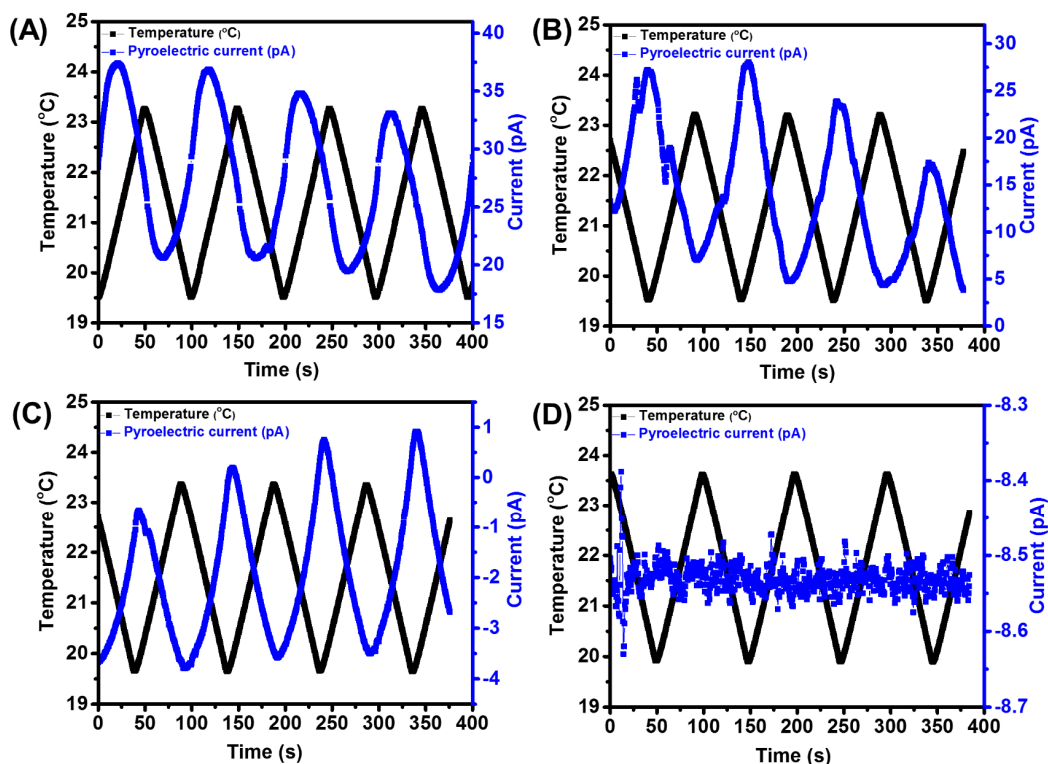
### 5.3. Results and Discussion

In a first set of experiments, the pyroelectric properties of PMETAC, PSPMA, PMPC and PHEMA were evaluated. The polymer brushes were subjected to a temperature oscillation and the open circuit current were measured in real-time. (**Figure 5.1**)



**Figure 5.1.** Graphic illustration of the pyroelectric current generated upon applying alternating sequence of temperature change to PE brushes.

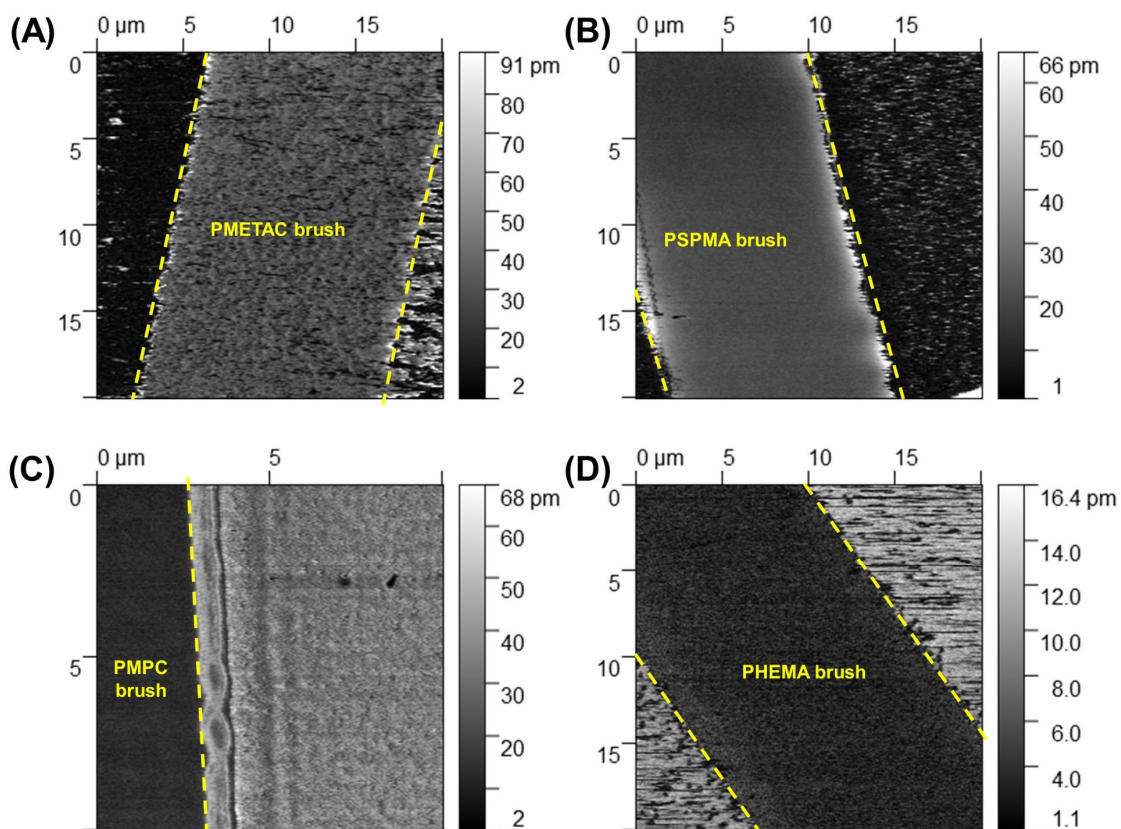
The results in **Figure 5.2** indicates that only PE brushes (here, PMETAC, PSPMA and PMPC) can generate pyroelectric current. As a control, no pyroelectric current was generated by PHEMA brushes.



**Figure 5.2.** Pyroelectric current response and temperature oscillations for (A) PMETAC brushes with dry film thicknesses of 160 nm, (B) PSPMA brushes with dry film thicknesses of 150 nm, (C) PMPC brushes with dry film thickness of 100 nm and (D) PHEMA brushes with dry film thickness of 100 nm.

Similarly, no pyroelectric current were observed in pristine fused silica, initiator modified fused silica and PtBMA brush coated fused silica, which further suggest that the pyroelectric current are only generated by PE brushes (**Figure S5.1**). Pyroelectric materials are always piezoelectric materials, characterizing the piezoelectric properties will help to better understand the pyroelectric properties. Single frequency piezoelectric force microscopy was used to characterize the inverse piezoelectric property. In **Figure 5.3A and B**, the piezoelectric response amplitude of PMETAC brushes and PSPMA brushes are 30 and 10 pm at 20 °C under driving voltage 1 V, respectively. No obvious

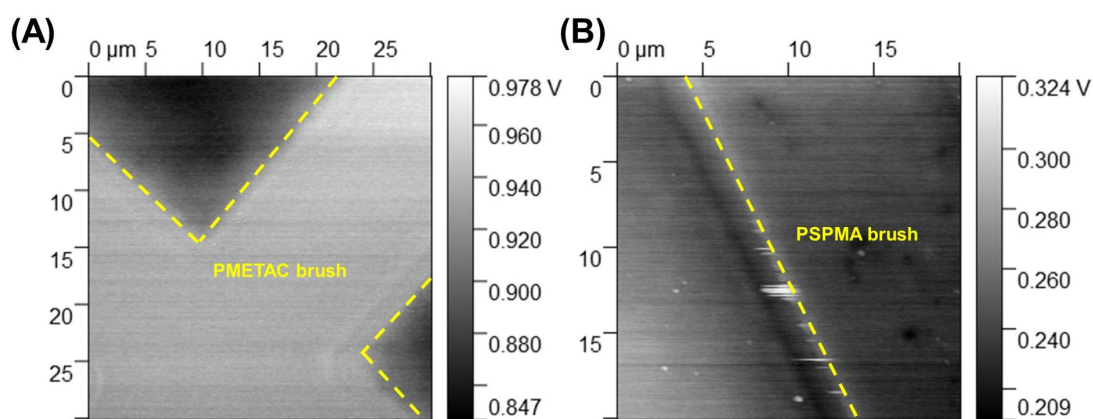
piezoelectric response was observed on both PMPC and PHEMA brushes. These results are consistent with the pyroelectric current measurement in **Figure 5.2**, which further suggest that the counterions are the main actor that affect the pyro/piezoelectrical properties by influencing the dipole moment inside the materials.



**Figure 5.3.** PFM piezoresponse amplitude of (A) PMETAC brushes with dry film thicknesses of 110 nm, (B) PSPMA brushes with dry film thicknesses of 80 nm, (C) PMPC brushes with dry film thickness of 100 nm and (D) PHEMA brushes with dry film thicknesses of 100 nm measured at 20 °C with driving voltage 1 V.

The results in **Figure 5.2** and **5.3** are good indications that there is a permanent dipole moment in the direction perpendicular to the substrate induced by the net charge. To

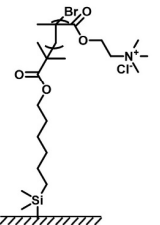
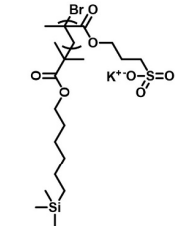
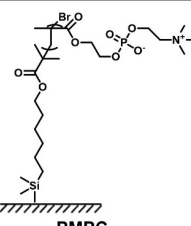
further prove our hypothesis, scanning kelvin probe microscopy (SKPM) was used to characterize the surface potential. In ideal case, the PE brushes should stay electrical neutral and every charge in the polymer side chain is compensate by the counterion. If there is a net charge inside the polymer materials, a net surface potential should be observed.



**Figure 5.4.** Scanning Kelvin Probe Microscopy measurement of (A) PMETAC brushes with dry film thicknesses of 110 nm, (B) PSPMA brushes with dry film thicknesses of 80 nm.

As is shown in **Figure 5.4A** and **B**, PMETAC brushes present +80 mV net positive surface potential and -10 mV for PSPMA brushes (here the silicon substrates of the PE brushes were conducting and were connected to the ground as a reference). These results suggest that there are positive charges accumulated on PMETAC brushes and negative charge on PSPMA brushes. This is also a good indication that the PE brushes are not electrical neutral and this result will be further confirmed with XPS measurement.

**Table 5.1.** Atomic concentration calculated from X-ray photoelectron spectra of PMETAC, PSPMA and PMPC brushes with dry film thicknesses of 110 nm, 200 nm and 150 nm, respectively at room temperature. (Calibrated at C<sub>1s</sub> 284.8 eV).

Atomic concentration table	C <sub>1s</sub>	O <sub>1s</sub>	N <sub>1s</sub>	Cl <sub>2p</sub>	Si <sub>2p</sub>	S <sub>2p</sub>	K <sub>2p</sub>	P <sub>2p</sub>
Relative sensitivity factors	0.314	0.733	0.499	0.954	0.368	0.717	1.552	0.525
 <p>PMETAC</p>	64.47	19.54	4.77	3.59	7.46	XX	XX	XX
 <p>PSPMA</p>	48.89	33.81	XX	XX	0.47	6.64	6.40	XX
 <p>PMPC</p>	59.62	30.74	4.71	XX	0.36	XX	XX	4.56

The results in **Table 5.1** indicate that the atom concentration of N (4.77%) is higher than Cl (3.59%) for PMETAC brushes whereas the atom concentration of S (6.64%) is roughly the same as K (6.40%) for PSPMA brushes. This result further confirmed

that there is a clear dipole moment concomitantly net charge in PMETAC brushes whereas the dipole moment in PSPMA is existed but relatively low.

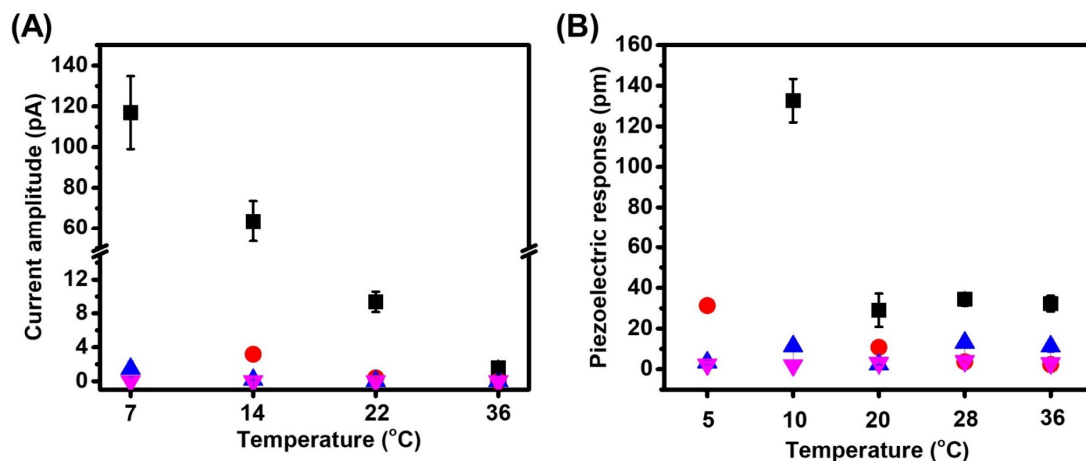


**Figure 5.5.** (A) Pyroelectric current amplitude of PMETAC brushes with dry film thicknesses of 110 nm (■), PSPMA brushes with dry film thicknesses of 200 nm (●), PMPC brushes with dry film thickness of 100 nm (▲) and PHEMA brushes with a dry film thickness of 100 nm (▼) measured at center temperature 7, 14, 22 and 36 °C varying at amplitude of 2 °C. (B) Piezoelectric response amplitude of PMETAC brushes with dry film thicknesses of 110 nm (■), PSPMA brushes with dry film thicknesses of 80 nm (●), PMPC brushes with dry film thickness of 100 nm (▲) and PHEMA brushes with dry film thickness of 100 nm (▼) measured at various temperatures with driving voltage 1 V.

There is also an interesting temperature effect. As shown in **Figure 5.5**, both the pyroelectric current and piezoelectric response amplitude for PMETAC and PSPMA brushes increase with decreasing temperatures. Here, we hypothesized that the  $T_g$  of these PE brushes may be in the range of 10-20 °C. Dipole moment are supposed to be

more aligned and rigid in glassy state, lifting the temperature above  $T_g$  will make the polymer chains changing from glassy to rubbery state, concomitantly increase the mobility of counterions. The result of ellipsometry measurement under different temperatures in **Figure S5.14** indicates that the  $T_g$  of PMETAC and PSPMA brushes at ambient atmosphere is 11.9 and 13.5 °C, which fit the hypothesis well. This  $T_g$  value of PMETAC brushes is similar to the value reported in solution before measured by electrochemical technique.<sup>267</sup>

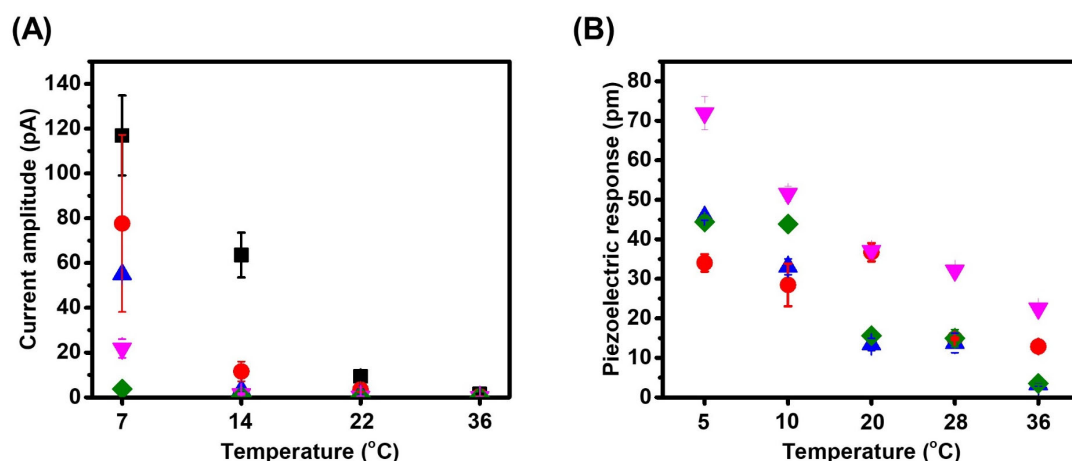


**Figure 5.6.** (A) Pyroelectric current amplitude of PMETAC brushes measured at center temperature 7, 14, 22 and 36 °C varying at amplitude of 2 °C. (■) Original PMETAC brushes with dry film thicknesses of 110 nm and PMETAC brushes after incubation in water (●), 0.2 M NaBr (▲), KSCN (▼) and NaNO<sub>3</sub> (◆) for 45 min. (B) Piezoelectric response amplitude of PMETAC brushes measured at 5, 10, 20, 28, 36 °C with driving voltage 1 V. PMETAC brushes after incubation in water (●), 0.2 M NaBr (▲), KSCN (▼) and NaNO<sub>3</sub> (◆) for 45 min at room temperature.

To further study how counterions will influence the pyroelectric property, counterion of PMETAC brushes were exchanged with  $\text{Br}^-$ ,  $\text{SCN}^-$  and  $\text{NO}_3^-$ . Pyroelectric current and piezoelectric response were measured under the same condition as shown in **Figure 5.6**. For all the samples, pyroelectric current and piezoelectric response increase with decreasing the temperature. Exchanging the counterion from  $\text{Cl}^-$  to  $\text{Br}^-$ ,  $\text{SCN}^-$  and  $\text{NO}_3^-$  shows a clearly decrease in pyroelectric current suggesting that the dipole moment inside the brushes decreases when counterions were changed (**Figure 5.6A**). The results here can be further explained by the charge interaction. In general, two main reasons determines the charge interaction. 1. Strength of ion specific dispersion interactions between counterions and charged group should increase from kosmotropic to chaotropic anions because of the increasing ionic polarizability. 2. Similar water affinity will have a higher interaction.<sup>263</sup> In the case of PMETAC brushes, quaternary amine is a weakly hydrated chaotrope, the same as  $\text{NO}_3^-$  and  $\text{SCN}^-$ . However,  $\text{Cl}^-$  and  $\text{Br}^-$  are in between chaotrope and kosmotrope and their water affinities are much higher than quaternary amine,  $\text{NO}_3^-$  and  $\text{SCN}^-$ . As a result, if the counterion was exchanged to  $\text{NO}_3^-$  or  $\text{SCN}^-$ , due to the higher interaction between counterions and the main polymer chain, the counterions are unlikely to be washed away, which result in an electrical neutral state. In the case of  $\text{Br}^-$  and  $\text{Cl}^-$ , due to weak interaction between the counterion and polymer backbone, except the condensed counterions, the free counterions were washed away from the brush surface which lead to a non-electrical neutral state. XPS results in **Table 5.2** further support this hypothesis. The atom concentration ratio of N and Cl in PMETAC is 1.64, N and Br in PMETAC+Br is 1.17 whereas the ratio between

N and S in PMETAC+SCN<sup>-</sup> and the ratio between N and O in PMETA + NO<sub>3</sub><sup>-</sup> indicates a 1:1 ratio between positive and negative charged atom. The results in **Table 5.2** are in consistent with the results shown in **Figure 5.6**. Since there are almost no net charge in the case of SCN<sup>-</sup> and NO<sub>3</sub><sup>-</sup>, there is almost no net dipole moment inside the brushes, which result in a very low pyroelectric current.

**Table 5.2.** Atomic concentration calculated from X-ray photoelectron spectra of PMETAC brush surfaces and brushes after incubation in 0.2 M NaBr, KSCN and NaNO<sub>3</sub> and NaAc for 45 min at room temperature. (Calibrated at C<sub>1s</sub> 284.8 eV).

Atomic concentration table	C <sub>1s</sub>	O <sub>1s</sub>	N <sub>1s</sub>	Cl <sub>2p</sub>	S <sub>2p</sub>	K <sub>2p</sub>	Br <sub>3d</sub>	Si <sub>2p</sub>
Relative sensitivity factors	0.314	0.733	0.499	0.954	0.717	1.552	1.149	0.368
PMETAC	67.48	18.47	5.91	3.59	XX	XX	XX	3.49
PMETAC+Br <sup>-</sup>	70.35	15.36	6.73	0.44	6.64	1.12	5.77	XX
PMETAC+SCN <sup>-</sup>	71.07	13.48	10.23	0.07	5.16	0.96	XX	XX
PMETAC+NO <sub>3</sub> <sup>-</sup>	63.13	26.27	10.60	XX	XX	XX	0.32	XX

However, the inverse piezoelectric response are not only related to the dipole moment in the materials, but also related to the modulus temperature and some other parameters.

More studies will be done to further explain the result in **Figure 5.6B**. **Figure S5.3-S5.7** are used to calculate the results in **Figure 5.6A**. **Figure S5.8-S5.11** are used to

calculate the result in **Figure 5.6B**. **Figure S5.13B** compares the pyroelectric current between PMETAC brushes and free PMETAC polymer prepared with the same thickness. The result indicates the pyroelectric current is much lower than in brushes state which further suggest that brush structure plays an important role in determining the pyroelectric properties because the dipole moment or net charge was created due to the separation between counterions and the main polymer chain. Free polymers may present a less net charge after drying because the separation is less prone in spin coated free polymer.

**Table 5.3.** Atomic concentration calculated from X-ray photoelectron spectra of PMETAC brush surfaces with dry film thicknesses of 10 nm and 20 nm. (Calibrated at C<sub>1s</sub> 284.8 eV).

Atomic concentration table	C <sub>1s</sub>	O <sub>1s</sub>	N <sub>1s</sub>	Cl <sub>2p</sub>	Si <sub>2p</sub>
Relative sensitivity factors	0.314	0.733	0.499	0.954	0.368
PMETAC 10 nm	68.67	16.55	7.36	5.73	1.6
PMETAC 20 nm	70.44	15.49	7.73	5.63	0.59

Since XPS spectroscopy can only detect the first 20 to 30 nm thickness from the top of the polymer brushes layer, the internal ratio between positive and negative charge remains question. **Table 5.3** presents the XPS results measured on PMETAC brushes with thicknesses of 10 and 20 nm. Similar to the result in **Table 5.2**, the ratios of N and

Cl are still not 1, the concentration of N is always higher than Cl which result in a positive net charges. These results were further confirmed by SKPM measurement in **Figure 5.7**. The surface potential of PMETAC in **Figure 5.7B** is higher than that of silicon substrate, which also suggest a positive charged surface. The results in **Table 5.3** and **Figure 5.7** indicate that the net charge in PMETAC brushes is positive and this is not only a surface effect but rather the whole brushes property.

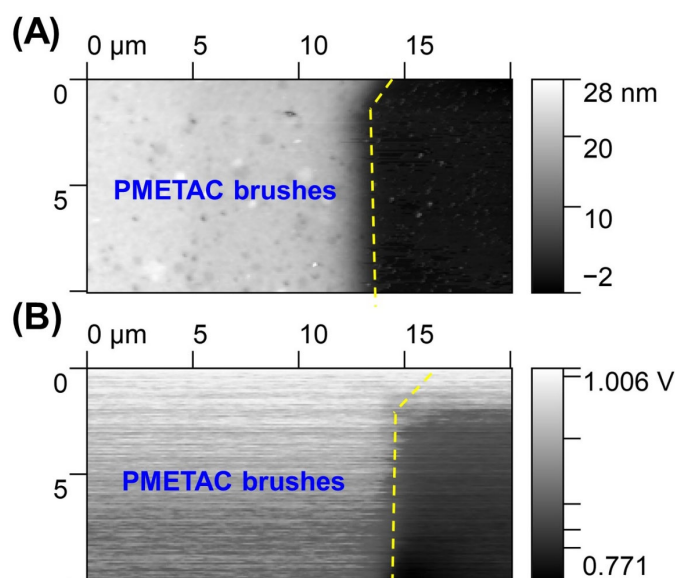


**Figure 5.7.** Scanning Kelvin Probe Microscopy measurement of PMETAC brushes with dry film thicknesses of 20 nm. (A) Topography (B) Surface potential.

#### 5.4. Conclusions

In **Chapter 5**, the pyro and piezoelectric properties of PE brushes was first reported here. A series of PE brushes has been prepared including PMETAC, PSPMA and PMPC brushes. In the first set of experiment, a clear pyroelectric current change was observed in the open circuit upon addition of an oscillation. No current change was detected for

non-PE brushes regardless of the hydrophilicity of the polymer brushes, which suggests that this effect is not caused by water molecules. A clear piezoelectric response was observed when applying a voltage (1 V) to the PE brushes with piezoelectric force microscopy, which suggests that there is a permanent dipole moment inside the materials. Surface potential measurements via scanning probe kelvin microscopy (SKPM) of PMETAC brushes results in a positive net surface charge, which indicates that the permanent dipole moment is originated from the net surface charge. The atom surface concentration measurement of PMETAC brushes via XPS spectroscopy shows that counterions, here chloride, is lower than that of nitrogen in positive charged quaternary amine, which further confirms the hypothesis that PMETAC brushes is in a non-neutral state. Moreover, decreasing the temperature range is accompanied by an increase in current and piezoelectric response. Since  $T_g$  of the brushes was found to be located in the selected temperature range, the enlargement of pyro/piezoelectric can be explained by the transition of glassy-rubbery state of the polymer brushes. Changing the counterions from weakly to strongly interacted with polymer backbone can further tune the pyroelectric properties. Moreover, these results further support our hypothesis that the pyroelectric current that is generated upon applying alternating sequence of temperature change originates from the existence of a permanent dipole moment in PMETAC brushes and this permanent dipole moment is generated by the non-neutral net charge within the brushes. However, although some questions remain unclear and the research in this chapter is still ongoing, we envision that the findings in this chapter will open up a new way in studying the electrical properties of PE brushes.

## 5.5. Supporting Information

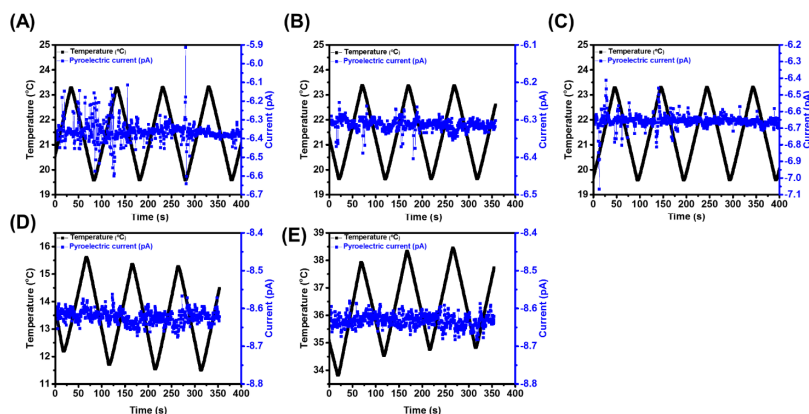


**Figure S5.1.** Pyroelectric current response and temperature oscillations for (A) pristine fused silica, (B) initiator modified fused silica, (C) PtBMA brushes with dry film thicknesses of 150 nm, (D) PHEMA brushes with dry film thicknesses of 100 nm measured from 12-16 °C, (E) PHEMA brushes with dry film thicknesses of 100 nm measured from 34-38 °C.

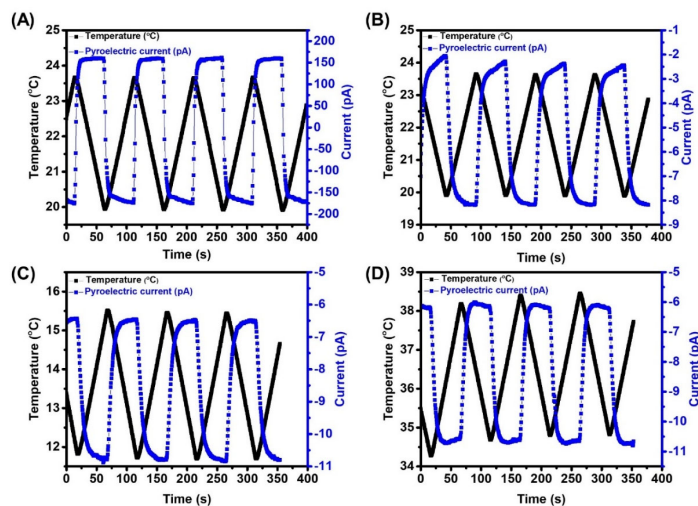


**Figure S5.2.** Pyroelectric current response and temperature oscillations for (A) PVDF film, (B) PVDF film on fused silica, (C) PVDF film on fused silica under temperature range from 11.5 to 15.5 °C, (D) PVDF film on fused silica 19.5 to 23.5 °C.

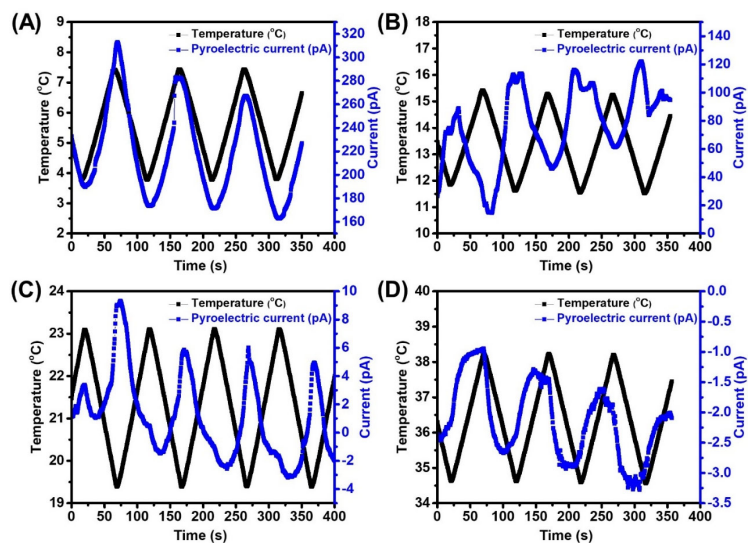


**Figure S5.3.** Pyroelectric current response and temperature oscillations ranging from (A) 4 to 8 °C, (B) 11.5 to 15.5 °C, (C) 19.5 to 23.5 °C, (D) 34.5 to 38.5 °C for PMETAC brushes with dry film thickness of 110 nm.

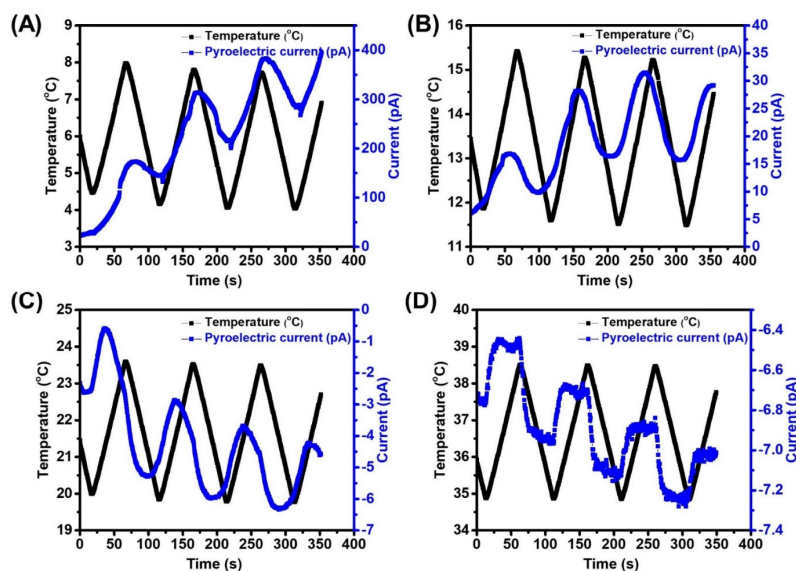


**Figure S5.4.** Pyroelectric current response and temperature oscillations ranging from (A) 4 to 8 °C, (B) 11.5 to 15.5 °C, (C) 19.5 to 23.5 °C, (D) 34.5 to 38.5 °C for PMETAC

brushes with a dry film thickness of 80 nm after incubation in water for 45 min at room temperature.

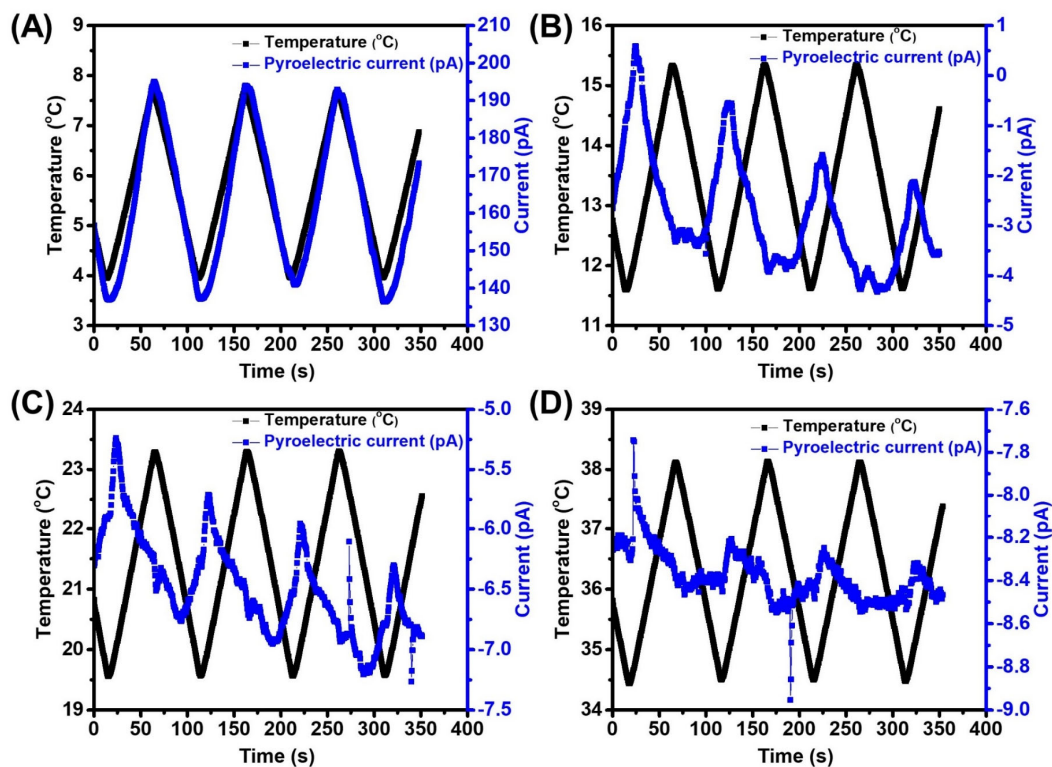


**Figure S5.5.** Pyroelectric current response and temperature oscillations ranging from (A) 4 to 8 °C, (B) 11.5 to 15.5 °C, (C) 19.5 to 23.5 °C, (D) 34.5 to 38.5 °C for PMETAC brushes with a dry film thickness of 100 nm after incubation in 0.2 M NaBr solution for 45 min at room temperature.

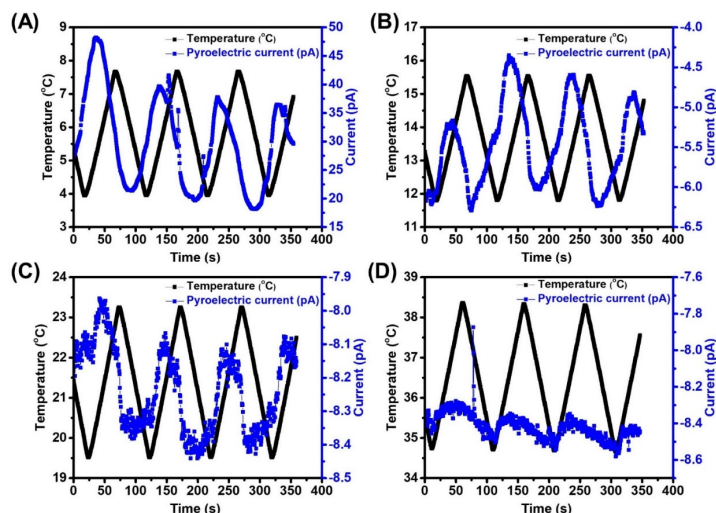


**Figure S5.6.** Pyroelectric current response and temperature oscillations ranging from (A) 4 to 8 °C, (B) 11.5 to 15.5 °C, (C) 19.5 to 23.5 °C, (D) 34.5 to 38.5 °C for PMETAC brushes with a dry film thickness of 93 nm after incubation in 0.2 M KSCN solution for 45 min at room temperature.

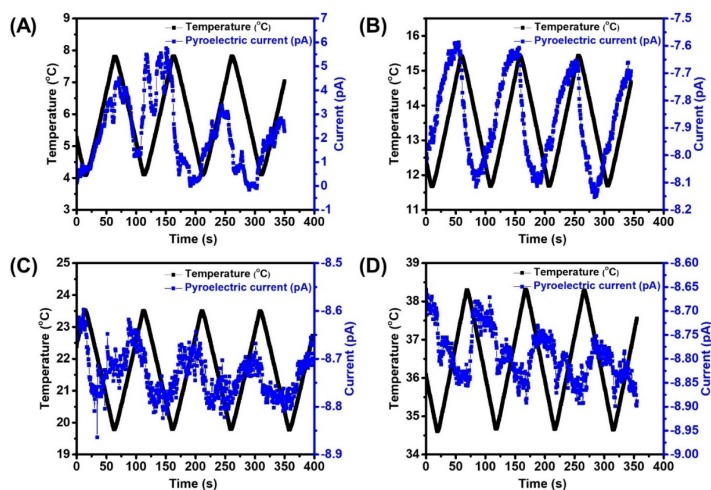


**Figure S5.7.** Pyroelectric current response and temperature oscillations ranging from (A) 4 to 8 °C, (B) 11.5 to 15.5 °C, (C) 19.5 to 23.5 °C, (D) 34.5 to 38.5 °C for PMETAC brushes with a dry film thickness of 93 nm after incubation in 0.2 M NaNO<sub>3</sub> solution for 45 min at room temperature.

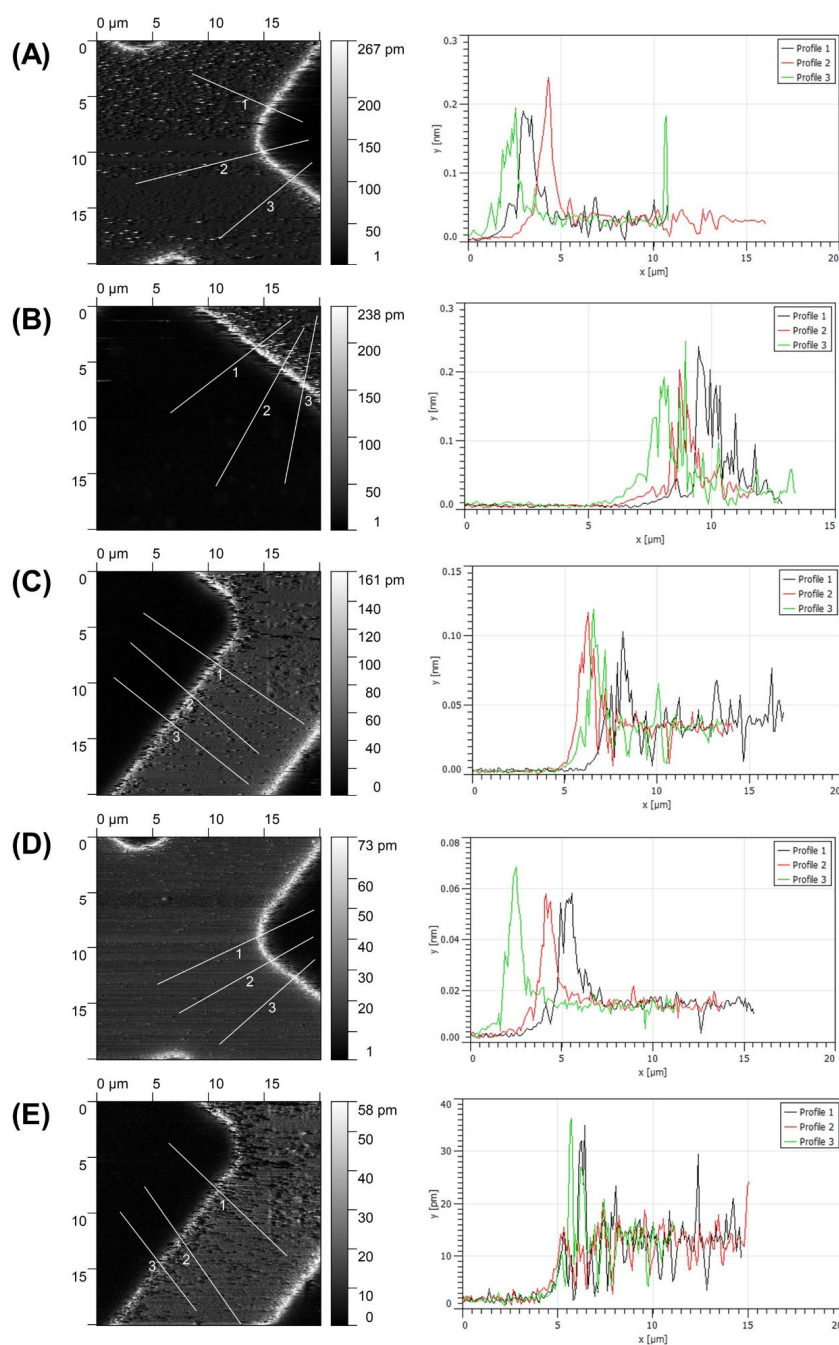


**Figure S5.8.** PFM piezoresponse amplitude of PMETAC brushes after incubation in water for 45 min at room temperature measured at (A) 5 °C, (B) 10 °C, (C) 20 °C, (D) 28 °C, (E) 36 °C with driving voltage 1 V.

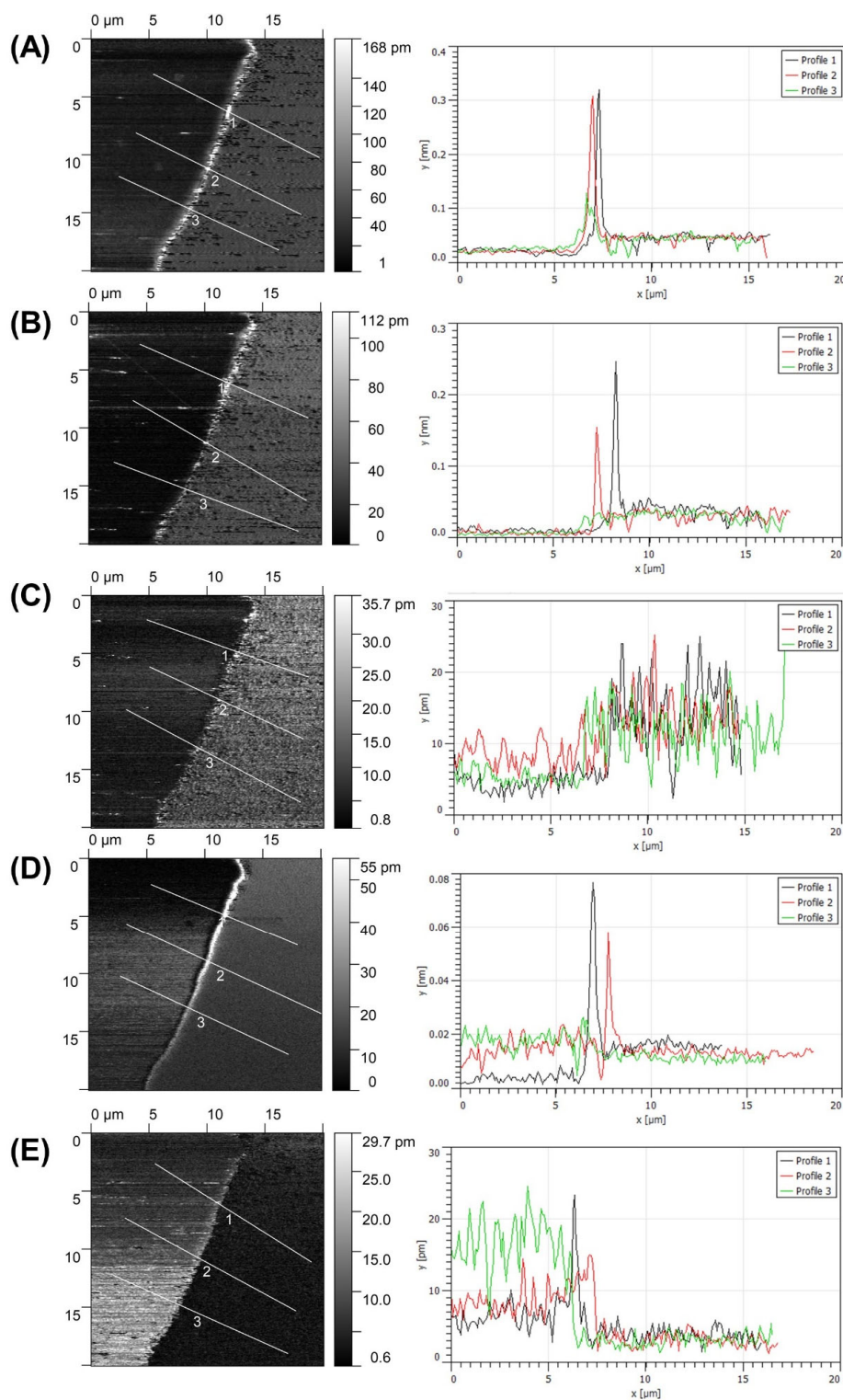


**Figure S5.9.** PFM piezoresponse amplitude of PMETAC brushes after incubation in 0.2 M NaBr for 45 min at room temperature measured at (A) 5 °C, (B) 10 °C, (C) 20 °C, (D) 28 °C, (E) 36 °C with driving voltage 1 V.

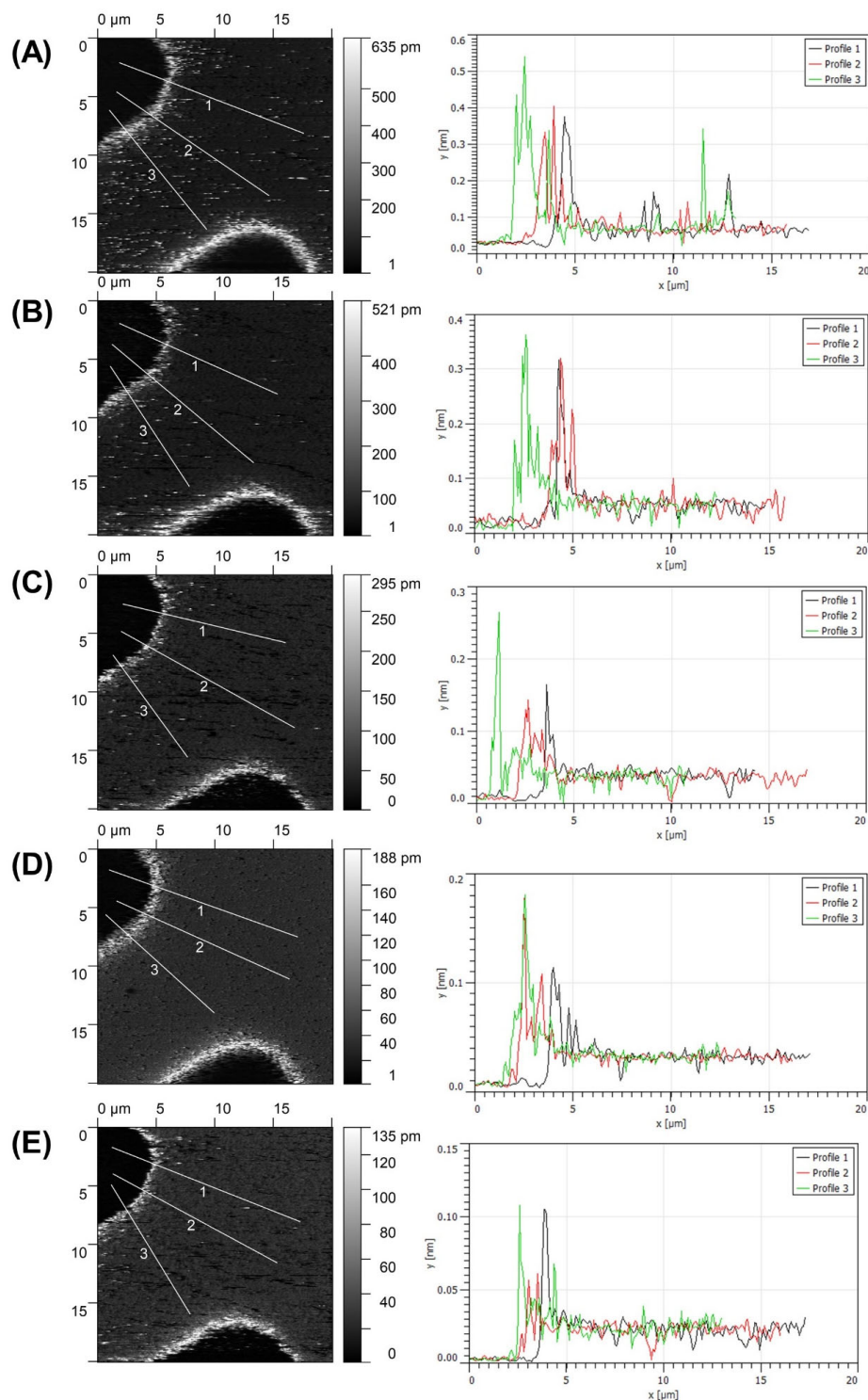


**Figure S5.10.** PFM piezoresponse amplitude of PMETAC brushes after incubation in 0.2 M KSCN for 45 min at room temperature measured at (A) 5 °C, (B) 10 °C, (C) 20 °C, (D) 28 °C, (E) 36 °C with driving voltage 1 V.

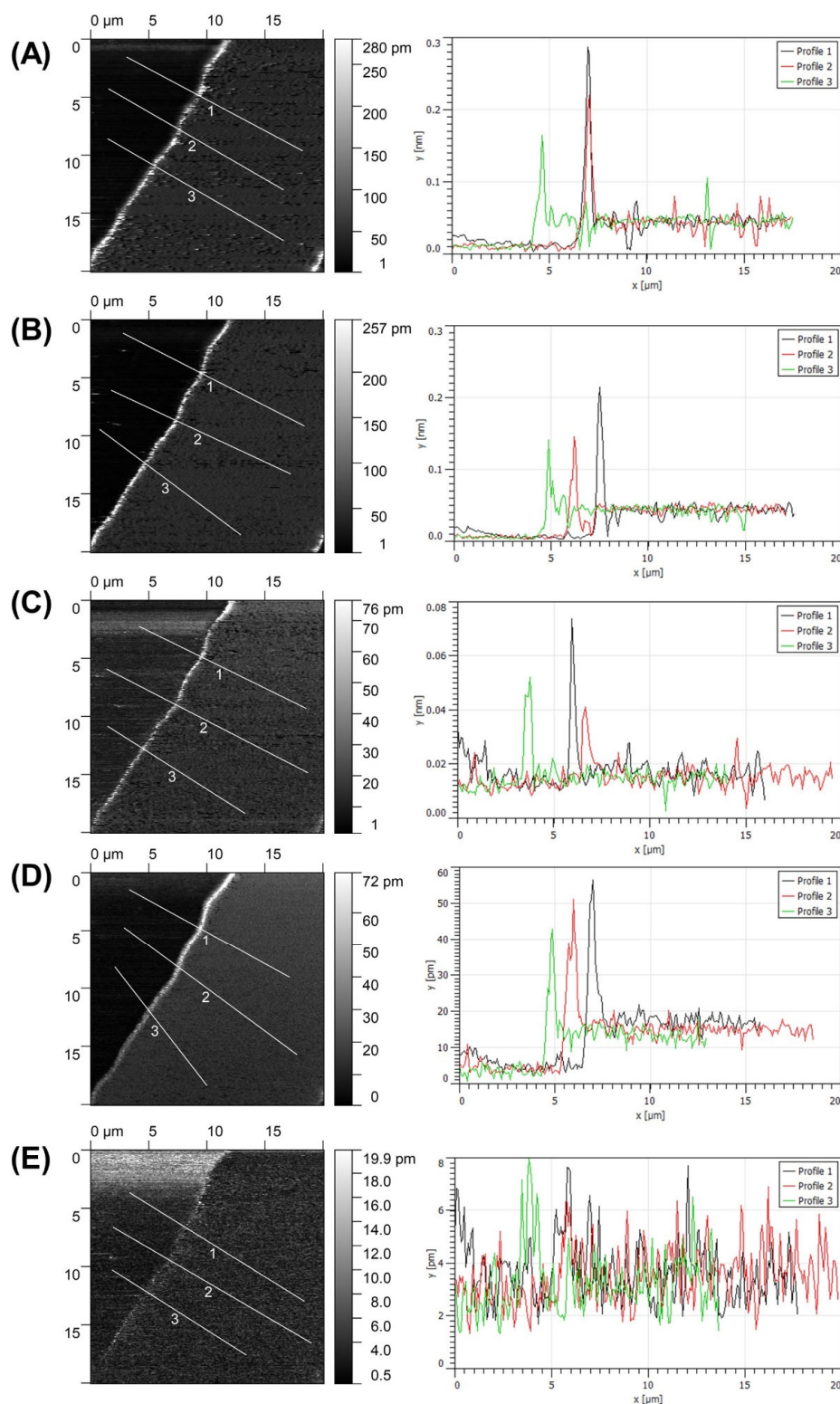


**Figure S5.11.** PFM piezoresponse amplitude of PMETAC brushes after incubation in 0.2 M NaNO<sub>3</sub> for 45 min at room temperature measured at (A) 5 °C, (B) 10 °C, (C) 20 °C, (D) 28 °C, (E) 36 °C with driving voltage 1 V.

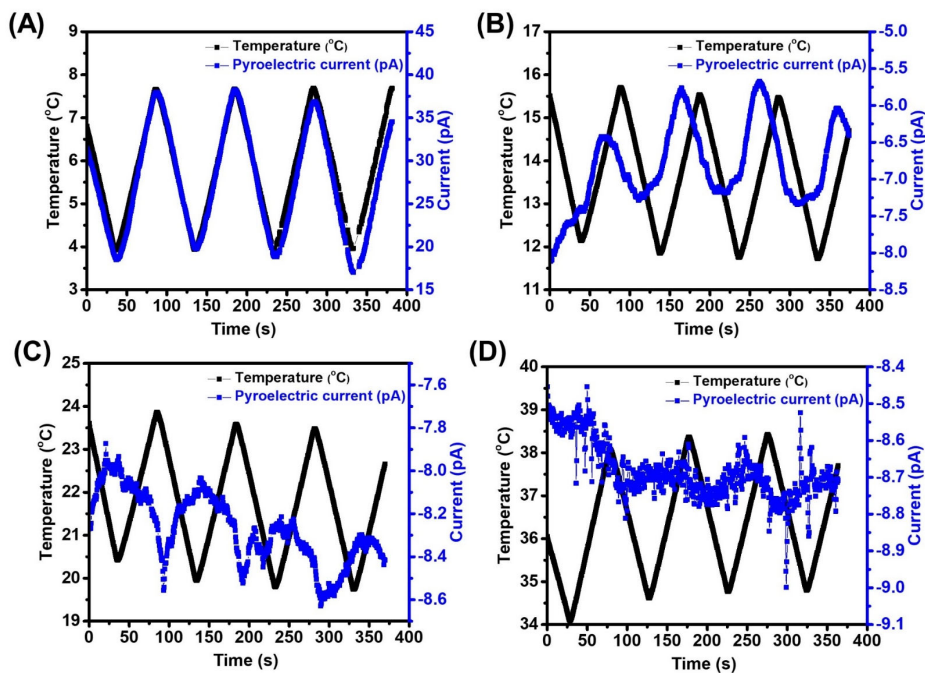


**Figure S5.12.** Pyroelectric current response and temperature oscillations ranging from (A) 4 to 8 °C, (B) 11.5 to 15.5 °C, (C) 19.5 to 23.5 °C, (D) 34.5 to 38.5 °C for PMETAC thin films on fused silica prepared via spin coating with a dry film thickness of 80 nm.

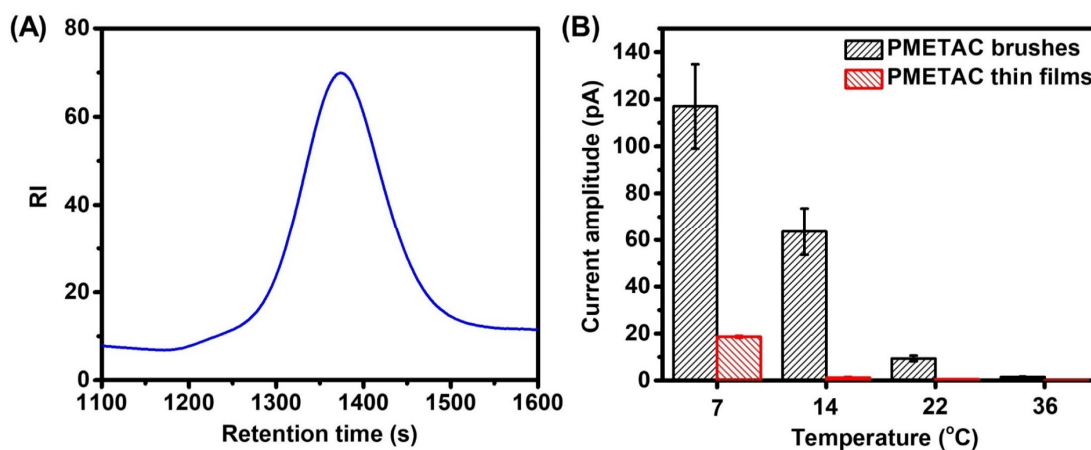


**Figure S5.13.** (A) GPC trace of PMETAC polymer with a molecular weight of 27.5 kDa in water. (B) Pyroelectric current amplitude of PMETAC brushes with a dry film thickness of 110 nm (black) and PMETAC spin coating thin films with a dry film thickness of 80 nm (red).

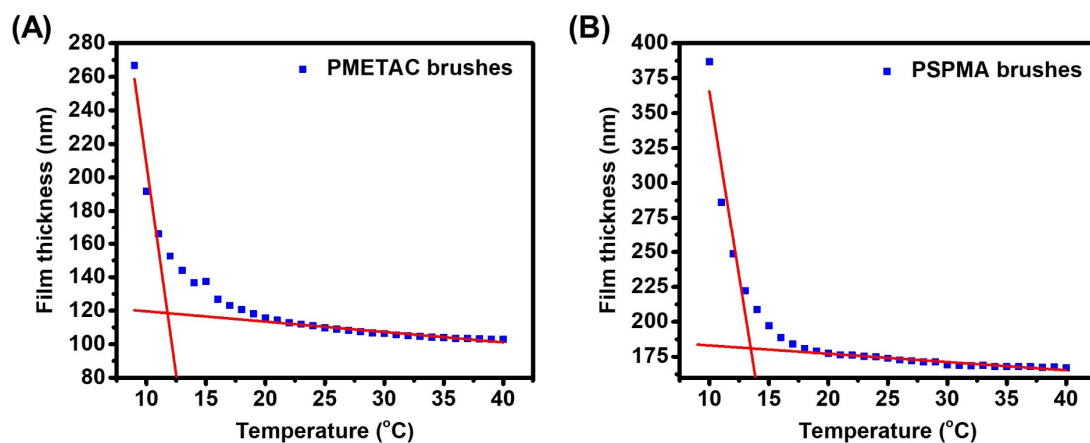


**Figure S5.14.** Evolution of ellipsometric thicknesses of (A) PMETAC and (B) PSPMA brush films as a function of temperature.

## 6. Conclusions and Perspectives

Controlled radical polymerization technique allows to prepare polymers with well-defined architecture, precisely defined molecular weight and narrow dispersities as well as complex functional groups. Ever since it was first realized 60 years ago, this technique has been used to prepare a wide range of polymers both at interfaces and in solution. Taking advantage of the assets of controlled radical polymerization, this thesis first studied the fundamental questions on the sensitivity of specific bonds to mechanical forces at interfaces and in solution (Chapter 2 and 3) and developed ultrathin polymer brush films with UV-light tunable bioadhesion properties or pyro/piezo electric properties.

Following a comprehensive introduction on the topic of controlled radical polymerization in **Chapter 1**, the present work has focused on the influences of weak mechanical forces on hydrolysis of siloxane/ester/amide bond at polymer substrate interface. More specifically, **Chapter 2** has investigated the degrafting and swelling properties of poly(*tert*-butyl methacrylate) (PtBMA) brushes in different water-miscible, organic solvents, viz. DMF, acetone and THF. In the presence of a sufficient quantity of water in the organic solvent, degrafting was also observed for PtBMA brushes. More importantly, however, the rate of degrafting depended on the nature of the organic solvent and the apparent initial rate constant of the degrafting reaction was found to correlate with the swelling ratio of the polymer brush in the different solvents. This correlation is the first, direct evidence in support of the hypothesis that degrafting is facilitated by a tension that acts on the bond(s) that tether the polymer chains to the

surface and which is amplified upon swelling of the polymer brush.

In **Chapter 3**, the hydrolysis of ester bonds, which are incorporated in the polymer backbone under mechanical force has been studied. The motivation for this research is that there are some controversy reports in the literature about whether ester bond hydrolysis is facilitated by mechanical forces. To study this question, two types of polystyrene, with (**PS(ester)**) and without (**PS(carbon)**) two ester bonds incorporated in the middle of the polymer chain, were prepared via ATRP. The degradation behavior of the PS under ultrasonication induced mechanical force were explored in both THF and THF water mixture. The degradation rate constant of **PS(ester)** increases upon addition of water whereas the rate constant of **PS(carbon)** doesn't change with or without water. These results suggest that ester hydrolysis contributes to the totally degradation process. FTIR and NMR were used to characterize the degradation product and the result from both techniques supported the hypothesis that ester hydrolysis occur during the degradation process. More importantly, the rate constant of ester hydrolysis, which was deconvoluted from the total degradation rate, increases with the increase of polymer molecular weight and ultrasound power density, concomitantly mechanical forces. This correlation between ester bond hydrolysis rate constant and mechanical forces supports the hypothesis that the hydrolysis of ester bond in polymer backbone is sensitive to mechanical forces. These findings are not only important as a fundamental point of view, but also contribute to the design of new biodegradable, mechanical sensitive materials which can be used for tissue engineering, drug delivery and some other biomedical applications.

**Chapter 4** presents an alternative approach to mediate adhesion between synthetic surfaces and tissue. The strategy presented here is based on the modification of the surface of interest with a thin polymer film that can be transformed on-demand, using UV-light as a trigger, from a non-adhesive into a reactive and tissue adhesive state. As a first proof-of-concept, the feasibility of two photoreactive, thin polymer film platforms have been explored. Both of these films, colloquially referred to as polymer brushes, have been prepared using surface-initiated atom transfer radical polymerization (SI-ATRP) of 2-hydroxyethyl methacrylate (HEMA). In the first part of this chapter, it is shown that direct UV-light irradiation of PHEMA brushes generates tissue-reactive aldehyde groups and facilitates adhesion to meniscus tissue. While this strategy is very straightforward from an experimental point of view, a main drawback is that the generation of the tissue reactive aldehyde groups uses the 250 nm wavelength region of the UV spectrum, which simultaneously leads to extensive photodegradation of the polymer brush. The second part of this report outlines the synthesis of PHEMA brushes that are modified with 4-[3-(trifluoromethyl)-3H-diazirin-3-yl]benzoic acid (TFMDA) moieties. UV-irradiation of the TFMDA containing brushes transforms the diazirine moieties into reactive carbenes that can insert into C-H, N-H and O-H bonds and mediate the formation of covalent bonds between the brush surface and meniscus tissue. The advantage of the TFMDA modified polymer brushes is that these can be activated with 365 nm wavelength UV light, which does not cause photodegradation of the polymer films. While technique presented in this chapter has used silicon wafers and fused silica substrates as a first proof-of-concept, the versatility of SI-ATRP should

enable the application of this strategy to a broad range of biomedically relevant surfaces.

**Chapter 5** has investigated the pyroelectric and piezoelectric behavior of polyelectrolyte brushes. A series of PE brushes has been prepared including PMETAC, PSPMA and PMPC. A clear pyroelectric current change was detected in the circuit upon the temperature change when the PE brushes was connected to an open circuit. As a control, no current change was detected for non-PE brushes regardless of the hydrophilicity of the polymer brushes, which suggests that this effect is not caused by water molecules. Moreover, decreasing the temperature range is accompanied by an increase in current. A clear piezoelectric response was observed when applying a voltage (1 V) to the PE brushes with piezoelectric force microscopy, which suggests that there is a permanent dipole moment inside the materials. Surface potential measurements via scanning probe kelvin microscopy (SKPM) of PMETAC brushes show a positive net surface charge, which further indicates that the concentration of counterions, here chloride, is lower than that of quaternary amine. XPS measurements further confirmed this result. We hypothesize that the pyroelectric current is generated upon applying alternating sequence of temperature change because of the existence of a permanent dipole moment in the materials. This permanent dipole moment is supposed to be generated by the uneven net charge balance within the brushes.

In this thesis, CPR was used to study the fundamental question of how external forces influences the hydrolysis behavior of different bonds in polymer backbone at interfaces and in solution and to develop light triggerable bioadhesives and pyro/piezoelectric polymer brushes which have never been studied before. However, some fundamental

questions and experimental challenges still remain. For example, capturing hydrolysis products at interfaces and in solution is challenging due to vanishing low concentrations of those products. The behavior and dynamics of water penetrating into polymer brushes and how it subsequently participates in the hydrolysis remains an open question. Moreover, the questions on how to tune the pyro/piezoelectric properties with counterions and how to enlarge the pyroelectric effect are still unclear. I believe this thesis will help in better understanding the intrinsic relationship between (weak) mechanical force and chemical reactions in polymer systems and pave a way to exploring new functional, pyro/piezoelectric materials with excellent performance.

## 7. References

- (1) Staudinger, H. Über Polymerisation. *Berichte der deutschen chemischen Gesellschaft (A and B Series)* **1920**, 53, 1073-1085.
- (2) Cowie, J. M. G.; Arrighi, V. CRC press: 2007.
- (3) Szwarc, M. 'Living' Polymers. *Nature* **1956**, 178, 1168-1169.
- (4) Szwarc, M. Living polymers and mechanisms of anionic polymerization. In *Living Polymers and Mechanisms of Anionic Polymerization*; Springer: 1983, pp 1-177.
- (5) Hirao, A.; Loykulant, S.; Ishizone, T. Recent advance in living anionic polymerization of functionalized styrene derivatives. *Prog. Polym. Sci.* **2002**, 27, 1399-1471.
- (6) Fayt, R.; Forte, R.; Jacobs, C.; Jérôme, R.; Ouhadi, T.; Teyssié, P.; Varshney, S. K. New initiator system for the living anionic polymerization of tert-alkyl acrylates. *Macromolecules* **1987**, 20, 1442-1444.
- (7) Varshney, S. K.; Hautekeer, J.; Fayt, R.; Jérôme, R.; Teyssié, P. Anionic polymerization of (meth) acrylic monomers. 4. Effect of lithium salts as ligands on the "living" polymerization of methyl methacrylate using monofunctional initiators. *Macromolecules* **1990**, 23, 2618-2622.
- (8) Wang, J.-S.; Jerome, R.; Bayard, P.; Baylac, L.; Patin, M.; Teyssie, P. Anionic Polymerization of Acrylic Monomers. 15. Living Anionic Copolymerization of Mixtures of Methyl Methacrylate and tert-Butyl Acrylate As Promoted by Dibenzo-18-Crown-6. *Macromolecules* **1994**, 27, 4615-4620.
- (9) Varshney, S. K.; Jerome, R.; Bayard, P.; Jacobs, C.; Fayt, R.; Teyssie, P. Anionic polymerization of (meth) acrylic monomers. 7. Macrocyclic crown ethers as promoters of the living polymerization of methyl methacrylate using monofunctional initiators. *Macromolecules* **1992**, 25, 4457-4463.
- (10) Baskaran, D.; Chakrapani, S.; Sivaram, S. Effect of chelation of the lithium cation on the anionic polymerization of methyl methacrylate using organolithium initiators. *Macromolecules* **1995**, 28, 7315-7317.
- (11) Miyamoto, M.; Sawamoto, M.; Higashimura, T. Living polymerization of isobutyl vinyl ether with hydrogen iodide/iodine initiating system. *Macromolecules* **1984**, 17, 265-268.
- (12) Faust, R.; Kennedy, J. P. Living carbocationic polymerization. *Polym. Bull.* **1986**, 15, 317-323.
- (13) Sawamoto, M. Modern cationic vinyl polymerization. *Prog. Polym. Sci.* **1991**, 16, 111-172.
- (14) Matyjaszewski, K.; Sigwalt, P. Unified approach to living and non-living cationic polymerization of alkenes. *Polym. Int.* **1994**, 35, 1-26.
- (15) Webster, O.; Hertler, W.; Sogah, D.; Farnham, W.; RajanBabu, T. V. Group-transfer polymerization. 1. A new concept for addition polymerization with organosilicon initiators. *J. Am. Chem. Soc.* **1983**, 105, 5706-5708.
- (16) Dicker, I. B.; Cohen, G. M.; Farnham, W. B.; Hertler, W. R.; Laganis, E. D.; Sogah, D. Y. Oxyanions catalyze group-transfer polymerization to give living polymers. *Macromolecules* **1990**, 23, 4034-4041.
- (17) Webster, O. W. Group transfer polymerization: a critical review of its mechanism and comparison with other methods for controlled polymerization of acrylic monomers. In *New Synthetic Methods*; Springer: 2003, pp 1-34.
- (18) Quirk, R. P.; Kim, J. S. Mechanistic aspects of silicon-mediated polymerization (group transfer polymerization) of methyl methacrylate with ester enolate anions as nucleophilic catalysts. *J. Phys. Org. Chem.* **1995**, 8, 242-248.

- (19) Borsig, E.; Lazar, M.; Capla, M.; Florian, S. Reinitiation reactions of poly(methyl-methacrylate) with labile bound fragments of initiator *Angew. Makromol. Chem.* **1969**, *9*, 89-95.
- (20) Otsu, T.; Yoshida, M.; Tazaki, T. A model for living radical polymerization. *Makromolekulare Chemie-Rapid Communications* **1982**, *3*, 133-140.
- (21) Braun, D. Initiation of free radical polymerization by thermal cleavage of carbon-carbon bonds. *Macromol. Symp.* **1996**, *111*, 63-71.
- (22) Johnson, C. H. J.; Moad, G.; Solomon, D. H.; Spurling, T. H.; Vearring, D. J. The application of supercomputers in modelling chemical reaction kinetics: Kinetic simulation of 'quasi-living' radical polymerization. *Aust. J. Chem.* **1990**, *43*, 1215-1230.
- (23) Fischer, H. The persistent radical effect in "living" radical polymerization. *Macromolecules* **1997**, *30*, 5666-5672.
- (24) Georges, M. K.; Veregin, R. P. N.; Kazmaier, P. M.; Hamer, G. K. Narrow molecular-weight resins by a free-radical polymerization process. *Macromolecules* **1993**, *26*, 2987-2988.
- (25) Kato, M.; Kamigaito, M.; Sawamoto, M.; Higashimura, T. Polymerization of methyl methacrylate with the carbon tetrachloride/dichlorotris-(triphenylphosphine)ruthenium(ii)/methylaluminum bis(2,6-di-tert-butylphenoxide) initiating system: possibility of living radical polymerization. *Macromolecules* **1995**, *28*, 1721-1723.
- (26) Wang, J.-S.; Matyjaszewski, K. Controlled/"living" radical polymerization. atom transfer radical polymerization in the presence of transition-metal complexes. *J. Am. Chem. Soc.* **1995**, *117*, 5614-5615.
- (27) Wang, J.-S.; Matyjaszewski, K. Controlled/"living" radical polymerization. halogen atom transfer radical polymerization promoted by a Cu(I)/Cu(II) redox process. *Macromolecules* **1995**, *28*, 7901-7910.
- (28) Percec, V.; Barboiu, B. "Living" radical polymerization of styrene initiated by arenesulfonyl chlorides and CuI(bpy)<sub>n</sub>Cl. *Macromolecules* **1995**, *28*, 7970-7972.
- (29) Kharasch, M. S.; Jensen, E. V.; Urry, W. H. Addition of carbon tetrachloride and chloroform to olefins. *Science* **1945**, *102*, 128-128.
- (30) Minisci, F. Free-radical additions to olefins in the presence of redox systems. *Acc. Chem. Res.* **1975**, *8*, 165-171.
- (31) Chiefari, J.; Chong, Y. K.; Ercole, F.; Krstina, J.; Jeffery, J.; Le, T. P. T.; Mayadunne, R. T. A.; Meijs, G. F.; Moad, C. L.; Moad, G.; Rizzardo, E.; Thang, S. H. Living free-radical polymerization by reversible addition-fragmentation chain transfer: the RAFT process. *Macromolecules* **1998**, *31*, 5559-5562.
- (32) Delduc, P.; Tailhan, C.; Zard, S. Z. A convenient source of alkyl and acyl radicals. *J. Chem. Soc., Chem. Commun.* **1988**, 308-310.
- (33) Nicolas, J.; Guillaneuf, Y.; Lefay, C.; Bertin, D.; Gigmes, D.; Charleux, B. Nitroxide-mediated polymerization. *Prog. Polym. Sci.* **2013**, *38*, 63-235.
- (34) Matyjaszewski, K.; Gaynor, S.; Greszta, D.; Mardare, D.; Shigemoto, T. 'Living' and controlled radical polymerization. *J. Phys. Org. Chem.* **1995**, *8*, 306-315.
- (35) Clay, P. A.; Gilbert, R. G. Molecular weight distributions in free-radical polymerizations. 1. model development and implications for data interpretation. *Macromolecules* **1995**, *28*, 552-569.
- (36) Dollin, M.; Szkurhan, A. R.; Georges, M. K. Rapid additive-free TEMPO-mediated stable free radical polymerizations of styrene. *J. Polym. Sci., Part A: Polym. Chem.* **2007**, *45*, 5487-5493.
- (37) Moad, G.; Rizzardo, E.; Solomon, D. H. Selectivity of the reaction of free radicals with styrene.

*Macromolecules* **1982**, *15*, 909-914.

(38) Moad, G.; Rizzardo, E.; Thang, S. H. Toward living radical polymerization. *Acc. Chem. Res.* **2008**, *41*, 1133-1142.

(39) Goto, A.; Fukuda, T. Kinetics of living radical polymerization. *Prog. Polym. Sci.* **2004**, *29*, 329-385.

(40) Hawker, C. J. Molecular weight control by a "living" free-radical polymerization process. *J. Am. Chem. Soc.* **1994**, *116*, 11185-11186.

(41) Schulte, T.; Studer, A. New seven- and eight-membered cyclic alkoxyamines for the living free radical polymerization. *Macromolecules* **2003**, *36*, 3078-3084.

(42) Li, I.; Howell, B.; Dineen, M.; Kastl, P.; Lyons, J.; Meunier, D.; Smith, P.; Priddy, D. Block copolymer preparation using sequential normal/living radical polymerization techniques. *Macromolecules* **1997**, *30*, 5195-5199.

(43) Connolly, T. J.; Baldovi, M.; Mohtat, N.; Scaiano, J. Photochemical synthesis of TEMPO-capped initiators for "living" free radical polymerization. *Tetrahedron Lett.* **1996**, *37*, 4919-4922.

(44) Dao, J.; Benoit, D.; Hawker, C. J. A versatile and efficient synthesis of alkoxyamine LFR initiators via manganese based asymmetric epoxidation catalysts. *J. Polym. Sci., Part A: Polym. Chem.* **1998**, *36*, 2161-2167.

(45) Bowman, D. F.; Gillan, T.; Ingold, K. U. Kinetic applications of electron paramagnetic resonance spectroscopy. III. Self-reactions of dialkyl nitroxide radicals. *J. Am. Chem. Soc.* **1971**, *93*, 6555-6561.

(46) Bowman, D. F.; Brokenshire, J. L.; Gillan, T.; Ingold, K. U. Kinetic applications of electron paramagnetic resonance spectroscopy. II. Self-reactions of N-alkyl nitroxides and N-phenyl nitroxide. *J. Am. Chem. Soc.* **1971**, *93*, 6551-6555.

(47) Catala, J.; Bubel, F.; Hammouch, S. O. Living radical polymerization: kinetic results. *Macromolecules* **1995**, *28*, 8441-8443.

(48) Benoit, D.; Chaplinski, V.; Braslau, R.; Hawker, C. J. Development of a universal alkoxyamine for "living" free radical polymerizations. *J. Am. Chem. Soc.* **1999**, *121*, 3904-3920.

(49) Benoit, D.; Grimaldi, S.; Robin, S.; Finet, J.-P.; Tordo, P.; Gnanou, Y. Kinetics and mechanism of controlled free-radical polymerization of styrene and n-butyl acrylate in the presence of an acyclic  $\beta$ -phosphonylated nitroxide. *J. Am. Chem. Soc.* **2000**, *122*, 5929-5939.

(50) Knoop, C. A.; Studer, A. Hydroxy- and silyloxy-substituted TEMPO derivatives for the living free-radical polymerization of styrene and n-butyl acrylate: synthesis, kinetics, and mechanistic studies. *J. Am. Chem. Soc.* **2003**, *125*, 16327-16333.

(51) Schmidt-Naake, G.; Stenzel, M. Studium der lebenden radikalischen Polymerisation mit der differential scanning calorimetry (DSC). *Angew. Makromol. Chem.* **1998**, *254*, 55-60.

(52) Butz, S.; Hillermann, J.; Schmidt-Naake, G.; Kressler, J.; Thomann, R.; Heck, B.; Stühn, B. Synthesis and microphase separation of diblock copolymers of styrene and p-chlorostyrene prepared by using N-oxyl capped macroinitiators. *Acta Polymerica* **1998**, *49*, 693-699.

(53) Bultz, E.; Bender, T. P. NMP of chloromethylstyrene with minimized PDI: the role of the initiator/nitroxide system and the meta isomer. *Macromolecules* **2011**, *44*, 3666-3669.

(54) Wan, X.; Tu, Y.; Zhang, D.; Zhou, Q. Nitroxide-mediated 'living' free radical synthesis of novel rod-coil diblock copolymers with polystyrene and mesogen-jacketed liquid-crystal polymer segments. *Polym. Int.* **2000**, *49*, 243-247.

(55) Gao, L. C.; Fan, X. H.; Shen, Z. H.; Chen, X.; Zhou, Q. F. Jacketed polymers: controlled

- synthesis of mesogen-jacketed polymers and block copolymers. *J. Polym. Sci., Part A: Polym. Chem.* **2009**, *47*, 319-330.
- (56) Moroni, M.; Hilberer, A.; Hadziioannou, G. Synthesis of a functional polymer with pendent luminescent phenylenevinylene units through nitroxide-mediated free-radical polymerization. *Macromol. Rapid Commun.* **1996**, *17*, 693-702.
- (57) Sessions, L. B.; Miinea, L. A.; Ericson, K. D.; Glueck, D. S.; Grubbs, R. B. Alkyne-functional homopolymers and block copolymers through nitroxide-mediated free radical polymerization of 4-(phenylethynyl) styrene. *Macromolecules* **2005**, *38*, 2116-2121.
- (58) Chang, C.; Zhu, J.; Zhang, Z.; Zhou, N.; Cheng, Z.; Zhu, X. Synthesizing and characterization of comb-shaped carbazole containing copolymer via combination of ring opening polymerization and nitroxide-mediated polymerization. *Polymer* **2010**, *51*, 1947-1953.
- (59) Lizotte, J. R.; Erwin, B. M.; Colby, R. H.; Long, T. E. Investigations of thermal polymerization in the stable free-radical polymerization of 2-vinylnaphthalene. *J. Polym. Sci., Part A: Polym. Chem.* **2002**, *40*, 583-590.
- (60) Huang, W.; Charleux, B.; Chiarelli, R.; Marx, L.; Rassat, A.; Vairon, J. P. Synthesis of water-soluble nitroxides and their use as mediators in aqueous-phase controlled radical polymerization. *Macromol. Chem. Phys.* **2002**, *203*, 1715-1723.
- (61) Bouix, M.; Gouzi, J.; Charleux, B.; Vairon, J. P.; Guinot, P. Synthesis of amphiphilic polyelectrolyte block copolymers using “living” radical polymerization. Application as stabilizers in emulsion polymerization. *Macromol. Rapid Commun.* **1998**, *19*, 209-213.
- (62) Cho, C. G.; You, Y. G.; Jang, H. Y.; Woo, J. K.; An, S. K. Synthesis of poly (styrene-*b*-styrenesulfonic acid) and its blend with PPO for proton exchange membrane. *J. Nanosci. Nanotechnol.* **2006**, *6*, 3665-3669.
- (63) Charleux, B.; Nicolas, J.; Guerret, O. Theoretical expression of the average activation-deactivation equilibrium constant in controlled/living free-radical copolymerization operating via reversible termination. Application to a strongly improved control in nitroxide-mediated polymerization of methyl methacrylate. *Macromolecules* **2005**, *38*, 5485-5492.
- (64) Ananchenko, G. S.; Fischer, H. Decomposition of model alkoxyamines in simple and polymerizing systems. I. 2, 2, 6, 6-tetramethylpiperidiny-N-oxyl-based compounds. *J. Polym. Sci., Part A: Polym. Chem.* **2001**, *39*, 3604-3621.
- (65) Mchale, R.; Aldabbagh, F.; Zetterlund, P. B. The role of excess nitroxide in the SG1 (N-tert-butyl-N-[1-diethylphosphono-(2, 2-dimethylpropyl)] nitroxide)-mediated polymerization of methyl methacrylate. *J. Polym. Sci., Part A: Polym. Chem.* **2007**, *45*, 2194-2203.
- (66) Ananchenko, G. S.; Souaille, M.; Fischer, H.; Le Mercier, C.; Tordo, P. Decomposition of model alkoxyamines in simple and polymerizing systems. II. Diastereomeric N-(2-methylpropyl)-N-(1-diethyl-phosphono-2, 2-dimethyl-propyl)-aminoxyl-based compounds. *J. Polym. Sci., Part A: Polym. Chem.* **2002**, *40*, 3264-3283.
- (67) Guillaneuf, Y.; Gimes, D.; Marque, S. R.; Tordo, P.; Bertin, D. Nitroxide-mediated polymerization of methyl methacrylate using an SG1-based alkoxyamine: how the penultimate effect could lead to uncontrolled and unliving polymerization. *Macromol. Chem. Phys.* **2006**, *207*, 1278-1288.
- (68) Dire, C.; Belleney, J.; Nicolas, J.; Bertin, D.; Magnet, S.; Charleux, B.  $\beta$ -Hydrogen transfer from poly (methyl methacrylate) propagating radicals to the nitroxide SG1: Analysis of the chain-end and determination of the rate constant. *J. Polym. Sci., Part A: Polym. Chem.* **2008**, *46*, 6333-6345.
- (69) Zang, L.; Wong, E. H.; Barner-Kowollik, C.; Junkers, T. Control of methyl methacrylate radical

- polymerization via Enhanced Spin Capturing Polymerization (ESCP). *Polymer* **2010**, *51*, 3821-3825.
- (70) Greene, A. C.; Grubbs, R. B. Synthesis and evaluation of N-phenylalkoxyamines for nitroxide-mediated polymerization. *Macromolecules* **2009**, *42*, 4388-4390.
- (71) Devonport, W.; Michalak, L.; Malmström, E.; Mate, M.; Kurdi, B.; Hawker, C. J.; Barclay, G. G.; Sinta, R. "Living" free-radical polymerizations in the absence of initiators: controlled autopolymerization. *Macromolecules* **1997**, *30*, 1929-1934.
- (72) Thomson, M. E.; Manley, A.-M.; Ness, J. S.; Schmidt, S. C.; Cunningham, M. F. Nitroxide-mediated surfactant-free emulsion polymerization of n-butyl methacrylate with a small amount of styrene. *Macromolecules* **2010**, *43*, 7958-7963.
- (73) Nicolas, J.; Brusseau, S.; Charleux, B. A minimal amount of acrylonitrile turns the nitroxide-mediated polymerization of methyl methacrylate into an almost ideal controlled/living system. *J. Polym. Sci., Part A: Polym. Chem.* **2010**, *48*, 34-47.
- (74) Nicolas, J.; Mueller, L.; Dire, C.; Matyjaszewski, K.; Charleux, B. Comprehensive modeling study of nitroxide-mediated controlled/living radical copolymerization of methyl methacrylate with a small amount of styrene. *Macromolecules* **2009**, *42*, 4470-4478.
- (75) Lessard, B.; Marić, M. Incorporating glycidyl methacrylate into block copolymers using poly (methacrylate-ran-styrene) macroinitiators synthesized by nitroxide-mediated polymerization. *J. Polym. Sci., Part A: Polym. Chem.* **2009**, *47*, 2574-2588.
- (76) Nicolas, J.; Couvreur, P.; Charleux, B. Comblike polymethacrylates with poly (ethylene glycol) side chains via nitroxide-mediated controlled free-radical polymerization. *Macromolecules* **2008**, *41*, 3758-3761.
- (77) Edeleva, M.; Marque, S. R.; Bertin, D.; Gigmes, D.; Guillaneuf, Y.; Morozov, S. V.; Bagryanskaya, E. G. Hydrogen-transfer reaction in nitroxide mediated polymerization of methyl methacrylate: 2, 2-Diphenyl-3-phenylimino-2, 3-dihydroindol-1-yloxyl nitroxide (DPAIO) vs. TEMPO. *J. Polym. Sci., Part A: Polym. Chem.* **2008**, *46*, 6828-6842.
- (78) Greene, A. C.; Grubbs, R. B. Nitroxide-mediated polymerization of methyl methacrylate and styrene with new alkoxyamines from 4-nitrophenyl 2-methylpropionat-2-yl radicals. *Macromolecules* **2010**, *43*, 10320-10325.
- (79) Matyjaszewski, K.; Paik, H.-j.; Zhou, P.; Diamanti, S. J. Determination of activation and deactivation rate constants of model compounds in atom transfer radical polymerization. *Macromolecules* **2001**, *34*, 5125-5131.
- (80) Tang, W.; Tsarevsky, N. V.; Matyjaszewski, K. Determination of equilibrium constants for atom transfer radical polymerization. *J. Am. Chem. Soc.* **2006**, *128*, 1598-1604.
- (81) Tang, W.; Matyjaszewski, K. Effect of ligand structure on activation rate constants in ATRP. *Macromolecules* **2006**, *39*, 4953-4959.
- (82) Tang, W.; Kwak, Y.; Braunecker, W.; Tsarevsky, N. V.; Coote, M. L.; Matyjaszewski, K. Understanding atom transfer radical polymerization: effect of ligand and initiator structures on the equilibrium constants. *J. Am. Chem. Soc.* **2008**, *130*, 10702-10713.
- (83) Matyjaszewski, K.; Gaynor, S.; Greszta, D.; Mardare, D.; Shigemoto, T. 'Living' and controlled radical polymerization. *J. Phys. Org. Chem.* **1995**, *8*, 306-315.
- (84) Matyjaszewski, K. Introduction to living polymeriz. Living and/or controlled polymerization. *J. Phys. Org. Chem.* **1995**, *8*, 197-207.
- (85) Kotani, Y.; Kamigaito, M.; Sawamoto, M. Living radical polymerization of para-substituted styrenes and synthesis of styrene-based copolymers with rhenium and iron complex catalysts.

*Macromolecules* **2000**, *33*, 6746-6751.

- (86) Kotani, Y.; Kamigaito, M.; Sawamoto, M. Re (V)-Mediated Living Radical Polymerization of Styrene: ReO<sub>2</sub>I (PPh<sub>3</sub>)<sub>2</sub>/R–I Initiating Systems. *Macromolecules* **1999**, *32*, 2420-2424.
- (87) Singha, N. K.; Klumperman, B. Atom-transfer radical polymerization of methyl methacrylate (MMA) using CuSCN as the catalyst. *Macromol. Rapid Commun.* **2000**, *21*, 1116-1120.
- (88) Matyjaszewski, K. Transition metal catalysis in controlled radical polymerization: atom transfer radical polymerization. *Chem. - Eur. J.* **1999**, *5*, 3095-3102.
- (89) Patten, T. E.; Matyjaszewski, K. Atom transfer radical polymerization and the synthesis of polymeric materials. *Adv. Mater.* **1998**, *10*, 901-915.
- (90) Matyjaszewski, K.; Xia, J. Atom transfer radical polymerization. *Chem. Rev.* **2001**, *101*, 2921-2990.
- (91) Xia, J.; Zhang, X.; Matyjaszewski, K. The effect of ligands on copper-mediated atom transfer radical polymerization. In *Transition Metal Catalysis in Macromolecular Design*; American Chemical Society: 2000; Vol. 760, pp 207-223.
- (92) Moad, G.; Rizzardo, E.; Thang, S. H. Living radical polymerization by the RAFT process. *Aust. J. Chem.* **2005**, *58*, 379-410.
- (93) Favier, A.; Charreyre, M.-T. Experimental requirements for an efficient control of free-radical polymerizations via the reversible addition-fragmentation chain transfer (RAFT) process. *Macromol. Rapid Commun.* **2006**, *27*, 653-692.
- (94) Moad, G.; Rizzardo, E.; Thang, S. H. Living radical polymerization by the RAFT process - a second update. *Aust. J. Chem.* **2009**, *62*, 1402-1472.
- (95) Moad, G.; Rizzardo, E.; Thang, S. H. Living radical polymerization by the RAFT process - a first update. *Aust. J. Chem.* **2006**, *59*, 669-692.
- (96) Krstina, J.; Moad, C. L.; Moad, G.; Rizzardo, E.; Berge, C. T.; Fryd, M. A new form of controlled growth free radical polymerization. *Macromol. Symp.* **1996**, *111*, 13-23.
- (97) Moad, G.; Rizzardo, E.; Thang, S. H. Living radical polymerization by the RAFT process a first update. *Aust. J. Chem.* **2006**, *59*, 669-692.
- (98) Braunecker, W. A.; Matyjaszewski, K. Controlled/living radical polymerization: features, developments, and perspectives. *Prog. Polym. Sci.* **2007**, *32*, 93-146.
- (99) Milner, S. Polymer brushes. *Science* **1991**, *251*, 905-914.
- (100) Zhao, B.; Brittain, W. J. Polymer brushes: surface-immobilized macromolecules. *Prog. Polym. Sci.* **2000**, *25*, 677-710.
- (101) Edmondson, S.; Osborne, V. L.; Huck, W. T. Polymer brushes via surface-initiated polymerizations. *Chem. Soc. Rev.* **2004**, *33*, 14-22.
- (102) Tsujii, Y.; Ohno, K.; Yamamoto, S.; Goto, A.; Fukuda, T. Structure and properties of high-density polymer brushes prepared by surface-initiated living radical polymerization. In *Surface-Initiated Polymerization I*; Jordan, R., Ed.; Springer Berlin Heidelberg: Berlin, Heidelberg, 2006, pp 1-45.
- (103) Barbey, R.; Lavanant, L.; Paripovic, D.; Schüwer, N.; Sugnaux, C.; Tugulu, S.; Klok, H.-A. Polymer brushes via surface-initiated controlled radical polymerization: synthesis, characterization, properties, and applications. *Chem. Rev.* **2009**, *109*, 5437-5527.
- (104) Zoppe, J. O.; Ataman, N. C.; Mocny, P.; Wang, J.; Moraes, J.; Klok, H.-A. Surface-initiated controlled radical polymerization: state-of-the-art, opportunities, and challenges in surface and interface engineering with polymer brushes. *Chem. Rev.* **2017**, *117*, 1105-1318.
- (105) Xie, G.; Khabibullin, A.; Pietrasik, J.; Yan, J.; Matyjaszewski, K. Polymer brushes by atom

transfer radical polymerization. *Polymer and Biopolymer Brushes: For Materials Science and Biotechnology* **2018**, 242.

(106) Brittain, W. J.; Minko, S. A structural definition of polymer brushes. *J. Polym. Sci., Part A: Polym. Chem.* **2007**, 45, 3505-3512.

(107) Jain, P.; Baker, G. L.; Bruening, M. L. Applications of polymer brushes in protein analysis and purification. *Annu. Rev. Anal. Chem.* **2009**, 2, 387-408.

(108) Galvin, C. J.; Genzer, J. Applications of surface-grafted macromolecules derived from post-polymerization modification reactions. *Prog. Polym. Sci.* **2012**, 37, 871-906.

(109) Azzaroni, O. Polymer brushes here, there, and everywhere: Recent advances in their practical applications and emerging opportunities in multiple research fields. *J. Polym. Sci., Part A: Polym. Chem.* **2012**, 50, 3225-3258.

(110) Krishnamoorthy, M.; Hakobyan, S.; Ramstedt, M.; Gautrot, J. E. Surface-initiated polymer brushes in the biomedical field: applications in membrane science, biosensing, cell culture, regenerative medicine and antibacterial coatings. *Chem. Rev.* **2014**, 114, 10976-11026.

(111) Hui, C. M.; Pietrasik, J.; Schmitt, M.; Mahoney, C.; Choi, J.; Bockstaller, M. R.; Matyjaszewski, K. Surface-initiated polymerization as an enabling tool for multifunctional (nano-) engineered hybrid materials. *Chem. Mater.* **2013**, 26, 745-762.

(112) Li, B.; Yu, B.; Ye, Q.; Zhou, F. Tapping the potential of polymer brushes through synthesis. *Acc. Chem. Res.* **2014**, 48, 229-237.

(113) Wu, L.; Glebe, U.; Boeker, A. Surface-initiated controlled radical polymerizations from silica nanoparticles, gold nanocrystals, and bionanoparticles. *Polym. Chem.* **2015**, 6, 5143-5184.

(114) Chen, W.-L.; Cordero, R.; Tran, H.; Ober, C. K. 50th anniversary perspective: polymer brushes: novel surfaces for future materials. *Macromolecules* **2017**, 50, 4089-4113.

(115) Hucknall, A.; Rangarajan, S.; Chilkoti, A. In pursuit of zero: polymer brushes that resist the adsorption of proteins. *Adv. Mater.* **2009**, 21, 2441-2446.

(116) Mei, Y.; Wu, T.; Xu, C.; Langenbach, K. J.; Elliott, J. T.; Vogt, B. D.; Beers, K. L.; Amis, E. J.; Washburn, N. R. Tuning cell adhesion on gradient poly (2-hydroxyethyl methacrylate)-grafted surfaces. *Langmuir* **2005**, 21, 12309-12314.

(117) Tugulu, S.; Klok, H.-A. Stability and nonfouling properties of poly (poly (ethylene glycol) methacrylate) brushes under cell culture conditions. *Biomacromolecules* **2008**, 9, 906-912.

(118) Ma, H.; Li, D.; Sheng, X.; Zhao, B.; Chilkoti, A. Protein-resistant polymer coatings on silicon oxide by surface-initiated atom transfer radical polymerization. *Langmuir* **2006**, 22, 3751-3756.

(119) Fan, X.; Lin, L.; Messersmith, P. B. Cell fouling resistance of polymer brushes grafted from Ti substrates by surface-initiated polymerization: effect of ethylene glycol side chain length. *Biomacromolecules* **2006**, 7, 2443-2448.

(120) Raynor, J. E.; Capadona, J. R.; Collard, D. M.; Petrie, T. A.; García, A. J. Polymer brushes and self-assembled monolayers: versatile platforms to control cell adhesion to biomaterials. *Biointerfaces* **2009**, 4, FA3-FA16.

(121) Banerjee, I.; Pangule, R. C.; Kane, R. S. Antifouling coatings: recent developments in the design of surfaces that prevent fouling by proteins, bacteria, and marine organisms. *Adv. Mater.* **2011**, 23, 690-718.

(122) Blaszykowski, C.; Sheikh, S.; Thompson, M. Surface chemistry to minimize fouling from blood-based fluids. *Chem. Soc. Rev.* **2012**, 41, 5599-5612.

(123) Yang, W. J.; Neoh, K.-G.; Kang, E.-T.; Teo, S. L.-M.; Rittschof, D. Polymer brush coatings for

- combating marine biofouling. *Prog. Polym. Sci.* **2014**, *39*, 1017-1042.
- (124) Moroni, L.; Gunnewiek, M. K.; Benetti, E. M. Polymer brush coatings regulating cell behavior: Passive interfaces turn into active. *Acta Biomater.* **2014**, *10*, 2367-2378.
- (125) Lowe, S.; O'Brien-Simpson, N. M.; Connal, L. A. Antibiofouling polymer interfaces: poly (ethylene glycol) and other promising candidates. *Polym. Chem.* **2015**, *6*, 198-212.
- (126) Mocny, P.; Klok, H.-A. Tribology of surface-grafted polymer brushes. *Molecular Systems Design & Engineering* **2016**, *1*, 141-154.
- (127) Dunlop, I. E.; Briscoe, W. H.; Titmuss, S.; Jacobs, R. M.; Osborne, V. L.; Edmondson, S.; Huck, W. T.; Klein, J. Direct measurement of normal and shear forces between surface-grown polyelectrolyte layers. *J. Phys. Chem. B* **2009**, *113*, 3947-3956.
- (128) Chen, M.; Briscoe, W. H.; Armes, S. P.; Cohen, H.; Klein, J. Robust, biomimetic polymer brush layers grown directly from a planar mica surface. *ChemPhysChem* **2007**, *8*, 1303-1306.
- (129) Zhang, Z. J.; Moxey, M.; Alswieleh, A.; Armes, S. P.; Lewis, A. L.; Geoghegan, M.; Leggett, G. J. Nanotribological investigation of polymer brushes with lithographically defined and systematically varying grafting densities. *Langmuir* **2017**, *33*, 706-713.
- (130) Wright, R. A.; Wang, K.; Qu, J.; Zhao, B. Oil- nsoluble polymer brush grafted nanoparticles as effective lubricant additives for friction and wear reductio. *Angew. Chem., Int. Ed.* **2016**, *55*, 8656-8660.
- (131) Morgese, G.; Trachsel, L.; Romio, M.; Divandari, M.; Ramakrishna, S. N.; Benetti, E. M. Topological polymer chemistry enters surface science: linear versus cyclic polymer brushes. *Angew. Chem., Int. Ed.* **2016**, *55*, 15583-15588.
- (132) Klein, J. Hydration lubrication. *Friction* **2013**, *1*, 1-23.
- (133) Kreer, T. Polymer-brush lubrication: a review of recent theoretical advances. *Soft Matter* **2016**, *12*, 3479-3501.
- (134) Benetti, E. M.; Divandari, M.; Ramakrishna, S. N.; Morgese, G.; Yan, W.; Trachsel, L. Loops and cycles at surfaces: the unique properties of topological polymer brushes. *Chemistry—A European Journal* **2017**, *23*, 12433-12442.
- (135) Morgese, G.; Benetti, E. M.; Zenobi-Wong, M. Molecularly engineered biolubricants for articular cartilage. *Adv. Healthcare Mater.* **2018**, 1701463.
- (136) Chen, M.; Briscoe, W. H.; Armes, S. P.; Klein, J. Lubrication at physiological pressures by polyzwitterionic brushes. *Science* **2009**, *323*, 1698-1701.
- (137) Paripovic, D.; Klok, H.-A. Polymer brush guided formation of thin gold and palladium/gold bimetallic films. *ACS Appl. Mater. & Interfaces* **2011**, *3*, 910-917.
- (138) Quintana, R.; Gosa, M.; Jańczewski, D.; Kutnyanszky, E.; Vancso, G. J. Enhanced stability of low fouling zwitterionic polymer brushes in seawater with diblock architecture. *Langmuir* **2013**, *29*, 10859-10867.
- (139) Bain, E. D.; Dawes, K.; Özcam, A. E.; Hu, X.; Gorman, C. B.; Šrogl, J. í.; Genzer, J. Surface-initiated polymerization by means of novel, stable, non-ester-based radical initiator. *Macromolecules* **2012**, *45*, 3802-3815.
- (140) Galvin, C. J.; Bain, E. D.; Henke, A.; Genzer, J. Instability of surface-grafted weak polyacid brushes on flat substrates. *Macromolecules* **2015**, *48*, 5677-5687.
- (141) Lego, B. a.; Skene, W.; Giasson, S. Swelling study of responsive polyelectrolyte brushes grafted from mica substrates: effect of pH, salt, and grafting density. *Macromolecules* **2010**, *43*, 4384-4393.
- (142) Zhu, Y.; Lv, B. e.; Zhang, P.; Ma, H. Swelling induced Au–S bond breakage is determined by the molecular composition of surface tethered copolymers—carboxylated poly (OEGMA-r-HEMA).

*Chem. Commun.* **2011**, 47, 9855-9857.

(143) Enomoto, K.; Takahashi, S.; Iwase, T.; Yamashita, T.; Maekawa, Y. Degradation manner of polymer grafts chemically attached on thermally stable polymer films: swelling-induced detachment of hydrophilic grafts from hydrophobic polymer substrates in aqueous media. *J. Mater. Chem.* **2011**, 21, 9343-9349.

(144) Melzak, K. A.; Yu, K.; Bo, D.; Kizhakkedathu, J. N.; Toca-Herrera, J. L. Chain length and grafting density dependent enhancement in the hydrolysis of ester-linked polymer brushes. *Langmuir* **2015**, 31, 6463-6470.

(145) Klok, H.-A.; Genzer, J. Expanding the polymer mechanochemistry toolbox through surface-initiated polymerization. *ACS Macro Lett.* **2015**, 4, 636-639.

(146) Ataman, N. C.; Klok, H.-A. Degrafting of poly (poly (ethylene glycol) methacrylate) brushes from planar and spherical silicon substrates. *Macromolecules* **2016**, 49, 9035-9047.

(147) May, P. A.; Moore, J. S. Polymer mechanochemistry: techniques to generate molecular force via elongational flows. *Chem. Soc. Rev.* **2013**, 42, 7497-7506.

(148) Caruso, M. M.; Davis, D. A.; Shen, Q.; Odom, S. A.; Sottos, N. R.; White, S. R.; Moore, J. S. Mechanically-induced chemical changes in polymeric materials. *Chem. Rev.* **2009**, 109, 5755-5798.

(149) Wiggins, K. M.; Brantley, J. N.; Bielawski, C. W. Methods for activating and characterizing mechanically responsive polymers. *Chem. Soc. Rev.* **2013**, 42, 7130-7147.

(150) Sheiko, S. S.; Sun, F. C.; Randall, A.; Shirvanyants, D.; Rubinstein, M.; Lee, H.-i.; Matyjaszewski, K. Adsorption-induced scission of carbon-carbon bonds. *Nature* **2006**, 440, 191-194.

(151) Li, Y. C.; Sheiko, S. S. Molecular mechanochemistry: engineering and implications of inherently strained architectures. In *Polymer Mechanochemistry*; Boulatov, R., Ed.; Springer Int Publishing Ag: Cham, 2015; Vol. 369, pp 1-36.

(152) Bao, Z.; Bruening, M. L.; Baker, G. L. Rapid growth of polymer brushes from immobilized initiators. *J. Am. Chem. Soc.* **2006**, 128, 9056-9060.

(153) Tugulu, S.; Harms, M.; Fricke, M.; Volkmer, D.; Klok, H. A. Polymer brushes as ionotropic matrices for the directed fabrication of microstructured calcite thin films. *Angew. Chem., Int. Ed.* **2006**, 45, 7458-7461.

(154) Sheiko, S. S.; Panyukov, S.; Rubinstein, M. Bond tension in tethered macromolecules. *Macromolecules* **2011**, 44, 4520-4529.

(155) Zerda, T.; Hoang, G. Effect of solvents on the hydrolysis reaction of tetramethyl orthosilicate. *Chem. Mater.* **1990**, 2, 372-376.

(156) Laidler, K. J.; Landskroener, P. A. The influence of the solvent on reaction rates. *Trans. Faraday Soc.* **1956**, 52, 200-210.

(157) Groote, R.; Jakobs, R. T.; Sijbesma, R. P. Mechanocatalysis: forcing latent catalysts into action. *Polym. Chem.* **2013**, 4, 4846-4859.

(158) Li, J.; Nagamani, C.; Moore, J. S. Polymer mechanochemistry: from destructive to productive. *Acc. Chem. Res.* **2015**, 48, 2181-2190.

(159) Bowser, B. H.; Craig, S. L. Empowering mechanochemistry with multi-mechanophore polymer architectures. *Polym. Chem.* **2018**, 9, 3583-3593.

(160) Willis-Fox, N.; Rognin, E.; Aljohani, T. A.; Daly, R. Polymer mechanochemistry: manufacturing is now a force to be reckoned with. *Chem* **2018**, 4, 2499-2537.

(161) Izak-Nau, E.; Campagna, D.; Baumann, C.; Göstl, R. Polymer mechanochemistry-enabled pericyclic reactions. *Polym. Chem.* **2020**, 11, 2274-2299.

- (162) Anderson, L.; Boulatov, R. Polymer mechanochemistry: a new frontier for physical organic chemistry. In *Advances in Physical Organic Chemistry*; Williams, I. H., Williams, N. H., Eds.; Academic Press: Elsevier Science Publishing: San Diego, United States, 2018; Vol. 52, pp 87-143.
- (163) Paulusse, J. M. J.; Sijbesma, R. P. Ultrasound in polymer chemistry: revival of an established technique. *J. Polym. Sci., Part A: Polym. Chem.* **2006**, *44*, 5445-5453.
- (164) Nguyen, T. Q.; Kausch, H.-H. Mechanochemical degradation in transient elongational flow. In *Macromolecules: Synthesis, Order and Advanced Properties; Advances in Polymer Science*; Springer: Berlin, Heidelberg, 1992; Vol. 100, pp 73-182.
- (165) Stratigaki, M.; Göstl, R. Methods for exerting and sensing force in polymer materials using mechanophores. *ChemPlusChem* **2020**, *85*, 1095-1103.
- (166) Brantley, J. N.; Wiggins, K. M.; Bielawski, C. W. Polymer mechanochemistry: the design and study of mechanophores. *Polym. Int.* **2013**, *62*, 2-12.
- (167) Brown, C. L.; Craig, S. L. Molecular engineering of mechanophore activity for stress-responsive polymeric materials. *Chem. Sci.* **2015**, *6*, 2158-2165.
- (168) Groote, R.; Jakobs, R. T. M.; Sijbesma, R. P. Mechanocatalysis: forcing latent catalysts into action. *Polym. Chem.* **2013**, *4*, 4846-4859.
- (169) Clough, J. M.; Balan, A.; Sijbesma, R. P. Mechanochemical reactions reporting and repairing bond scission in polymers. In *Polymer Mechanochemistry*; Boulatov, R., Ed.; Springer International Publishing: Cham, Switzerland, 2015; Vol. 369, pp 209-238.
- (170) Akbulatov, S.; Tian, Y.; Kapustin, E.; Boulatov, R. Model studies of the kinetics of ester hydrolysis under stretching force. *Angew. Chem., Int. Ed.* **2013**, *52*, 6992-6995.
- (171) Tong, R.; Lu, X.; Xia, H. A facile mechanophore functionalization of an amphiphilic block copolymer towards remote ultrasound and redox dual stimulus responsiveness. *Chem. Commun.* **2014**, *50*, 3575-3578.
- (172) Li, F.; Xie, C.; Cheng, Z.; Xia, H. Ultrasound responsive block copolymer micelle of poly(ethylene glycol)-poly(propylene glycol) obtained through click reaction. *Ultrason. Sonochem.* **2016**, *30*, 9-17.
- (173) Lin, Y.-K.; Yu, Y.-C.; Wang, S.-W.; Lee, R.-S. Temperature, ultrasound and redox triple-responsive poly(n-isopropylacrylamide) block copolymer: synthesis, characterization and controlled release. *RSC Advances* **2017**, *7*, 43212-43226.
- (174) Shao, C.; Duan, H.; Min, Y.; Zhang, X. Diphenyl cyclopropanone-centered polymers for site-specific co-releasing and chain dissociation. *Chin. Chem. Lett.* **2020**, *31*, 299-302.
- (175) Wang, J.; Klok, H.-A. Swelling-induced chain stretching enhances hydrolytic degrafting of hydrophobic polymer brushes in organic media. *Angew. Chem., Int. Ed.* **2019**, *58*, 9989-9993.
- (176) Bain, E. D.; Dawes, K.; Özcam, A. E.; Hu, X.; Gorman, C. B.; Šrogl, J.; Genzer, J. Surface-initiated polymerization by means of novel, stable, non-ester-based radical initiator. *Macromolecules* **2012**, *45*, 3802-3815.
- (177) Ko, Y.; Genzer, J. Spontaneous degrafting of weak and strong polycationic brushes in aqueous buffer solutions. *Macromolecules* **2019**, *52*, 6192-6200.
- (178) Rodriguez-Galan, A.; Franco, L.; Puiggali, J. Degradable poly(ester amide)s for biomedical applications. *Polymers* **2011**, *3*, 65-99.
- (179) Campoccia, D.; Doherty, P.; Radice, M.; Brun, P.; Abatangelo, G.; Williams, D. F. Semisynthetic resorbable materials from hyaluronan esterification. *Biomaterials* **1998**, *19*, 2101-2127.
- (180) Nair, L. S.; Laurencin, C. T. Biodegradable polymers as biomaterials. *Prog. Polym. Sci.* **2007**,

32, 762-798.

- (181) Woodruff, M. A.; Hutmacher, D. W. The return of a forgotten polymer—polycaprolactone in the 21st century. *Prog. Polym. Sci.* **2010**, *35*, 1217-1256.
- (182) Kim, K.; Hasneen, A.; Paik, H.-j.; Chang, T. MALDI-TOF MS characterization of polystyrene synthesized by ATRP. *Polymer* **2013**, *54*, 6133-6139.
- (183) Berkowski, K. L.; Potisek, S. L.; Hickenboth, C. R.; Moore, J. S. Ultrasound-induced site-specific cleavage of azo-functionalized poly (ethylene glycol). *Macromolecules* **2005**, *38*, 8975-8978.
- (184) Duan, H.-Y.; Wang, Y.-X.; Wang, L.-J.; Min, Y.-Q.; Zhang, X.-H.; Du, B.-Y. An Investigation of the selective chain scission at centered diels–alder mechanophore under ultrasonication. *Macromolecules* **2017**, *50*, 1353-1361.
- (185) Graessley, W. W. Polymer chain dimensions and the dependence of viscoelastic properties on concentration, molecular weight and solvent power. *Polymer* **1980**, *21*, 258-262.
- (186) Kryger, M. J.; Ong, M. T.; Odom, S. A.; Sottos, N. R.; White, S. R.; Martinez, T. J.; Moore, J. S. Masked cyanoacrylates unveiled by mechanical force. *J. Am. Chem. Soc.* **2010**, *132*, 4558-4559.
- (187) Malhotra, S. L. Ultrasonic solution degradations of poly(alkyl methacrylates). *J. Macromol. Sci., Chem.* **1986**, *23*, 729-748.
- (188) Robb, M. J.; Moore, J. S. A retro-staudinger cycloaddition: mechanochemical cycloelimination of a  $\beta$ -lactam mechanophore. *J. Am. Chem. Soc.* **2015**, *137*, 10946-10949.
- (189) Sato, T.; Nalepa, D. E. Shear degradation of cellulose derivatives. *J. Appl. Polym. Sci.* **1978**, *22*, 865-867.
- (190) Kryger, M. J.; Munaretto, A. M.; Moore, J. S. Structure–mechanochemical activity relationships for cyclobutane mechanophores. *J. Am. Chem. Soc.* **2011**, *133*, 18992-18998.
- (191) Nguyen, T. Q. Kinetics of mechanochemical degradation by gel permeation chromatography. *Polym. Degrad. Stab.* **1994**, *46*, 99-111.
- (192) Nguyen, T. Q.; Liang, Q. Z.; Kausch, H.-H. Kinetics of ultrasonic and transient elongational flow degradation: a comparative study. *Polymer* **1997**, *38*, 3783-3793.
- (193) Basedow, A. M.; Ebert, K. H. Ultrasonic degradation of polymers in solution. In *Physical Chemistry; Advances in Polymer Science*; Springer: Berlin, Heidelberg, 1977; Vol. 22, pp 83-148.
- (194) Schaefer, M.; Icli, B.; Weder, C.; Lattuada, M.; Kilbinger, A. F. M.; Simon, Y. C. The role of mass and length in the sonochemistry of polymers. *Macromolecules* **2016**, *49*, 1630-1636.
- (195) Niezette, J.; Linkens, A. Contribution to the ultrasonic degradation of polystyrene solutions. *Polymer* **1978**, *19*, 939-942.
- (196) Marx-Figini, M. Studies on the ultrasonic degradation of cellulose macromolecular properties. *Angew. Makromol. Chem.* **1997**, *250*, 85-92.
- (197) Li, Y.; Niu, Z.; Burdyńska, J.; Nese, A.; Zhou, Y.; Kean, Z. S.; Dobrynin, A. V.; Matyjaszewski, K.; Craig, S. L.; Sheiko, S. S. Sonication-induced scission of molecular bottlebrushes: implications of the “hairy” architecture. *Polymer* **2016**, *84*, 178-184.
- (198) Vijayalakshmi, S. P.; Madras, G. Effect of initial molecular weight and solvents on the ultrasonic degradation of poly(ethylene oxide). *Polym. Degrad. Stab.* **2005**, *90*, 116-122.
- (199) Jellinek, H. H. G. Degradation of long chain molecules by ultrasonic waves. viii. rate constants and the cavitation process. *J. Polym. Sci.* **1959**, *37*, 485-497.
- (200) Price, G. J.; Smith, P. F. Ultrasonic degradation of polymer solutions: 2. the effect of temperature, ultrasound intensity and dissolved gases on polystyrene in toluene. *Polymer* **1993**, *34*, 4111-4117.
- (201) Noltingk, B. E.; Neppiras, E. A. Cavitation produced by ultrasonics. *Proc. Phys. Soc., London*,

*Sect. B* **1950**, 63, 674-685.

- (202) Thomas, B. B.; Alexander, W. J. Ultrasonic degradation of cellulose nitrate. II. Effects of temperature, solvent, and other process variables. *J. Polym. Sci.* **1957**, 25, 285-303.
- (203) Bender, M. L.; Turnquest, B. W. General basic catalysis of ester hydrolysis and its relationship to enzymatic hydrolysis. *J. Am. Chem. Soc.* **1957**, 79, 1656-1662.
- (204) Khanlari, S.; Dubé, M. A. Bioadhesives: a review. *Macromolecular Reaction Engineering* **2013**, 7, 573-587.
- (205) Mehdizadeh, M.; Yang, J. Design strategies and applications of tissue bioadhesives. *Macromol. Biosci.* **2013**, 13, 271-288.
- (206) Palacio, M. L.; Bhushan, B. Bioadhesion: a review of concepts and applications. *Philosophical Transactions of the Royal Society A: Mathematical, Physical and Engineering Sciences* **2012**, 370, 2321-2347.
- (207) Bouten, P. J.; Zonjee, M.; Bender, J.; Yauw, S. T.; van Goor, H.; van Hest, J. C.; Hoogenboom, R. The chemistry of tissue adhesive materials. *Prog. Polym. Sci.* **2014**, 39, 1375-1405.
- (208) Kaul, A.; Hutfless, S.; Le, H.; Hamed, S. A.; Tymitz, K.; Nguyen, H.; Marohn, M. R. Staple versus fibrin glue fixation in laparoscopic total extraperitoneal repair of inguinal hernia: a systematic review and meta-analysis. *Surg. Endosc.* **2012**, 26, 1269-1278.
- (209) Raja, P. R. Cyanoacrylate adhesives: a critical review. *Rev. Adhes. Adhes.* **2016**, 4, 398-416.
- (210) Bhagat, V.; Becker, M. L. Degradable adhesives for surgery and tissue engineering. *Biomacromolecules* **2017**, 18, 3009-3039.
- (211) Ghobril, C.; Grinstaff, M. The chemistry and engineering of polymeric hydrogel adhesives for wound closure: a tutorial. *Chem. Soc. Rev.* **2015**, 44, 1820-1835.
- (212) Bré, L. P.; Zheng, Y.; Pêgo, A. P.; Wang, W. Taking tissue adhesives to the future: from traditional synthetic to new biomimetic approaches. *Biomater. Sci.* **2013**, 1, 239-253.
- (213) Zhu, W.; Chuah, Y. J.; Wang, D.-A. Bioadhesives for internal medical applications: a review. *Acta Biomater.* **2018**, 74, 1-16.
- (214) Mogal, V.; Papper, V.; Chaurasia, A.; Feng, G.; Marks, R.; Steele, T. Novel on-d emand bioadhesion to soft tissue in wet environments. *Macromol. Biosci.* **2014**, 14, 478-484.
- (215) Lang, N.; Pereira, M. J.; Lee, Y.; Friehs, I.; Vasilyev, N. V.; Feins, E. N.; Ablasser, K.; O'Cearbhaill, E. D.; Xu, C.; Fabozzo, A. A blood-resistant surgical glue for minimally invasive repair of vessels and heart defects. *Sci. Transl. Med.* **2014**, 6, 218ra216-218ra216.
- (216) Yang, Y.; Zhang, J.; Liu, Z.; Lin, Q.; Liu, X.; Bao, C.; Wang, Y.; Zhu, L. Tissue-integratable and biocompatible photogelation by the imine crosslinking reaction. *Adv. Mater.* **2016**, 28, 2724-2730.
- (217) Hong, Y.; Zhou, F.; Hua, Y.; Zhang, X.; Ni, C.; Pan, D.; Zhang, Y.; Jiang, D.; Yang, L.; Lin, Q. A strongly adhesive hemostatic hydrogel for the repair of arterial and heart bleeds. *Nat. Commun.* **2019**, 10, 2060.
- (218) Shirzaei Sani, E.; Kheirkhah, A.; Rana, D.; Sun, Z.; Foulsham, W.; Sheikhi, A.; Khademhosseini, A.; Dana, R.; Annabi, N. Sutureless repair of corneal injuries using naturally derived bioadhesive hydrogels. *Sci. Adv.* **2019**, 5, eaav1281.
- (219) Feng, G.; Djordjevic, I.; Mogal, V.; O'Rourke, R.; Pokholenko, O.; Steele, T. W. Elastic light tunable tissue adhesive dendrimers. *Macromol. Biosci.* **2016**, 16, 1072-1082.
- (220) Nanda, H. S.; Shah, A. H.; Wicaksono, G.; Pokholenko, O.; Gao, F.; Djordjevic, I.; Steele, T. W. Nonthrombogenic hydrogel coatings with carbene-cross-linking bioadhesives. *Biomacromolecules* **2018**, 19, 1425-1434.

- (221) Granskog, V.; Andrén, O. C. J.; Cai, Y.; González-Granillo, M.; Felländer-Tsai, L.; von Holst, H.; Haldosen, L.-A.; Malkoch, M. Linear dendritic block copolymers as promising biomaterials for the manufacturing of soft tissue adhesive patches using visible light initiated thiol–ene coupling chemistry. *Adv. Funct. Mater.* **2015**, *25*, 6596-6605.
- (222) Walker, B. W.; Lara, R. P.; Yu, C. H.; Sani, E. S.; Kimball, W.; Joyce, S.; Annabi, N. Engineering a naturally-derived adhesive and conductive cardiopatch. *Biomaterials* **2019**, *207*, 89-101.
- (223) Shah, A. H.; Pokholenko, O.; Nanda, H. S.; Steele, T. W. J. Non-aqueous, tissue compliant carbene-crosslinking bioadhesives. *Mater. Sci. Eng., C* **2019**, *100*, 215-225.
- (224) Trujillo-de Santiago, G.; Sharifi, R.; Yue, K.; Sani, E. S.; Kashaf, S. S.; Alvarez, M. M.; Leijten, J.; Khademhosseini, A.; Dana, R.; Annabi, N. Ocular adhesives: design, chemistry, crosslinking mechanisms, and applications. *Biomaterials* **2019**, *197*, 345-367.
- (225) Barbey, R.; Lavanant, L.; Paripovic, D.; Schuwer, N.; Sugnaux, C.; Tugulu, S.; Klok, H.-A. Polymer brushes via surface-initiated controlled radical polymerization: synthesis, characterization, properties, and applications. *Chem. Rev.* **2009**, *109*, 5437-5527.
- (226) Yu, Q.; Zhang, Y.; Wang, H.; Brash, J.; Chen, H. Anti-fouling bioactive surfaces. *Acta Biomater.* **2011**, *7*, 1550-1557.
- (227) Vaisocherová, H.; Brynda, E.; Homola, J. Functionalizable low-fouling coatings for label-free biosensing in complex biological media: advances and applications. *Anal. Bioanal. Chem.* **2015**, *407*, 3927-3953.
- (228) Xu, F. J.; Neoh, K. G.; Kang, E. T. Bioactive surfaces and biomaterials via atom transfer radical polymerization. *Prog. Polym. Sci.* **2009**, *34*, 719-761.
- (229) Schüwer, N.; Klok, H. A. A potassium-selective quartz crystal microbalance sensor based on crown-ether functionalized polymer brushes. *Adv. Mater.* **2010**, *22*, 3251-3255.
- (230) Tugulu, S.; Silacci, P.; Stergiopoulos, N.; Klok, H.-A. RGD—Functionalized polymer brushes as substrates for the integrin specific adhesion of human umbilical vein endothelial cells. *Biomaterials* **2007**, *28*, 2536-2546.
- (231) Bilgic, T.; Klok, H.-A. Oligonucleotide immobilization and hybridization on aldehyde-functionalized poly (2-hydroxyethyl methacrylate) brushes. *Biomacromolecules* **2015**, *16*, 3657-3665.
- (232) Xu, D.; Yu, W. H.; Kang, E. T.; Neoh, K. G. Functionalization of hydrogen-terminated silicon via surface-initiated atom-transfer radical polymerization and derivatization of the polymer brushes. *J. Colloid Interface Sci.* **2004**, *279*, 78-87.
- (233) Neises, B.; Steglich, W. Simple Method for the Esterification of Carboxylic Acids. *Angew. Chem., Int. Ed. Engl.* **1978**, *17*, 522-524.
- (234) Alang Ahmad, S.; Hucknall, A.; Chilkoti, A.; Leggett, G. J. Protein patterning by UV-induced photodegradation of poly (oligo (ethylene glycol) methacrylate) brushes. *Langmuir* **2010**, *26*, 9937-9942.
- (235) Ducker, R. E.; Janusz, S.; Sun, S.; Leggett, G. J. One-step photochemical introduction of nanopatterned protein-binding functionalities to oligo (ethylene glycol)-terminated self-assembled monolayers. *J. Am. Chem. Soc.* **2007**, *129*, 14842-14843.
- (236) Jeyachandran, Y.; Terfort, A.; Zharnikov, M. Controlled modification of protein-repelling self-assembled monolayers by ultraviolet light: the effect of the wavelength. *J. Phys. Chem. C* **2012**, *116*, 9019-9028.
- (237) Reynolds, N. P.; Tucker, J. D.; Davison, P. A.; Timney, J. A.; Hunter, C. N.; Leggett, G. J. Site-specific immobilization and micrometer and nanometer scale photopatterning of yellow fluorescent protein on glass surfaces. *J. Am. Chem. Soc.* **2009**, *131*, 896-897.

- (238) Tizazu, G.; el Zubir, O.; Patole, S.; McLaren, A.; Vasilev, C.; Mothersole, D. J.; Adawi, A.; Hunter, C. N.; Lidzey, D. G.; Lopez, G. P. Micrometer and nanometer scale photopatterning of proteins on glass surfaces by photo-degradation of films formed from oligo (ethylene glycol) terminated silanes. *Biointerphases* **2012**, 7, 54.
- (239) Ul-Haq, E.; Patole, S.; Moxey, M.; Amstad, E.; Vasilev, C.; Hunter, C. N.; Leggett, G. J.; Spencer, N. D.; Williams, N. H. Photocatalytic nanolithography of self-assembled monolayers and proteins. *ACS Nano* **2013**, 7, 7610-7618.
- (240) Pranantyo, D.; Xu, L. Q.; Neoh, K.-G.; Kang, E.-T.; Ng, Y. X.; Teo, S. L.-M. Tea stains-inspired initiator primer for surface grafting of antifouling and antimicrobial polymer brush coatings. *Biomacromolecules* **2015**, 16, 723-732.
- (241) Feng, W.; Brash, J. L.; Zhu, S. Non-biofouling materials prepared by atom transfer radical polymerization grafting of 2-methacryloxyethyl phosphorylcholine: separate effects of graft density and chain length on protein repulsion. *Biomaterials* **2006**, 27, 847-855.
- (242) Iwata, R.; Suk-In, P.; Hoven, V. P.; Takahara, A.; Akiyoshi, K.; Iwasaki, Y. Control of nanobiointerfaces generated from well-defined biomimetic polymer brushes for protein and cell manipulations. *Biomacromolecules* **2004**, 5, 2308-2314.
- (243) Bochyńska, A. I.; Van Tienen, T. G.; Hannink, G.; Buma, P.; Grijpma, D. W. Development of biodegradable hyper-branched tissue adhesives for the repair of meniscus tears. *Acta Biomater.* **2016**, 32, 1-9.
- (244) Bochyńska, A. I.; Hannink, G.; Grijpma, D. W.; Buma, P. Tissue adhesives for meniscus tear repair: an overview of current advances and prospects for future clinical solutions. *J. Mater. Sci. Mater. Med.* **2016**, 27, 85.
- (245) Bochyńska, A. I.; Hannink, G.; Buma, P.; Grijpma, D. W. Adhesion of tissue glues to different biological substrates. *Polym. Adv. Technol.* **2017**, 28, 1294-1298.
- (246) Hu, Y.; Goodeal, N.; Chen, Y.; Ganose, A. M.; Palgrave, R. G.; Bronstein, H.; Blunt, M. O. Probing the chemical structure of monolayer covalent-organic frameworks grown via Schiff-base condensation reactions. *Chem. Commun.* **2016**, 52, 9941-9944.
- (247) Di Giovannantonio, M.; Kosmala, T.; Bonanni, B.; Serrano, G.; Zema, N.; Turchini, S.; Catone, D.; Wandelt, K.; Pasini, D.; Contini, G. Surface-enhanced polymerization via schiff-base coupling at the solid-water interface under pH control. *J. Phys. Chem. C* **2015**, 119, 19228-19235.
- (248) Brash, D. E.; Rudolph, J. A.; Simon, J. A.; Lin, A.; McKenna, G. J.; Baden, H. P.; Halperin, A. J.; Ponten, J. A role for sunlight in skin cancer: UV-induced p53 mutations in squamous cell carcinoma. *Proc. Natl. Acad. Sci.* **1991**, 88, 10124-10128.
- (249) Ananthaswamy, H. N.; Pierceall, W. E. Molecular mechanisms of ultraviolet radiation carcinogenesis. *Photochem. Photobiol.* **1990**, 52, 1119-1136.
- (250) Ritter, E.; Przybylski, P.; Brzezinski, B.; Bartl, F. Schiff Bases in Biological Systems. *Curr. Org. Chem.* **2009**, 13, 241-249.
- (251) Halloran, M. W.; Lumb, J. P. Recent applications of diazirines in chemical proteomics. *Chemistry—A European Journal* **2019**, 25, 4885-4898.
- (252) Preston, G. W.; Wilson, A. J. Photo-induced covalent cross-linking for the analysis of biomolecular interactions. *Chem. Soc. Rev.* **2013**, 42, 3289-3301.
- (253) Murale, D. P.; Hong, S. C.; Haque, M. M.; Lee, J. S. Photo-affinity labeling (PAL) in chemical proteomics: a handy tool to investigate protein-protein interactions (PPIs). *Proteome Sci.* **2017**, 15.
- (254) Hermanson, G. T.; Academic press: 2013.

- (255) Léonard, D.; Chevolot, Y.; Bucher, O.; Sigrist, H.; Mathieu, H. ToF-SIMS and XPS study of photoactivatable reagents designed for surface glycoengineering. Part I. N-(m-(3-(trifluoromethyl) diazirine-3-yl) phenyl)-4-maleimido-butyramide (mad) on silicon, silicon nitride and diamond. *Surf. Interface Anal.* **1998**, *26*, 783-792.
- (256) Yu, J.; Jackson, N. E.; Xu, X.; Morgenstern, Y.; Kaufman, Y.; Ruths, M.; de Pablo, J. J.; Tirrell, M. Multivalent counterions diminish the lubricity of polyelectrolyte brushes. *Science* **2018**, *360*, 1434-1438.
- (257) Yu, J.; Mao, J.; Yuan, G.; Satija, S.; Jiang, Z.; Chen, W.; Tirrell, M. Structure of polyelectrolyte brushes in the presence of multivalent counterions. *Macromolecules* **2016**, *49*, 5609-5617.
- (258) Yu, J.; Jackson, N. E.; Xu, X.; Brettmann, B. K.; Ruths, M.; de Pablo, J. J.; Tirrell, M. Multivalent ions induce lateral structural inhomogeneities in polyelectrolyte brushes. *Sci. Adv.* **2017**, *3*, eaao1497-eaao1497.
- (259) Karzbrun, E.; Tayar, A. M.; Noireaux, V.; Bar-Ziv, R. H. Programmable on-chip DNA compartments as artificial cells. *Science* **2014**, *345*, 829-832.
- (260) Drummond, T. G.; Hill, M. G.; Barton, J. K. Electrochemical DNA sensors. *Nat. Biotechnol.* **2003**, *21*, 1192-1199.
- (261) Jin, Y.; Wu, C.; Yang, Y.; Wu, J.; He, Z.; Wang, J. Inhibiting condensation freezing on patterned polyelectrolyte coatings. *ACS Nano* **2020**, *14*, 5000-5007.
- (262) Chen, T.; Ferris, R.; Zhang, J.; Ducker, R.; Zauscher, S. Stimulus-responsive polymer brushes on surfaces: Transduction mechanisms and applications. *Prog. Polym. Sci.* **2010**, *35*, 94-112.
- (263) Kou, R.; Zhang, J.; Chen, Z.; Liu, G. Counterion specificity of polyelectrolyte brushes: role of specific ion-pairing interactions. *ChemPhysChem* **2018**, *19*, 1404-1413.
- (264) Manning, G. S. Counterion binding in polyelectrolyte theory. *Acc. Chem. Res.* **1979**, *12*, 443-449.
- (265) Wang, J.; Karami, P.; Ataman, N. C.; Pioletti, D. P.; Steele, T. W. J.; Klok, H.-A. Light-activated, bioadhesive, poly(2-hydroxyethyl methacrylate) brush coatings. *Biomacromolecules* **2020**, *21*, 240-249.
- (266) Ramstedt, M.; Cheng, N.; Azzaroni, O.; Mossialos, D.; Mathieu, H. J.; Huck, W. T. S. Synthesis and characterization of poly(3-sulfopropylmethacrylate) brushes for potential antibacterial applications. *Langmuir* **2007**, *23*, 3314-3321.
- (267) Alonso-García, T.; Rodríguez-Presa, M. J.; Gervasi, C.; Moya, S.; Azzaroni, O. Electrochemical determination of the glass transition temperature of thin polyelectrolyte brushes at solid-liquid interfaces by impedance spectroscopy. *Anal. Chem.* **2013**, *85*, 6561-6565.

# Curriculum Vitae

---

## PERSONAL INFORMATION

**Name:** Jian Wang

**Date of Birth:** 10/07/1989

**Gender:** Male

**Email:** jian.wang@epfl.ch

**Marital Status:** Married, two children

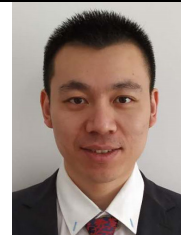
**Phone number:** +41 787158268

**Citizenship:** People's Republic of China

**ORCID:** 0000-0003-0459-5833

**Address:** EPFL-STI-IMX-LP, MXD 131, Station 12, CH-1015 Lausanne (Switzerland)

---



## EDUCATION

**09. 2008-06. 2012:** **Bachelor Degree. Major: Chemical engineering.** College of Chemistry, Jilin University, P. R. China.

**09. 2012-06. 2015:** **Master Degree. Major: Polymer chemistry and physics.** Department of Chemistry, Renmin University of China, P. R. China. **Advisor: Prof. Yapei Wang**

**11. 2015-now:** PhD student, Institute of Materials, Ecole Polytechnique Fédérale de Lausanne (EPFL). **Advisor: Prof. Harm-Anton Klok**

---

## SUPERVISION OF STUDENTS

1. Jing Zhao (undergraduate student in Renmin University of China). "Fabrication of multifunctional paper based-sensor via printing chemistry" (06. 2013-06. 2015).
  2. Jean-Ludovic Genilloud (master student in EPFL) Master semester project "The influence of stretching forces on mechanophores in polymer backbones" (09. 2017-12. 2017).
  3. Dharmawan Philip (master student in EPFL) Master semester project "The thermal electric properties of polymer brushes" (03. 2019-06.2019).
- 

## PRIZES, AWARDS, FELLOWSHIPS

1. Swiss National Science Foundation "Early Postdoc Mobility" Fellowship (05. 2020)
2. "Chemistry travel award" from the Swiss Academy of Science and the Swiss Chemical Society (04. 2019)

3. “Best poster award” in the 8<sup>th</sup> International Symposium on Polymer Chemistry, PC2018 in Changchun, China. (June 6-9 2018).
  4. Fellowship for studying abroad from China Scholarship Council (11. 2015 – 10. 2019)
  5. “Best poster award” in the 29<sup>th</sup> Chinese Chemical Society Congress in Beijing, China (August 4-7 2014)
  6. “Guanghua” scholarship (290 quotas per year all over China) (12. 2013)
  7. “Quintessence student” of Renmin University of China (12. 2013)
  8. “Excellent postgraduate” of Renmin University of China (12. 2013)
  9. The first prize scholarship of Renmin University of China (06. 2013)
  10. The first prize scholarship of Renmin University of China (09. 2012)
  11. Excellent graduation design of college of chemistry, Jilin University (06. 2012)
  12. The third prize scholarship of Jilin University (06. 2011)
- 

## **PERSONAL SKILLS**

**Language skills:** Chinese, mother tongue; English, fluent spoken and written.

**Experimental skills:** Preparation of micro/nanoparticles via emulsion method, micro/nanofabrication technique, photolithography, atom transfer radical polymerization (ATRP), post-polymerization modification, functionalization of silica nanoparticles, silicon, fused silica and PDMS flat surfaces, UV-oxidation reaction.

**Characterization skills:** Electrochemical working station, Optical microscopy, SEM, NMR, GPC/SEC, ATR-FTIR, AFM, ellipsometry, DSL, TGA, XPS, water contact angle measurement, MALDI-TOF, Instron instrument.

**IT skills:** MS office, OriginLab, Chembiodraw, 3ds Max, LabVIEW.

---

## **LIST OF PUBLICATIONS**

1. **J. Wang** and H-A. Klok\*, *Angew. Chem. Int. Ed.* **2019**, 58, 9989-9993.
2. **J. Wang**, P. Karami, N. C. Ataman, D. P. Pioletti, T. W. J. Steele, and H-A. Klok\*, *Biomacromolecules* **2020**, 21, 240-249.
3. **J. Wang** and H-A. Klok\*, “Mechanical Acceleration of Hydrolysis in Polymer Incorporating Main Chain Ester Bonds”, submitted.
4. **J. Wang**, K. Chu, D. Damjanovic and H-A. Klok\*, “Pyroelectric Properties of Polyelectrolyte Brushes”, in preparation.
5. J. Zoppe, N. Ataman, P. Mocny, **J. Wang**, J. Moraes, and H-A. Klok\*, *Chem. Rev.* **2017**, 117, 1105–1318.
6. **J. Wang**, J. Zhao, Y. Li, M. Yang, Z. Sun\* and Y. Wang\*, *ACS Macro Lett.* **2015**, 4, 392-397.

7. **J. Wang**, X. Zhang, X. Huang, S. Wang, Q. Qian, W. Du and Y. Wang\*, *Small* **2013**, 9, 3759-3764. (Highlight by nanowerk)
  8. H. Jia, **J. Wang** (co-first author), X. Zhang and Y. Wang\*, *ACS Macro Lett.* **2014**, 3, 86-91.
  9. X. Dou, **J. Wang**, X. Lu, M. Zhang, Y. Qin\*, Y. Wang, P. Zhang, and Z-X. Guo\*, *RSC Adv.*, **2016**, 6, 112241.
  10. Q. Qian, **J. Wang**, F. Yan and Y. Wang\*, *Angew. Chem. Int. Ed.* **2014**, 53, 4465-4468. (Back cover) (Highlight by NatureChina)
  11. S. Zhang, S. Liao, Y. Cao, **J. Wang**, R. Li, Z. Wang and Y. Wang\*, *J. Mater. Chem. B*, **2017**, 5, 4966-4972.
  12. Y. Cao, Z. Wang, S. Liao, **J. Wang** and Y. Wang\*, *Chem. Eur. J.* **2016**, 22, 1152–1158.
  13. X. Huang, R. Fang, D. Wang, **J. Wang**, H. Xu\* and Y. Wang, *Small*. **2015**, 11, 1537-1541.
  14. R. Ma, F. Cao, **J. Wang**, G. Zhu and G. Pang\* , *Materials Letters*, **2011**, 65, 2880-2882
-